

High Strain Rate Behaviour of Cervical Spine Segments in Flexion and Extension

by

Jeffrey Barker

A thesis

presented to the University of Waterloo

in fulfillment of the

thesis requirement for the degree of

Master of Applied Science

in

Mechanical Engineering

Waterloo, Ontario, Canada, 2012

© Jeffrey Barker 2012

AUTHOR'S DECLARATION

I hereby declare that I am the sole author of this thesis. This is a true copy of the thesis, including any required final revisions, as accepted by my examiners.

I understand that my thesis may be made electronically available to the public.

Jeffrey B. Barker

Abstract

Cervical Spine injuries are a common occurrence during motor vehicle accidents, and they represent a significant economic cost to society. Numerical Finite Element (FE) models have been formulated to investigate the response of the neck under various loading scenarios and to improve vehicle safety. The Global Human Body Models Consortium (GHBMC) was formed to develop a detailed FE model capable of simulating occupant response and predicting subsequent soft tissue injuries in the cervical spine.

The objective of this thesis was to validate the neck region of the GHBMC model at the segment level in flexion and extension, and at rotation rates observed during car crash scenarios. Nine cervical spines, under the age of 50, were procured from post mortem human subjects and they were dissected into segments. A segment consisted of two vertebrae with the ligaments and the intervertebral disc intact, and the muscle, nervous, and cardiovascular tissues removed. A custom built fixture was built to test each specimen three times in flexion and extension at two rotation rates: a low rate (one degree per second) and a high rate (500 degrees per second). To avoid damaging the specimens after the first test, the segments were only rotated up to ten degrees for the segments at the C2-C3 through C5-C6 level, and up to eight degrees for the C6-C7 and C7-T1 level. The segment response was represented by plots of the moment against the angle of rotation in the sagittal plane. The segment models were simulated at the same low and high rotation rates, and the model results were evaluated against the experimental response.

The low speed experimental results were compared to existing quasi-static studies, but there was not an elevated rotation rate study at each segment level to compare with the high rate response. The segment response from the existing data was generally weaker than the results of this thesis because the earlier studies tested older specimens, and the existing studies applied a step-wise loading protocol instead of a continuous one.

A statistical analysis was conducted to determine the significance of the difference between the low and high rate experimental response. At the maximum angle of rotation, the analysis found moderate evidence ($p < 0.05$) of increased segment stiffness at the high rotation rate for the C5-C6 and C6-C7 segments in flexion and extension, and weak evidence of increased stiffness for the C3-C4 and C4-C5 segments in flexion and extension, and for the C2-C3 and C7-T1 segments in extension. Below six degrees of rotation, there was no statistical evidence that the low and high speed responses were significantly different for any segment.

In flexion, the model response was within one standard deviation of the experimental mean at the C6-C7 and C7-T1 segment level. For the C2-C3 through C5-C6 segment levels, the model was stiffer than the experimental mean. In extension, the model was within one standard deviation at every segment level except at the C2-C3 and C7-T1 segment levels where the model response was weaker than the experimental response. For the high rate model analysis, the model predicted that the high rate simulations were stiffer than the low rate simulation at every segment level; however the difference was much greater in flexion than in extension.

Recommendations for further research included studying the high rate behaviour of the intervertebral discs under compressive and bending loading, and investigating the translational and rotational displacement of the spine during flexion and extension and compare the results with the model. The procurement of more post mortem human subjects would increase the sample size and it could improve the significance of the statistical analysis, and additional spines would permit the analysis of other effects, such as the influence of gender.

Acknowledgements

I would like to thank my supervisors, Dr. Naveen Chandrashekar and Dr. Duane Cronin, for their guidance and providing me with an opportunity to conduct research at the University of Waterloo.

I am pleased to thank the Global Human Body Models Consortium (GHBMC) for their financial support and their leadership throughout the project. In particular, I would like to thank Dr. Yibing Shi and Dr. Zine Ben Aoun for sharing their knowledge and providing feedback over the past two years.

I want to thank my office mates and fellow students in the GHBMC project, especially Jeff Moulton for his help with designing and building the testing machine, and Steve Mattucci for his contribution to the dissection and preparation of the testing specimens.

And finally I would like to thank my family for supporting me throughout my school career. They have always pushed me to pursue a better education and I would not be in this position today without them.

Table of Contents

AUTHOR'S DECLARATION	ii
Abstract	iii
Acknowledgements	v
Table of Contents	vi
List of Figures	ix
List of Tables	xii
Chapter 1 Introduction.....	1
1.1 Motivation for Research.....	1
1.2 Research Objectives and Approach.....	2
1.3 Thesis Organization.....	3
Chapter 2 Anatomy of the Cervical Spine.....	4
2.1 Planes and Directions	4
2.2 The Human spine.....	6
2.2.1 Cervical Spine	7
Chapter 3 Literature Review	24
3.1 Experimental Testing.....	24
3.2 Flexion and Extension Studies	27
3.3 Cervical Spine Range of Motion	32
3.4 Biological Tissues in the Cervical Spine.....	32
3.4.1 Collagen.....	33
3.4.2 Bone.....	34
3.4.3 Intervertebral Discs	37
3.4.4 Ligaments	45
3.5 Age Related Properties	52

3.6 Numerical and mathematical models of the cervical spine	53
Chapter 4 Low and High Rate Experimental Testing Procedure	58
4.1 Cadaver Morphology.....	58
4.2 Testing Preparation.....	59
4.3 Testing Apparatus.....	65
4.4 Testing Procedure.....	68
4.4.1 Reporting of Results	68
4.4.2 Preconditioning.....	73
4.4.3 Preload.....	75
4.4.4 Flexion and Extension Tests.....	75
4.5 Data acquisition.....	77
4.6 Statistical Analysis	78
Chapter 5 Segment Finite Element Model Description.....	79
5.1 Vertebrae	80
5.2 Intervertebral Discs	82
5.3 Ligaments	85
5.4 Facet joints	87
5.5 Application of Flexion and Extension Moments.....	89
Chapter 6 Experimental and Model Results.....	91
6.1 Experimental Results.....	91
6.2 Model Results.....	94
6.3 Discussion	98
6.3.1 Strain Rate Effects.....	98
6.3.2 Comparison with Existing Studies	100
6.3.3 Influence of the Fixed Axis Machine	104

Chapter 7 Summary and Recommendations	107
7.1 Recommendations	109
Appendix – Individual Segment Test Results	111
References	117

List of Figures

Figure 2-1: Anatomical Planes	4
Figure 2-2: Human Spine	6
Figure 2-3: Cervical Spine.....	7
Figure 2-4: Cervical Spine Range of Motion	8
Figure 2-5: C1 – Axis, Superior View.....	9
Figure 2-6: C2 – Atlas, Superior Posterior View	10
Figure 2-7: C5 Vertebra.....	11
Figure 2-8: Mechanics of Flexion, Extension, Lateral Bending, and Axial Rotation	12
Figure 2-9: Cervical Spine Ligaments.....	14
Figure 2-10: Posterior Longitudinal Ligament.....	15
Figure 2-11: Ligamentum Flavum.....	16
Figure 2-12: Facet Joint.....	17
Figure 2-13: Facet Joint Angle	18
Figure 2-14: Intervertebral Disc	20
Figure 2-15: Annulus Fibrosus Layers	21
Figure 2-16: The Angle of the Annulus Fibrosus.....	22
Figure 3-1: Flexion Extension Apparatus.....	24
Figure 3-2: Flexion Apparatus.....	25
Figure 3-3: Fixed Axis of Rotation Machine.....	25
Figure 3-4: Flexion/Extension Results	28
Figure 3-5: Flexion/Extension Results - Camacho et al. 1997, Nightingale et al. 2002, 2007, Wheeldon et al. 2006.....	30
Figure 3-6: Strain Rate Sensitivity of Collagen.....	33
Figure 3-7: Osteons and the Haversian Canal	35
Figure 3-8: Strain Rate Sensitivity of Bone.....	37
Figure 3-9: Circumferential Tensile Stress Strain Response of the Outer Annulus Fibrosus	38
Figure 3-10: Site Specific Properties of the Annulus Fibrosus - Circumferential Direction.....	39
Figure 3-11: Radial Stress Strain Curve of the Annulus Fibrosus – Fujita et al. 1997	41
Figure 3-12: Stress Strain Response of the ALL, PLL, and LF – Chazel et al. 1985.....	46
Figure 3-13: Summary of High Rate Ligament Testing - Failure Force	50
Figure 3-14: Summary of High Rate Ligament Testing - Failure Elongation.....	50

Figure 3-15: Summary of High Rate Ligament Testing - Failure Stress.....	51
Figure 3-16: Summary of High Rate Ligament Testing - Failure Strain.....	51
Figure 3-17: Comparison of Cervical Spine Finite Element Model with Flexion Extension Segment Studies (Adapted from Panzer et al. 2011).....	56
Figure 4-1: Spine Dissection	60
Figure 4-2: C6-C7 Segment Ready for Potting	62
Figure 4-3: Potting Procedure	63
Figure 4-4: Half Potted Specimen	64
Figure 4-5: Fixed Axis Machine.....	65
Figure 4-6: Upper and Lower Pot Holders	66
Figure 4-7: Servomotor and Rotating Bracket	67
Figure 4-8: Load Cell at 45 degree angle	69
Figure 4-9: Raw Data - Forces and Moments	70
Figure 4-10: Adjustment of Force Moment Reading	71
Figure 4-11: Sample Resultant Moment Graph.....	72
Figure 4-12: Precondition - Finding the Center Point	74
Figure 4-13: Angular Rotation and Velocity versus Time	76
Figure 5-1: Full GHBM Neck Model	79
Figure 5-2: Top and Side View of C1 through C4	80
Figure 5-3: Top and Side View of C5 through T1	81
Figure 5-4: Vertebra Cortical Shell [red] and Cancellous Interior [green]	82
Figure 5-5: Nucleus Pulposus [left], Ground Substance [center], Annulus Fibrosus Layer [right]	83
Figure 5-6: Stress Strain Curves for each Annulus Fibrosus Layer	84
Figure 5-7: 7 Beam Elements Representing the ALL	85
Figure 5-8: Quasi-static Load Curves of each Ligament.....	86
Figure 5-9: Closeup of Model Facet Joints	87
Figure 5-10: Rigid Bodies attached to the Vertebrae for Moment Application	90
Figure 6-1: C2-C3, C3-C4, C4-C5 Experimental Results – Low and High Speed Tests.....	92
Figure 6-2: C5-C6, C6-C7 & C7-T1 Experimental Results - Low and High Speed Tests.....	93
Figure 6-3: C2-C3, C3-C4 & C4-C5 Experimental Testing vs. Model Results	96
Figure 6-4: C5-C6, C6-C7 & C7-T1 Experimental Testing vs. Model Results	97
Figure 6-5: C3-C4 & C4-C5 Comparison with results from Nightingale et al. (2002, 2007) and Wheeldon et al. (2006)	102

Figure 6-6: C5-C6, C6-C7 & C7-T1 Comparison with results from Nightingale et al. (2002, 2007) and Wheeldon et al. (2006) 103

Figure 6-7: Sample Shear and Compression Force Curves Plotted against Rotation..... 104

List of Tables

Table 3-1: Flexion/Extension Range of Motion - Panjabi et al. 2001	31
Table 3-2: Cervical Spine Segment Range of Motion in Degrees - Dvorak et al. 1991.....	32
Table 3-3: Site Specific Elastic Properties of the Annulus Fibrosus (Elliot et al. 2001).....	40
Table 3-4: Elastic Properties of Single Annulus Fibrosus Fibre	42
Table 3-5: Failure Properties of a Single Annulus Fibrosus Fibre	42
Table 3-6: Failure Properties of the Cervical Spine Ligaments – Myklebust et al. (1988).....	46
Table 3-7: Failure and Elastic Properties of the Cervical Spine Ligaments (Pryzbylski et al. 1996).....	47
Table 3-8: Properties of the Middle and Lower Cervical Spine Ligaments	48
Table 4-1: Cervical Spine Donor Morphology	59
Table 4-2: Average Dimensions (with Standard Deviation) of Donor Vertebral Bodies.....	61
Table 5-1: Mechanical Properties of Cortical and Cancellous Bone in the Model	81
Table 5-2: Mechanical Properties in the model of the Articular Cartilage.....	88
Table 6-1: P-value of the Statistical Test Comparing Low and High Rate (Maximum Rotation)	94
Table 6-2: Statistical Comparison for Rotation Rate Effects (2° Rotation)	98
Table 6-3: Statistical Comparison for Rotation Rate Effects (4° Rotation)	99
Table 6-4: Statistical Comparison for Rotation Rate Effects (6° Rotation)	99
Table 6-5: Shear and Compressive Average Forces for Flexion and Extension at every Segment Level	106

Chapter 1

Introduction

1.1 Motivation for Research

The cervical spine is frequently injured during motor vehicle collisions. Fourteen percent of all car crashes result in an injury to the cervical spine (National Highway Traffic Safety Administration - National Automotive Sampling System 2010, <http://www.nhtsa.gov/NASS>). In order to improve motor vehicle safety, cars have to be tested in various crash scenarios to determine their crash worthiness. The process of designing, building, and crashing vehicles is iterative and very expensive. To reduce the costs and design time, finite element (FE) models of the vehicle and the occupant have been developed (Halldin et al. 2000, Van der Horst 2002, Meyer et al. 2004, Panzer et al. 2011) to simulate these car crash scenarios before actually building and crash testing the vehicle.

Finite element models of crash test dummies, and even human body models, are limited by their kinematic accuracy and their ability to predict injury. Currently, the available body models are used to predict global kinematics which can then be related to injury based on certain parameters, such as peak accelerations or force interactions between body parts and the vehicle. However, on a global scale, the models cannot accurately predict local soft tissue injury. Major automotive companies and their part suppliers have formed the Global Human Body Models Consortium (GHBMC) to develop a new FE model of the entire human body that addresses the lack of local injury prediction capabilities of current FE models.

In general, finite element models are limited in scope by the experimental validation. A FE model of the cervical spine must be validated for numerous testing scenarios and at varying intensities of loading. For the case of car crash testing, the model must be validated for different possible scenarios, such as frontal, side and rear impacts. If the cervical spine model is only compared against experimental frontal impacts, model results from rear impact simulations cannot be considered legitimate. However, before the FE neck model is validated on the global scale, the model must be built in stages, beginning with the material properties and geometry of the fundamental tissues. Once the geometry and material properties are obtained, the model is built up and validated in intermediate stages called segments. A segment consists of two vertebrae with the associated intervertebral disc and ligaments intact. After the segments are validated, the whole cervical spine model can be assembled. This thesis will focus on the segment level experimental testing and validation of the cervical spine model in flexion and extension.

Serious injuries often result from high speed car crashes, and if a FE model is used to simulate such an event, the model should be validated against high speed experimental data. Many studies have analyzed the quasi-static stiffness of the neck in flexion and extension (Moroney et al. 1988, Wen et al. 1993, Camacho et al. 1997,

Winklestein et al. 2000), but very few studies have looked into the dynamic response of the neck (Voo et al. 1998, Nightingale et al. 2002 & 2007). Another limitation of the literature is the age of the human donor spines. US census data from 2009 shows that almost 50% of drivers involved in car crashes are under the age of 35 (Table 1114, United States Census Bureau, 2009), so the FE model should be representative of a young healthy person. Due to a lack of young donor spines, most studies use specimens over the age of 50, but it has been shown that tissue properties weaken with aging, especially above the age of 50 (Iida et al. 2002, Stemper et al. 2010). Therefore the experimental testing from this thesis will only test cervical spines from donors aged 50 and under.

Tensile testing of cervical spine ligaments has revealed a positive correlation between strain rate and ligament stiffness and failure stress, and a negative correlation with failure strain (Shim et al. 2005, Ivancic et al. 2007, Bass et al. 2007, Mattucci et al. 2012). The strain rate effect on the compression loading of intervertebral disc has not been researched because the discs are too thin to test at high strain rates. However, the soft tissue building block of the disc, the annulus fibrosus, is made up of collagen fibres similar to ligaments, so the disc should also be strain rate dependent. During flexion and extension, the segment is loaded in bending and some of the ligaments are loaded in tension. It is hypothesized that since the ligaments are strain rate sensitive, the stiffness of the spine in flexion and extension should also show strain rate sensitivity.

1.2 Research Objectives and Approach

The first objective of this thesis is to conduct and interpret high speed experimental testing of the cervical spine at the segment level in flexion and extension. In flexion and extension, the data is reported as a relationship of the moment and the change in angle between two adjacent vertebral bodies. The second objective is to use the data obtained from the experimental testing to validate a finite element model of the cervical spine segments of a full cervical spine model capable of predicting soft tissue injury during motor vehicle car crash simulations. In this thesis, the model, which has already been developed before the research work in this thesis was conducted, is validated at the segment level only.

Nine cadaver cervical spines under the age of 50 were procured for testing. The spines were dissected into segments consisting of two vertebrae along with the ligaments and the intervertebral disc. The vertebrae were potted into liquid resin which hardened after a few minutes in plastic cups. The inferior vertebra was fixed to a six axis load cell and the superior vertebra was coupled to a servomotor that controlled the angular displacement in flexion and extension. A new experimental testing apparatus was custom built to rotate the superior vertebra about the fixed inferior vertebra in flexion and extension about a fixed axis.

The segments were rotated at two angular displacement rates. The first angular displacement rate, representing quasi-static conditions, was one degree per second. The dynamic rate was 500 degrees per second, and it was determined from 22 g frontal impact simulations of an existing finite element model of the cervical spine (Panzer et al. 2011). The moment-rotation relationship was reported for each segment test. The experimental procedure, including the boundary conditions, was recreated in the model simulation using commercial FE software and the moment-rotation relationship of the model was compared with the experimental testing results.

1.3 Thesis Organization

The second chapter of this thesis reviews the anatomy of the human cervical spine. This chapter discusses the geometry, composition, and purpose of the vertebrae, the ligaments, and the intervertebral discs. The muscles are not discussed in this thesis because they are not included in the segment models and they were removed before experimental testing.

Chapter three reviews the existing research relevant to the cervical spine and this thesis. This section first looks at studies done in flexion and extension at the whole spine and segment level, and describes the gap in the literature that will be addressed later on in this thesis. Afterwards, the chapter examines the research done on the cervical spine ligaments, vertebrae, and the intervertebral disc and its two main building blocks, the annulus fibrosus and nucleus pulposus. The mechanical properties of the biological tissues in the cervical spine are discussed in this chapter along with important concepts, such as viscoelasticity and strain rate dependency.

The fourth chapter discusses the methodology, which includes the experimental procedure, the statistical analysis of the results, and the model simulation.

The fifth chapter presents the GHBMC model. All the individual biological tissues are displayed along with the associated material models and numerical values for the model parameters.

The results of the experimental testing and the model validation are found in chapter six. The experimental and model results are compared against each other and against previous studies.

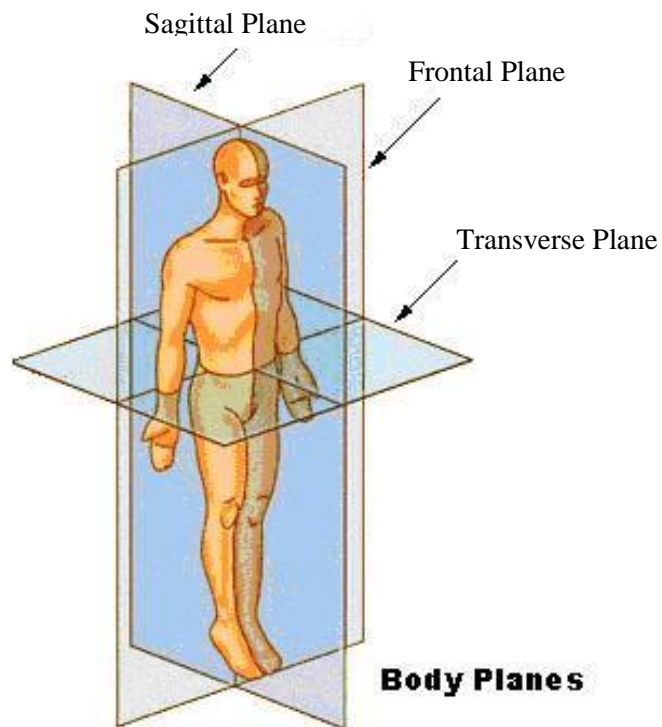
Chapter seven is the final chapter and it summarizes the research and the conclusions of the findings. Recommendations are made for improving the test procedure and for further experimental testing.

Chapter 2

Anatomy of the Cervical Spine

2.1 Planes and Directions

The human body in a standing position is divided into three anatomical planes (Figure 2-1). The transverse plane is parallel to the ground and splits the body into superior and inferior parts. The sagittal plane separates the right and the left side of the body, while the frontal plane divides the body from front to back.



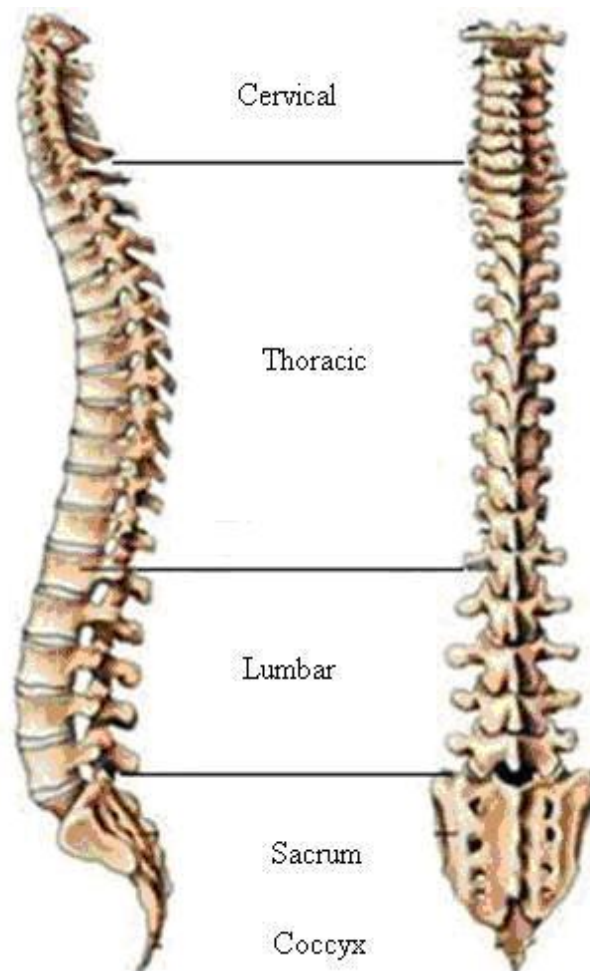
(Adapted from National Cancer Institute)

Figure 2-1: Anatomical Planes

There are several anatomical terms used to describe the direction or the relative position within the human body. The superior and inferior directions are perpendicular to the transverse plane and point towards the head and feet respectively. In the frontal plane, the anterior direction points towards the front (chest) of the body and the posterior direction points towards the back. For the sagittal plane, there is no left or right distinction because they are interchangeable depending on the point of view. Instead of left or right, there are the medial and lateral directions: the medial direction points towards the midsagittal plane and the lateral direction points away from it. There are three terms used to describe the depth relative to the surface of the body: superficial is on the outside, deep is in the center and intermediate is in between.

2.2 The Human spine

The human spinal column consists of 24 vertebrae and it is divided into three sections: cervical, thoracic, and lumbar, plus the sacrum and the coccyx (Figure 2-2). The cervical spine, which has seven vertebrae, is located at the superior end of the spine and is generally referred to as the neck. The thoracic spine consists of 12 vertebrae and it is in the middle section of the spine. The lumbar spine, located inferiorly to the thoracic spine, has only five vertebrae, but they are the largest in the spine. The sacrum and the coccyx are two unique bones at the inferior end of the spine.



(Adapted from www.back.com)

Figure 2-2: Human Spine

2.2.1 Cervical Spine

The seven vertebrae in the cervical spine are labeled C1 to C7 (Figure 2-3). C1 is located at the superior end and it is in contact with the base of the skull. C7 is found at the inferior end of the cervical spine and it interfaces with the first thoracic vertebrae. The purpose of the cervical spine is to protect the spinal cord and allow the head to move in flexion, extension, lateral bending and axial rotation. The skull-C1-C2 complex is unique from the rest of the cervical spine. The C0-C1 joint, or skull-C1, allows for significant rotation in flexion and extension, while the majority of the whole spine's axial rotation happens between C1 and C2.

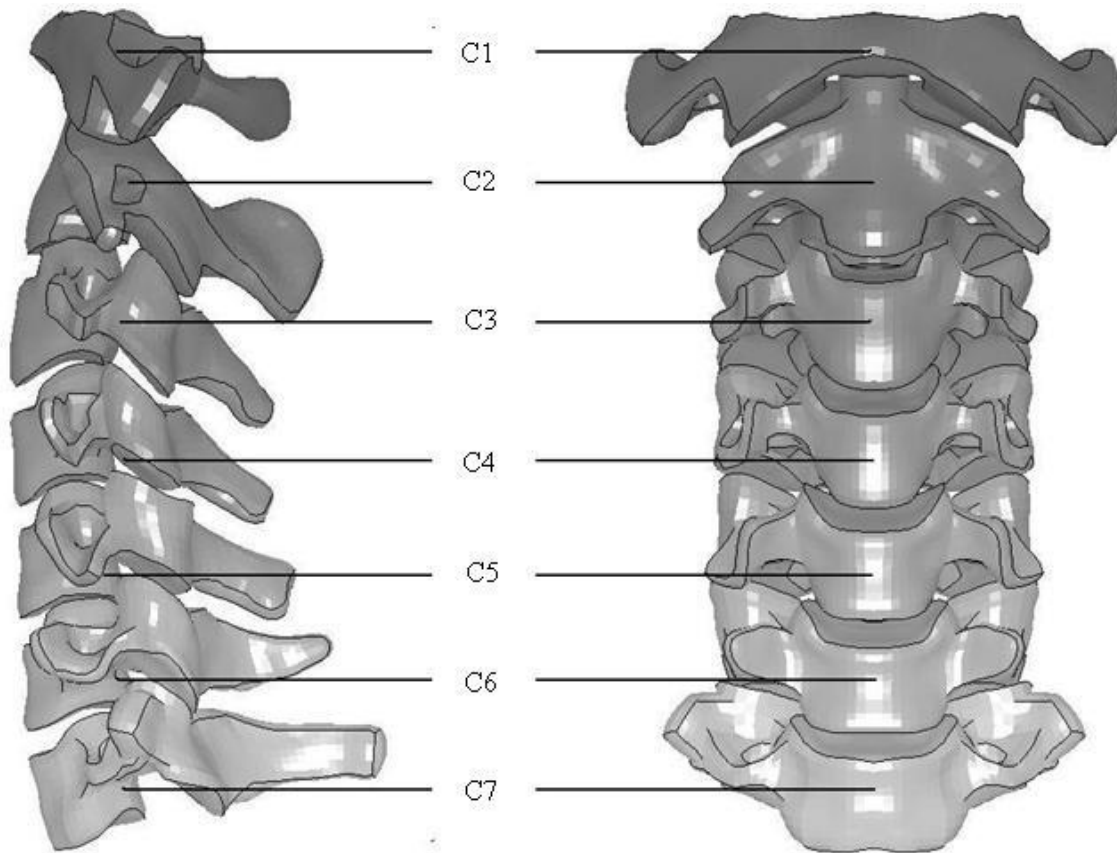
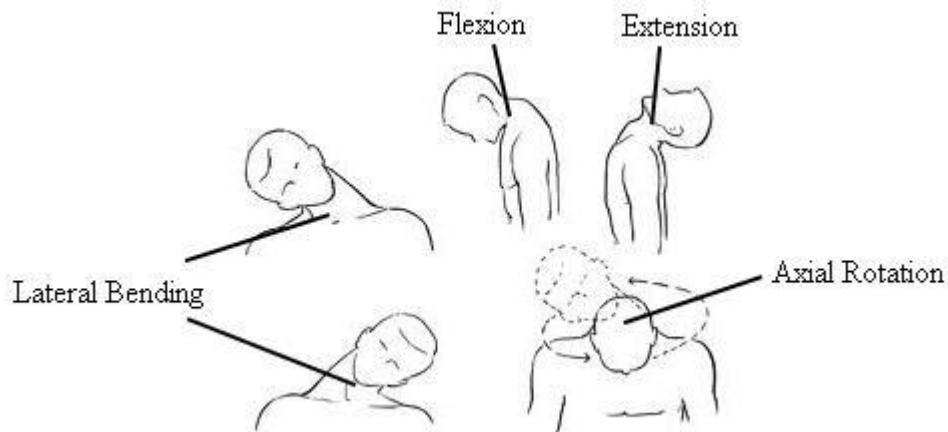


Figure 2-3: Cervical Spine

The cervical spine allows four types of movements: flexion, extension, lateral bending, and axial rotation (Figure 2-4). Flexion is referring to the head bending forward to look at the ground and extension is the action of bending the head backward to look up. Flexion and extension are both rotations about the axis normal to the sagittal plane. During frontal and rear impacts, the neck rotates in flexion and extension due to inertia of the head. Lateral bending is when the head rotates about the axis normal to the frontal plane and axial rotation describes the twisting motion of the head about the normal axis of the transverse plane.



(Adapted from www.drpaulose.com)

Figure 2-4: Cervical Spine Range of Motion

The first cervical spine vertebra, the axis or C1, is shaped like a ring (Figure 2-5). The occipital condyles at the base of the skull rest on top of the superior articular facets of C1 – all the weight of the head is passed on to the spine through this interface. The articular facets have a concave shape in the sagittal plane while the occipital condyles are convex. The concave-convex joint between the skull and C1 allows for a large range of motion in flexion and extension, but almost no axial rotation, lateral bending, or translation in any direction.

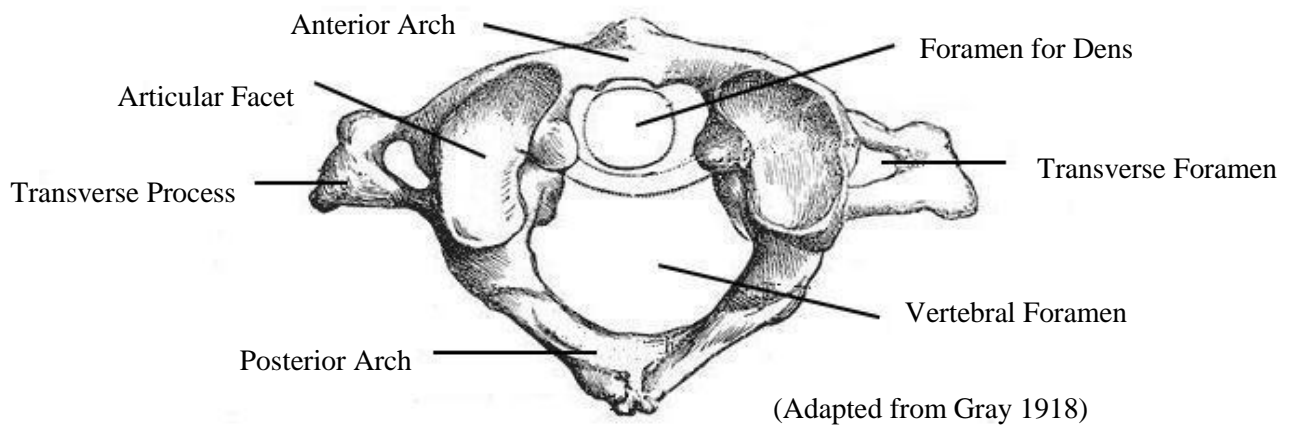


Figure 2-5: C1 – Axis, Superior View

The interior side of the anterior arch of the C1 is where the C1 contacts with the dens of C2 (Figure 2-6). The dens is pressed against the arch by the atlas' strong transverse ligament. The atlas can rotate about the dens, but it cannot bend in the sagittal or frontal plane and it cannot translate in any direction. When the head rotates, the majority of this rotation in the spine takes place at the atlas-axis joint.

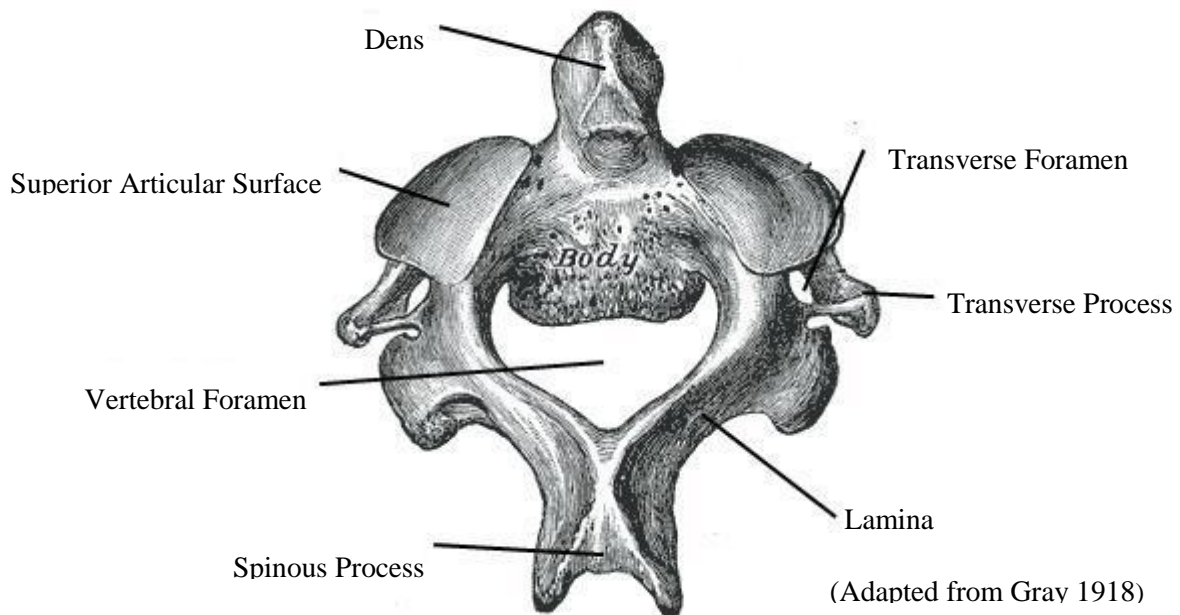


Figure 2-6: C2 – Atlas, Superior Posterior View

The C3 through C7 vertebrae have the same basic features (Figure 2-7). The vertebral body is the largest bony section of the vertebrae. The superficial surface of the vertebrae consists of cortical bone while the interior is made up of cancellous bone. Cartilaginous end plates are found on the superior and inferior surface of each vertebra. The end plate is only a few millimeter thick and its purpose is to feed nutrients to the intervertebral disc and to secure the disc to the vertebra. The pedicles protrude out of the vertebral body in the lateral and posterior direction while the transverse processes are attached to the anterior edge of the vertebral body. The transverse processes and the pedicles, located laterally from the vertebral body, form cavities called the transverse foramen. Blood vessels and nerves pass through the transverse foramen. At the end of the pedicles are the articular processes. The superior and inferior surfaces of the articular processes are sloped relative to the transverse plane. Adjacent articular processes are connected to one another via the facet joints. The spinous process is located at the posterior end of the vertebrae, and it is connected to the articular processes via the lamina (Moore et al. 1999).

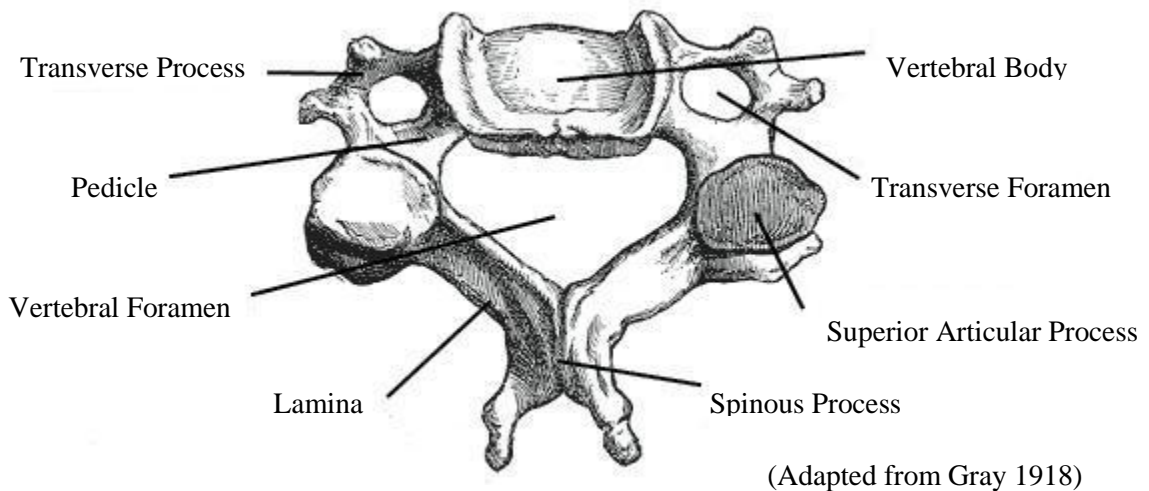
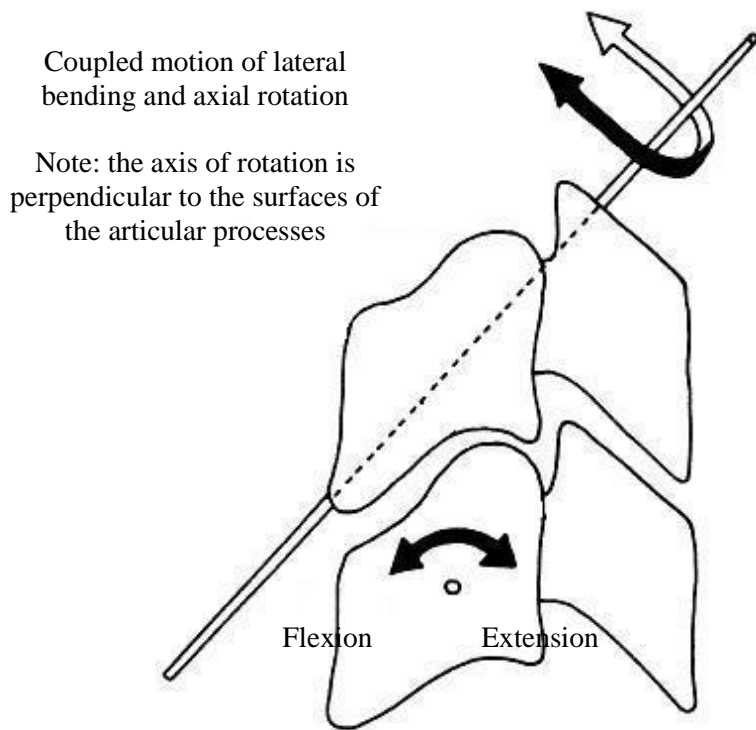


Figure 2-7: C5 Vertebra

The superior and inferior surfaces of the vertebral bodies are not flat and parallel to the transverse plane as they are elsewhere in the spine (Figure 2-8). The inferior surface is concave downwards in the sagittal plane (from front to back), and the superior surface is concave upwards in the transverse plane (side to side). When they are fitted together, the two surfaces form a “saddle” joint that permits a rocking motion in the sagittal plane (flexion and extension) and in a plane parallel to the surfaces of the articular processes (Bogduk et al. 2000). The rocking motion, or rotation, about the axis perpendicular to the plane of the surface of the articular processes can be resolved into components in the transverse plane (axial rotation) and in the frontal plane (lateral bending). Therefore, axial rotation and lateral bending are always coupled together in the cervical spine from C2 to T1.



(Adapted from Bogduk et al. 2000)

Figure 2-8: Mechanics of Flexion, Extension, Lateral Bending, and Axial Rotation

The soft tissues, along with the bony structure of the vertebrae, determine the range of motion of the spine. The soft tissues include the ligaments, the intervertebral discs, the tendons, and the muscles. The muscles (and the tendons that attach the muscles to the bone) were not considered in this thesis because their active tissues can not be tested in vitro. For the finite element segment models in this thesis, the muscles and tendon were omitted, but they were included in the full spine model.

Ligaments are referred to as uniaxial structures because they can only resist one type of load (tension) in one primary direction, which is dictated by the fibre orientation. The cervical spine ligaments serve three main functions. Firstly, the ligaments permit physiological motion between adjacent vertebrae and maintain the stability of the spine. Second, they protect the spinal cord by shielding the cord from any protrusions into the vertebral foramen. Lastly, they can absorb and dissipate energy during dynamic loading events (White et al. 1990). The ligament fibres are made up of two proteins: collagen and elastin. Collagen, which is more common, has a high tensile strength but is not as elastic as elastin. Elastin can stretch farther and its response is elastic; the stress strain loading and unloading curves are almost identical for this material.

There are six ligaments in the cervical spine: the anterior longitudinal ligament, the posterior longitudinal ligament, the ligamentum flavum, the interspinous ligament and the two capsular ligaments (Figure 2-9).

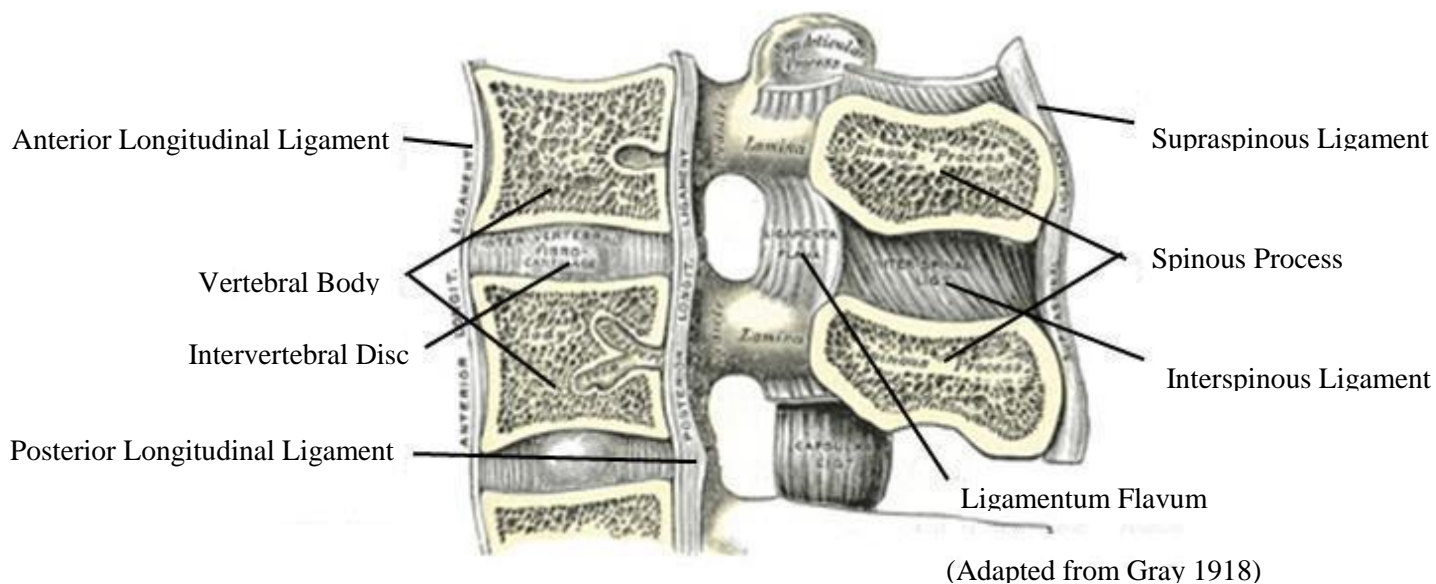
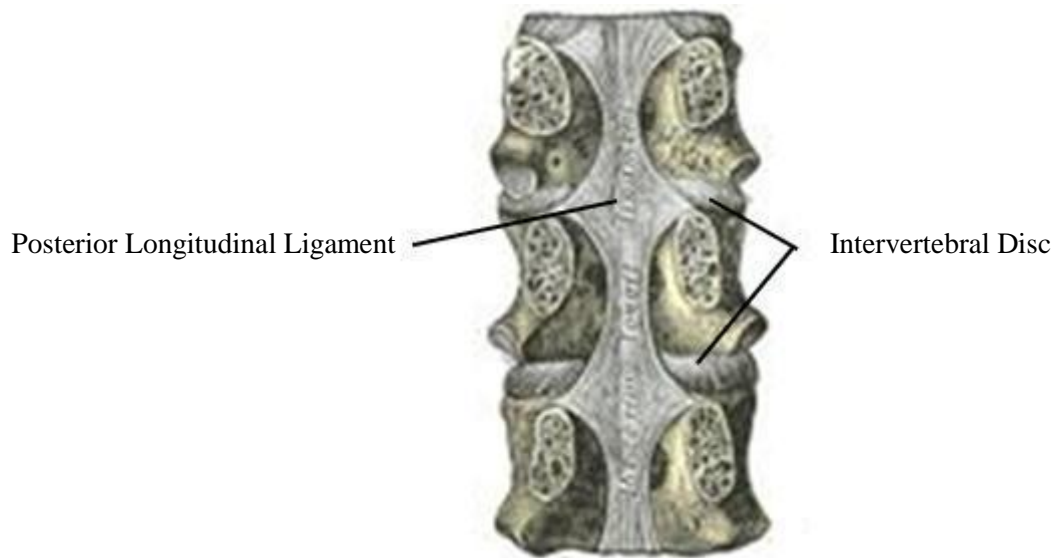


Figure 2-9: Cervical Spine Ligaments

The anterior longitudinal ligament (ALL) runs all the way down the anterior surface of every vertebral body along the spine from the axis to the sacrum. There are several layers of fibres that make up the ALL. The superficial fibres (visible fibres on the surface) are the longest and stretch for as many as four or five vertebrae. The intermediate fibres extend two or three vertebrae while the deep fibres only span one vertebral disc. The fibre ends are primarily attached at the intervertebral discs (Gray 1918), or at the superior and inferior ends of the vertebral bodies (White et al. 1990), but not at the middle. The ALL is thicker opposite the vertebra and thinner opposite the disc (Gray 1918), while the breadth of the ligament is fairly constant along the length of the cervical spine. The ALL prevents hyper-extension and translational motion.

The posterior longitudinal ligament (PLL) runs down the posterior side of the vertebral bodies from the transverse ligament in the C1-C2 joint down to the sacrum (Figure 2-10). It shields the spinal cord from any protrusions into the vertebral foramen by the intervertebral disc. The PLL is similar to the ALL in that they are both longitudinal ligaments spanning the length of the spine along the vertebral bodies. Both ligaments are more firmly attached to the disc than to the vertebral body, which allows for blood vessels to pass between the middle of the vertebral body surface and the ligament. However, there are significant differences. The fibres of the PLL are more densely packed than those in the ALL, and the width of the PLL is not constant (Gray 1918). The PLL is wider at the intervertebral disc, but narrows opposite of the vertebral body. The PLL is activated during flexion and resists translational motion.



(Adapted from Gray 1918)

Figure 2-10: Posterior Longitudinal Ligament

The ligamentum flavum (LF) connects the lamina of adjacent vertebrae and provides a barrier around the posterior side of the vertebral foramen (Figure 2-11). Unlike the longitudinal ligaments, the LF only extends from one vertebra to another, starting at the C2-C3 level. The LF is really two ligaments divided by the sagittal plane; each ligament starts at the root of the articular processes and ends at the point where the spinous process and lamina converge. The elastin to collagen ratio of the LF is between 2:1 (Nachemson et al. 1968) and 4:1 (Viejo-Fuertes et al. 1998), while all other cervical spine ligaments are composed primarily of collagen. The LF resists flexion.

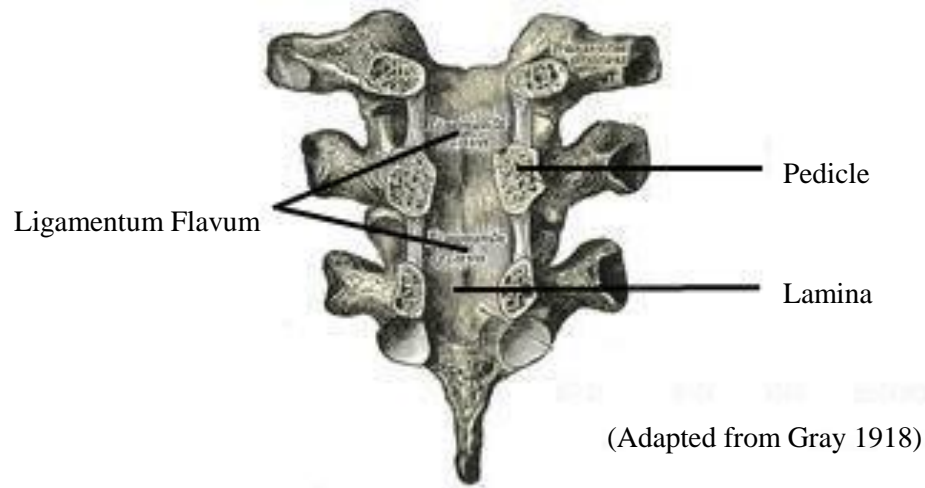


Figure 2-11: Ligamentum Flavum

The interspinous ligament attaches neighbouring spinous processes. The ligament is very narrow and the anterior edge is in contact with the ligamentum flavum while the posterior edge touches the supraspinous ligament. Since the ligament is so narrow in the cervical spine, it has very weak tensile properties. Even though it is not strong, the ligament does resist flexion due to its long moment arm from the center of rotation.

The capsular ligaments join the articular processes of two vertebrae and form a joint called the facet joint. The facet joints resist lateral bending and axial rotation and they are not in tension when the

spine is in flexion or extension, but they do limit the motion when the articular processes come into contact. The superior and inferior surfaces of the articular process are sloped at an angle relative to the transverse plane, and the fibre orientation is perpendicular to these surfaces (White 1990). Adjacent surfaces are usually at the same angle and therefore they are parallel to each other.

Each pair of vertebrae is separated by two facet joints that are located posterior and laterally relative to the intervertebral disc. The facet joint is a synovial joint: the bony surfaces of the articular processes that form the joint are covered by a thin layer of low friction articular cartilage to allow for sliding. The joint is lubricated by the synovial fluid, and the fluid is held inside the joint by the surrounding capsular ligament (Figure 2-12).

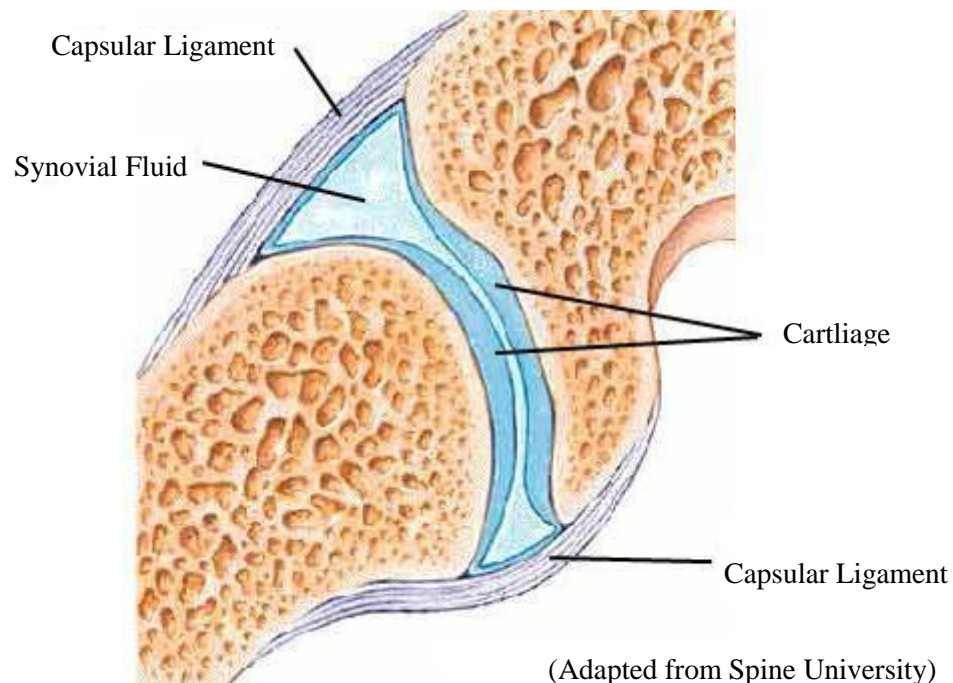
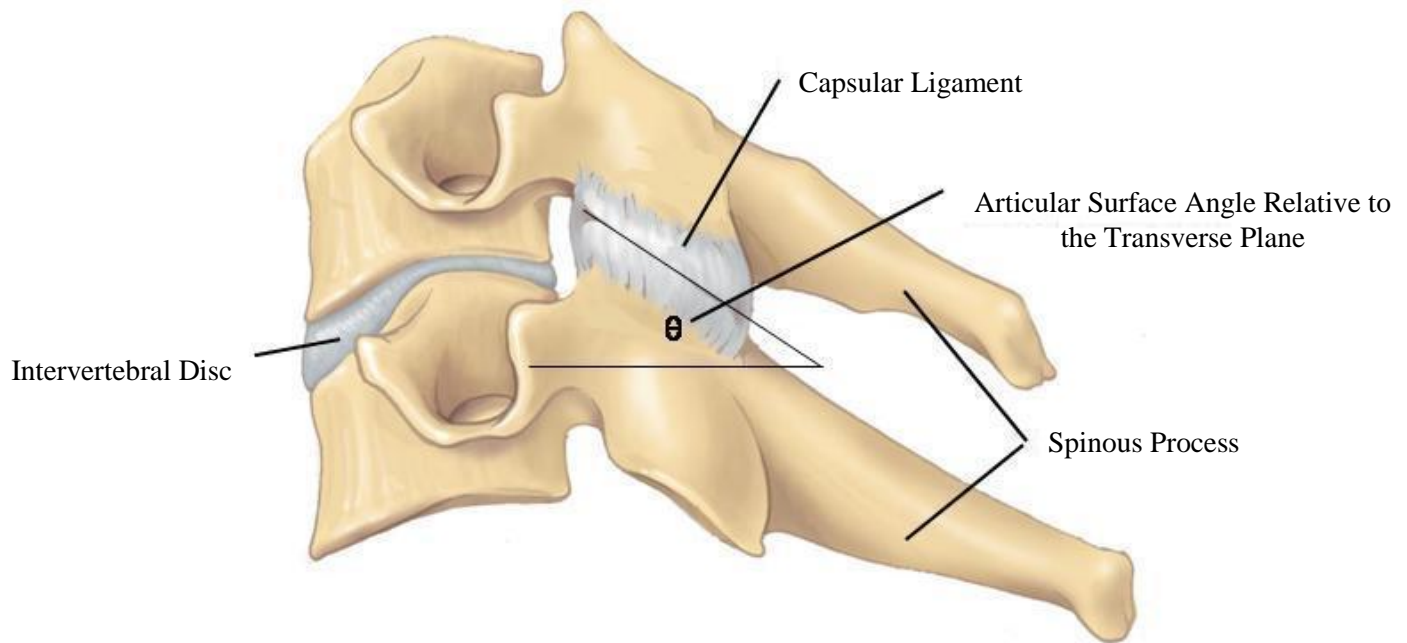


Figure 2-12: Facet Joint

The geometry of the facet joints limit relative vertebral movement in flexion and extension and couple the motions of lateral bending and axial rotation together. The surfaces are sloped at an angle relative to the transverse plane when viewed from the sagittal plane (Figure 2-13). The surfaces slope downwards from the anterior edge to the posterior edge and the angle varies depending on the spinal level. In flexion and extension, the articular surfaces glide over each, allowing for large range of motions while in lateral bending, the slope of the surfaces forces the vertebrae to rotate axially at the same time, producing a coupled motion. The degree of coupling and the range of motion are determined by the gap in the joint and the angle of the surfaces.

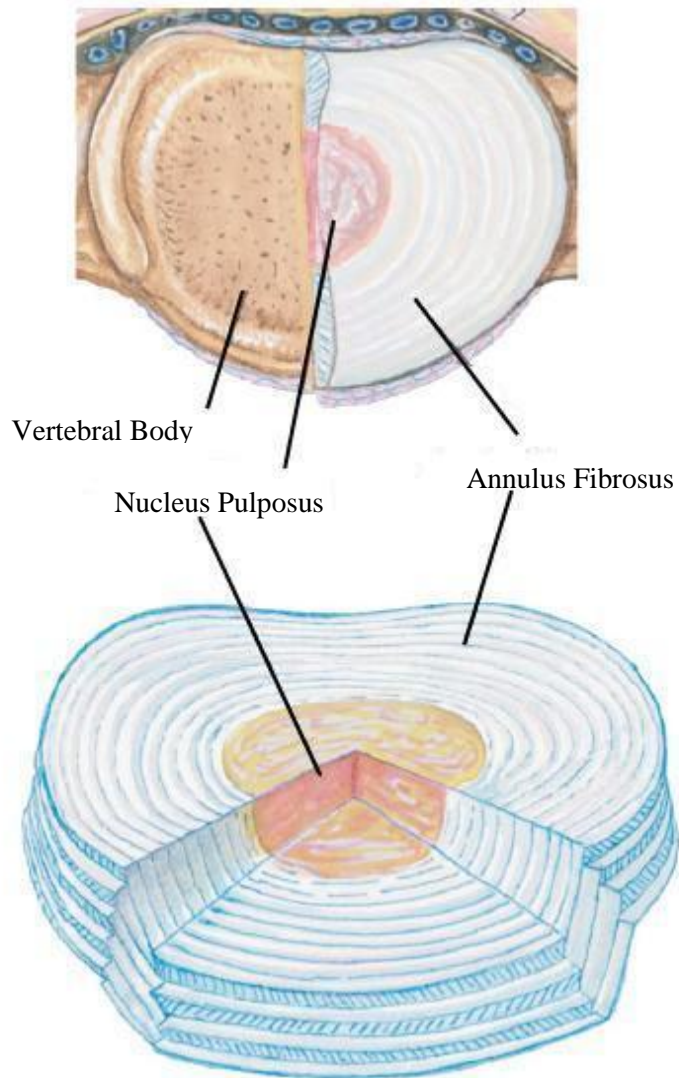


(Adapted from Spine Universe)

Figure 2-13: Facet Joint Angle

The intervertebral disc is a deformable soft tissue located in between adjacent vertebral bodies. The plane of the disc is parallel to the transverse plane. The disc consists of a fluid interior, called the nucleus pulposus, and it is contained by layers of fibres called the annulus fibrosus (Figure 2-14). During compression, the nucleus pulposus tries to relieve pressure by flowing outwards. This radial expansion is resisted by the annulus fibrosus as the fibres around the circumference are put under tension.

The annulus fibrosus consists of layers, or lamellae, of fibres laminated together to form a composite structure. Each lamella is a composite structure with several collagen fibres oriented in the same direction surrounded by a ground matrix substance. The purpose of the disc is to transmit compressive loads through the spine into the fibres. The axial stresses in the transverse plane are transmitted into radial and circumferential tensile stresses in the lamellae of the annulus fibrosus. The ability of the annulus fibrosus to transmit load is dependent on the mechanical properties of the individual collagen fibres, and the geometry of the lamellae.

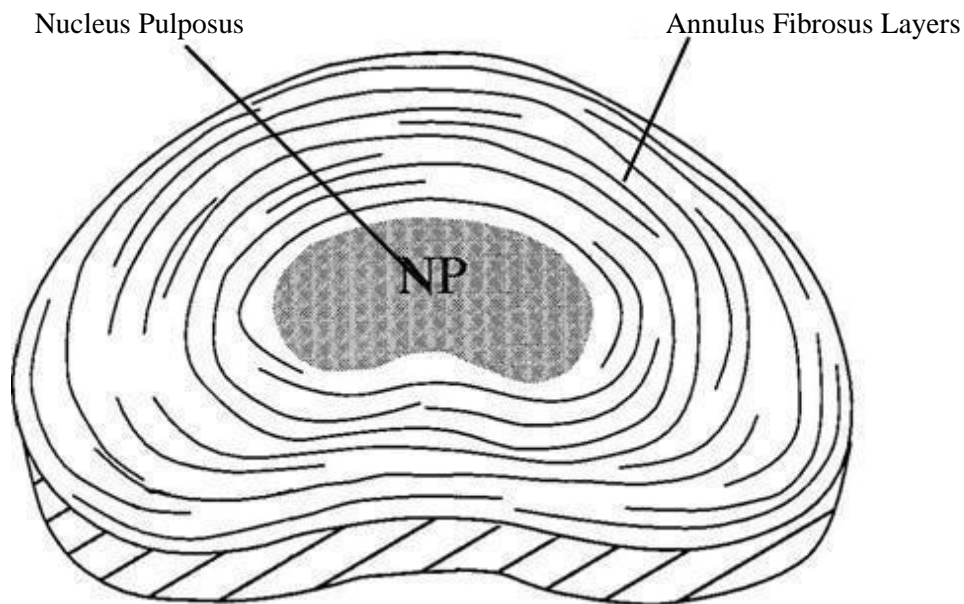


(Adapted from Caner et al. 2007)

Figure 2-14: Intervertebral Disc

Researchers have discovered that the geometry of the annulus fibrosus consists of numerous layers. The number of lamella in the annulus fibrosus varies with age, and circumferential position and they are not continuous and distinct from each other around the entire circumference (Figure 2-15). For young discs (< 30 years old), there are between 15 and 25 distinct and continuous lamellae, but there

are another 40 lamellae that are not complete or entirely separate from adjacent lamellae (Marchand et al. 1990).



(Adapted from Elliot et al. 2000)

Figure 2-15: Annulus Fibrosus Layers

The fibre orientation of adjacent lamellae is never the same; the angle of the fibre orientation relative to the axis of the transverse plane alternates from positive to negative for consecutive lamellae (Figure 2-16). The absolute value of this angle varies with radial position. At the outer edge of the disc, this angle has been found to be about 60 degrees, but towards the center of the disc, the angle changes to only 45 degrees (Cassidy et al. 1989). So, for example, the outermost lamella might have a fibre angle of +60 degrees, the next lamella will have an angle of -60, and moving towards the center, the angle will gradually drop towards 45.

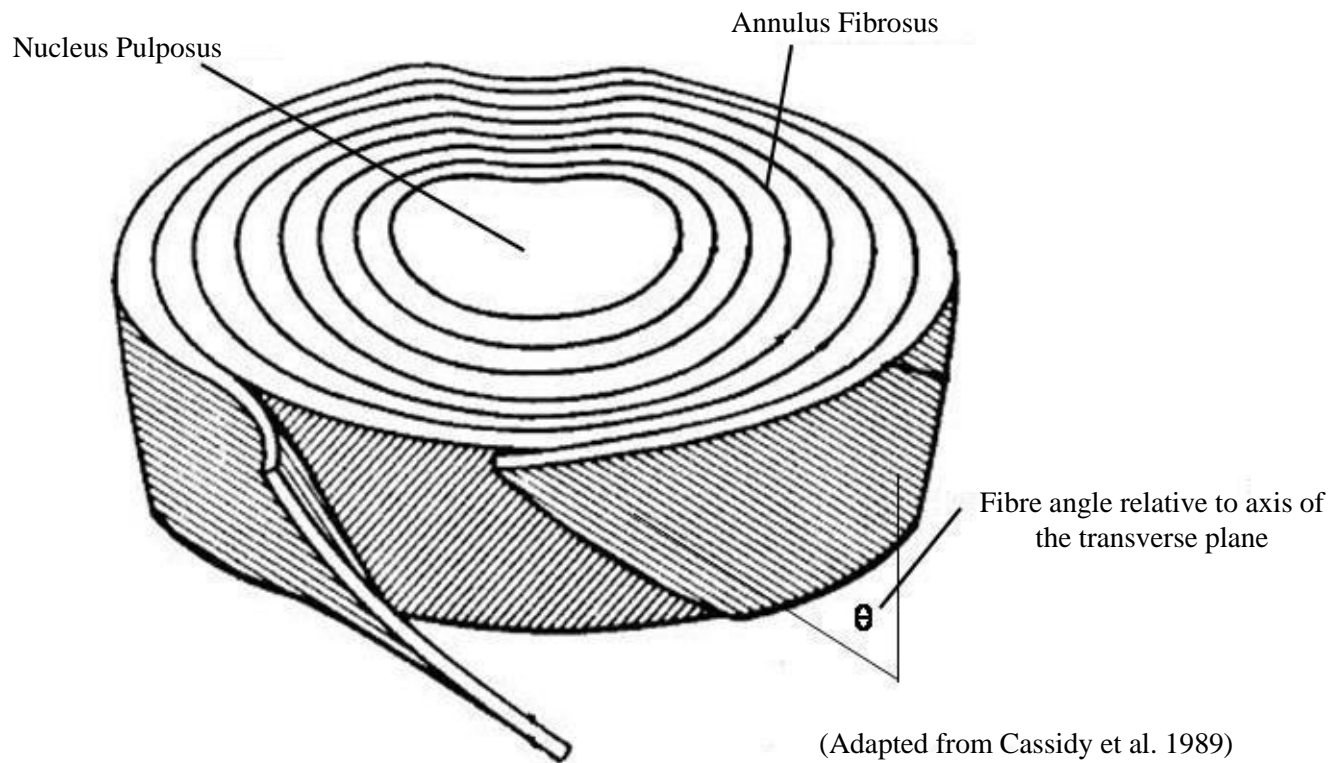


Figure 2-16: The Angle of the Annulus Fibrosus

Lamella thickness also varies with respect to radial position. Lamellae at the edge of the disc are thinner (130 μm) than those closer to the nucleus (200 μm). However, the border between the annulus fibrosus and nucleus is gradual instead of distinct and sudden. Another interesting feature of the annulus fibrosus is the fibres are crimped instead of being straight. Under a no-load condition, it appears as though the fibres have been compressed slightly and they have a wavy appearance. When a small compressive load is applied to the disc, the tensile stress in the fibres stays at zero because the initial strain causes the fibres to straighten out before carrying any load (Cassidy et al. 1989, Pezowicz et al. 2005).

In flexion, the anterior portion of the disc is put under compression. The range of motion in flexion is limited by the resistance of the disc to compression, the initial thickness of the disc, the structure of the vertebral body, and the tensile strength of the PLL, LF, and ISL. At some point, the vertebrae can not be rotated in flexion anymore without rupturing the disc, tearing a ligament, or fracturing the vertebral endplate or the vertebra itself. If the disc is thicker, then there is more room for rotation. In extension, the posterior edge of the disc is in compression and the adjacent spinous processes rotate towards each other. The spinous processes eventually come into contact and prevent further rotation unless one of the spinous processes is fractured. Extension is also limited by the tensile strength of the ALL, and the compressive strength of the intervertebral disc.

Chapter 3

Literature Review

3.1 Experimental Testing

Numerous studies have been performed to establish the moment-rotation properties of the cervical spine in all four modes of loading: flexion, extension, lateral bending and axial rotation. However the majority of the research was focused on flexion and extension at quasi-static loading rates. In vitro testing has been done using three different equipment arrangements. The three apparatuses attached the inferior vertebra of a whole spine or segment to a load cell, and applied the load to the superior vertebrae. The difference in the equipment setup was the way the moment was applied to the superior vertebrae. The first apparatus was called a pure moment device. Pure moment devices do as their name says: apply a pure moment to the free vertebra without any shear or normal forces (Figure 3-1). The moment was usually applied by a system of weights and pulleys. The second equipment setup, called a lever arm apparatus, attached one end of a flat bar to the superior vertebrae and applied a downwards force at the other end of the bar to induce rotation through a lever action (Figure 3-2). The downwards force was applied by a pneumatic piston cylinder. The third setup, called a fixed axis device, used a servomotor to rotate the superior vertebra about the inferior vertebra. The superior vertebra cannot translate in any direction. It can only rotate about the axis of the servomotor (Figure 3-3).

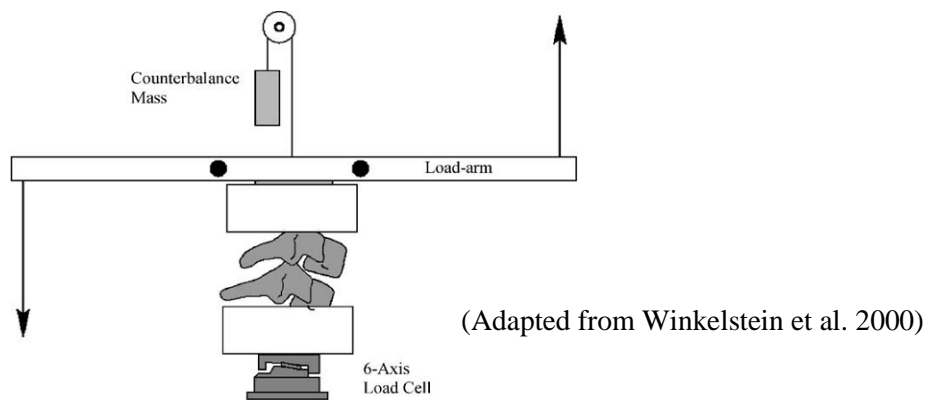


Figure 3-1: Flexion Extension Apparatus

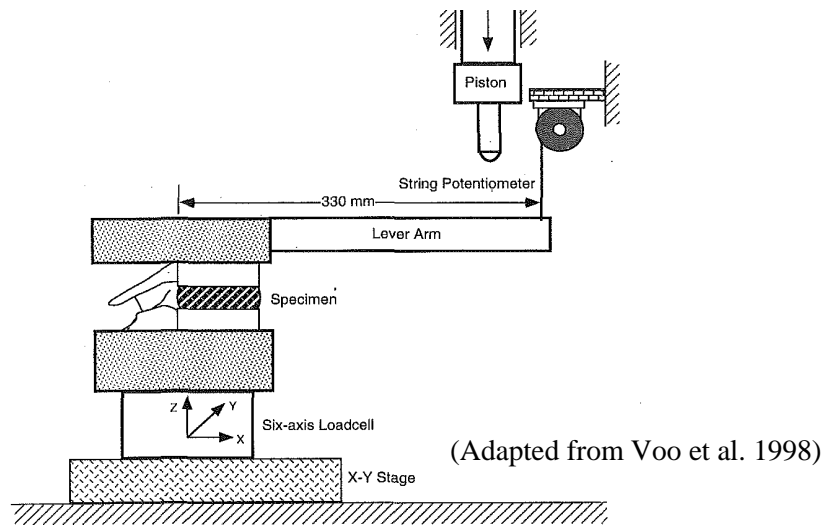


Figure 3-2: Flexion Apparatus

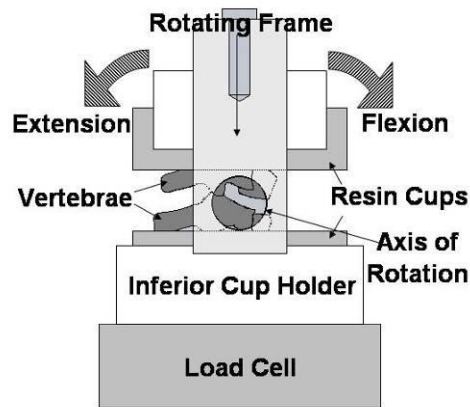


Figure 3-3: Fixed Axis of Rotation Machine

The type of machine used for testing can influence the results. It is important to determine the loading condition of the machine in order to interpret the results and understand their limitations. The pure moment apparatus is preferred by those who want to eliminate all normal and shear forces and focus solely on the response of the specimen to the pure moment. However, a compressive or tensile preload can be applied to the segment, and the magnitude of the preload can change the results. Cripton et al. (2000) published a study analyzing how the preload affects the moment recorded by the load cell attached to the fixed vertebra. The study compared the applied forces and moments with those recorded by the load cell and stated that the differences are called “artefact”

forces and moments produced by the setup. It was reported that there is a tradeoff between artifact forces and moment; there will always be one or the other present. The preload condition determines if there is primarily an artifact moment and little artifact force or vice versa.

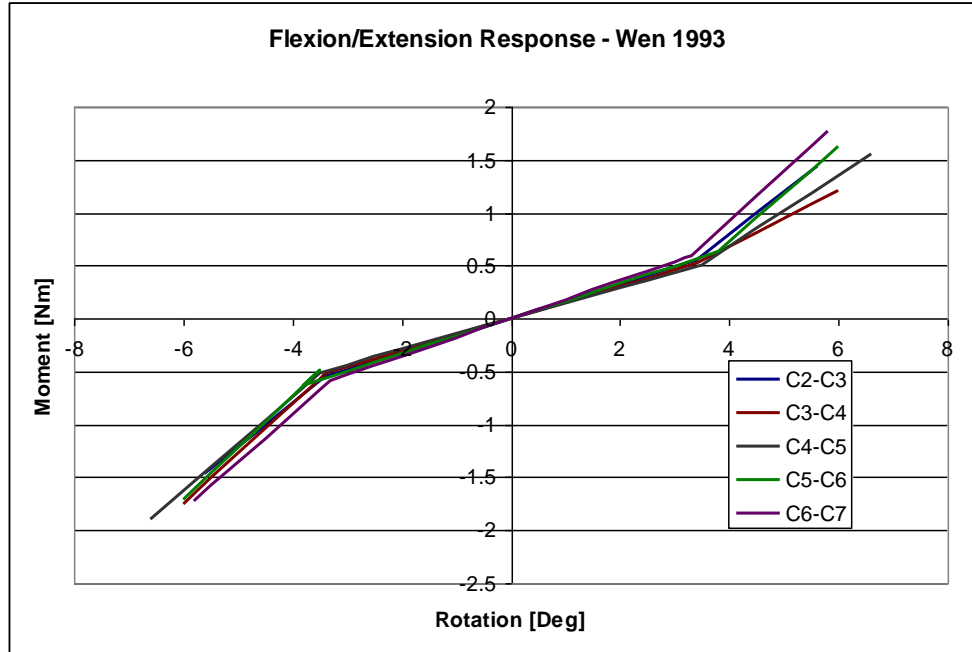
The fixed axis and lever arm machines could not produce a pure moment. For these apparatuses, the displacement was the independent variable and the moment was then measured by a load cell. This switch of dependent and independent variables was advantageous for researchers looking to vary the rate of loading. It was very difficult to vary the moment at a high rate because it required the load cell to feedback the current load. If the feedback signal was filtered, then the signal would have been delayed, and if it was not filtered, the signal can be oscillatory and this could result in an unstable system. The displacement feedback, measured by an encoder, was smooth and instantaneous and the rotation rate was easily manipulated.

The viscoelastic nature of human tissue presented another variable for researchers to consider: creep or stress relaxation time. Some flexion/extension studies applied the moment in a stepwise manner and held the load at each step, while other studies employed a continuous loading procedure. Goertzen et al. (2004) studied the difference between the step and continuous loading procedure and came to the plausible conclusion that segments tested with the stepwise loading procedure appear to have more flexibility than those segments tested with a continuous load. For load-controlled testing, the load at each step was held and creep occurs. The rotation increased over time, so the flexibility of the segment (quotient of rotation and moment) increased too. For displacement-controlled tests, the displacement was held constant, the moment decreased with time, and the flexibility increased with time.

3.2 Flexion and Extension Studies

Moroney et al. (1988) was one of the first studies to analyze cervical spine segments. Anthropometric data was not available for the 16 spines tested. The spines were sectioned into 35 segments; some of the segments were completely intact while others had the facet joints and the posterior arches removed. The testing apparatus applied a pure moment to the segment. The inferior vertebra in the segment was fixed while the superior vertebra was allowed to translate and rotate in any direction no matter the type of loading. The loads were applied by a system of pulleys and the displacement in all six axes was measured by a system of mechanical gauges. This study researched the segment response to all forms of loading: compression, shear, lateral bending, flexion, extension and axial rotation. The rotation at 1.8Nm moment was reported along with the mean stiffness.

Wen et al. (1993) tested 56 segments from 29 human donor spines with an average age of 66. The segments, ranging from C2-C3 to C6-C7 were tested in flexion, lateral bending and axial rotation with a pure moment applied by a system of cables. Each segment was loaded and unloaded in small increments up to a maximum moment of 1.5 Nm or 4.5 Nm depending on the test and the segment. The load, unload cycle was repeated three times and the third test was the only one recorded and each load increment was held for 15 seconds before the displacement was measured. They described the moment-rotation curve as two separate regions: a neutral zone of low stiffness, and an elastic zone, where the stiffness increases and it is close to linear (Figure 3-4). The response of the C4-C5 segment in flexion and extension was plotted, showing high variability amongst the different spines, but no curve fits were published to compare with other data. Instead, the end point of the neutral zone and the secant stiffness was reported. The neutral zone and elastic stiffness was very similar for all segment levels.



(Adapted from Wen et al. 1993)

Figure 3-4: Flexion/Extension Results

Camacho et al. (1997) used a pure moment machine to test 10 whole cervical spines. The donor age ranged from 53 to 80 (mean 66, standard deviation 8.2). The spine was placed upside down so the head was fixed to a six axis load cell and the moment was applied to the T2. Optical markers placed on each vertebra measured the relative rotation. No preconditioning procedure was reported. The spines were tested in flexion and extension up to 1.5 Nm in 0.1 Nm steps and the specimens were allowed to creep 50 seconds before the cameras recorded the position (Figure 3-5). On the x-axis of Figure 3-5 the moment is plotted, and the measured rotation is plotted on the y-axis. The positive moment-rotation indicates flexion, while negative values represent extension

Nightingale et al. (2002 and 2007) conducted an extensive study of the cervical spine in flexion and extension. The 2002 study used female spines only and the 2007 paper discussed the response of male spines. Segments were preconditioned for 30 cycles up to 1.5Nm. The studies used a pure-moment apparatus to apply moments in 0.5 Nm steps up to 3.5 Nm while recording the rotation. The load was held for 30 seconds at each step. The segments were tested to failure after 3.5Nm at a rate of 90 Nm/s, split almost evenly between flexion and extension. The 2002 study tested 16 segments at the C0-C2 level, 11 at the C3-C4 level, 10 at the C5-C6 level, and 10 at the C7-T1 level, and reported

the rotation-moment relationship (Figure 3-5). The donor age ranged from 33 to 66 years, with a mean of 51, and a standard deviation of 8.8. The 2007 study tested 16 male segments at the C0-C2 level, 13 at the C4-C5 level and 12 at the C6-C7 level. The donor age ranged from 51 to 74 years, with a mean of 66, and a standard deviation of 7.2. The study published the average rotation-moment curves for each segment levels (Figure 3-5).

Wheeldon et al. (2006) tested seven spines aged 20-51 (mean age of 33.4 and standard deviation of 11.7). The spines were tested completely intact (C2-T1) and a moment was applied to the entire spine to the C2 while the T1 was fixed to a load cell. Markers were placed on each vertebra to measure deflection and rotation. This study only went up to moments of 2 Nm in 0.5 Nm increments (Figure 3-5). The study did not specify if the segments were allowed to creep before the position was measured.

For the Camacho, Nightingale and Wheeldon studies, the moment-angular displacement data was fitted with a nonlinear, natural logarithmic function where θ is the angular displacement, M is the moment, and A and B are the fitting constants (Figure 3-5).

$$\theta = A \times \ln(BM + 1)$$

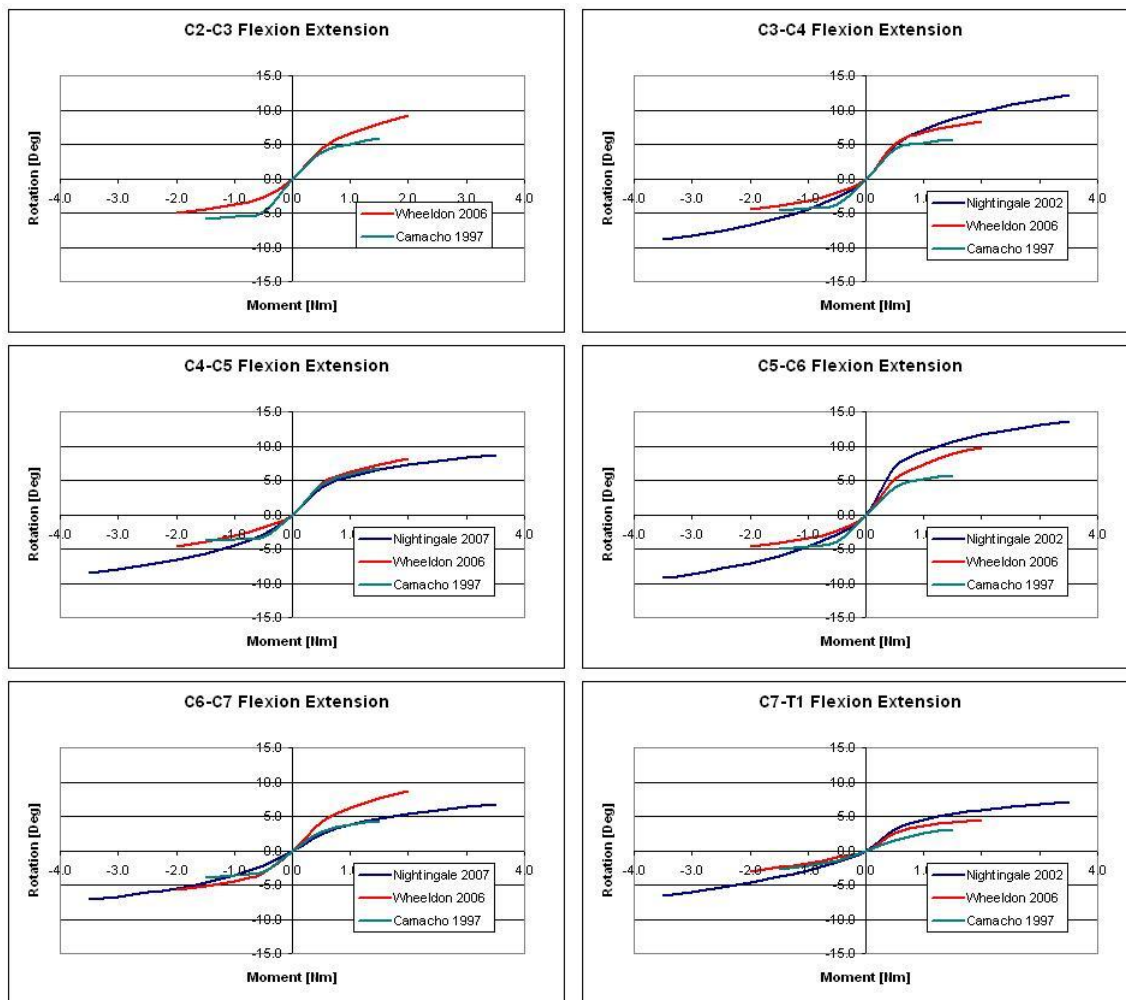


Figure 3-5: Flexion/Extension Results - Camacho et al. 1997, Nightingale et al. 2002, 2007, Wheeldon et al. 2006

Panjabi et al (2001) built a pure moment apparatus to tests 16 whole spines (one C0-C5, five C0-C6, two C0-C7, and eight C2-C7) +/- 1.0 Nm in 0.33 Nm increments. The age of the spine donors was not reported. The spines were tested in flexion, extension, lateral bending and axial rotation, and the displacements and rotations were measured by attaching optical markers to each vertebra. The objective of this study was to find the range of motion of each segment. Range of motion is a subjective term because it can be defined in different ways; *in vivo* it can be defined as the maximum rotation in a certain mode of loading while *in vitro* testing, it can be defined as the motion recorded

under an arbitrary load or moment. In this study, the range of motion was measured as the rotation of the spine under the 1.0 Nm load (Table 3-1).

Table 3-1: Flexion/Extension Range of Motion - Panjabi et al. 2001

	C2-C3		C3-C4		C4-C5		C5-C6		C6-C7	
	Mean	St.Dev								
Flexion [deg]	3.5	1.3	4.3	2.9	5.3	3.0	5.5	2.6	3.7	2.1
Extension [deg]	2.7	1.0	3.4	2.1	4.8	1.9	4.4	2.8	3.4	1.9

Panjabi et al. (2005) tested the spine's response to whiplash. A sled apparatus was built to simulate the conditions of a 3.5g, 5g, 6.5g, and 8g impact. The rotation of each vertebra was measured to determine the range of motion during the impact event. The data from this study compares the impact g-force with the rotation instead of moment-rotation.

Voo et al. (1998) was the only study that has compared the static and dynamic responses. The study used a lever arm to apply a rotation to the superior segment while the inferior segment was fixed to a load cell. The lever arm was 33 cm arm long from the center of the segment to the point of loading. The loading was applied by a vertically positioned piston cylinder with a maximum velocity of 500 cm/s. The moment-rotation relationship was recorded. The study only tested C4-C5 segments (five specimens aged 62 to 84) in flexion. The static test was repeated three times, and at no point did the load exceed 6 Nm. The dynamic test was then performed up to failure. The static rotation rate was 3.2 deg/s and the dynamic rate was between 1000 and 2000 deg/s. The dynamic rate was not constant because while the piston velocity could be constant in the vertical direction, the moment arm length increased as it rotated. The static and dynamic response compared the slope of tangent lines applied to the two moment-rotation curves. The tangent lines were arbitrarily applied at a rotation of 15 degrees. The study found that the stiffness increased from 1.03 to 1.50 Nm/deg due to dynamic effects and the maximum rotation went from 14.0 to 29.3 degrees.

3.3 Cervical Spine Range of Motion

Several studies have tried to establish the range of motion of the entire cervical spine. The in vivo range of motion can be measured passively or actively. The active range of motion is measured by requiring a volunteer to flex or extend their neck as far as possible, while in passive measurements, another person rotates the neck of the volunteer as far as possible in flexion and extension without any attempted resistance from the volunteer and without causing pain. The range of motion of extension and flexion for each segment level was reported as one combined number for all studies. Dvorak et al. (1988) compared the two methods for young male subjects and found that the passive range of motion was higher than the active range of motion. Dvorak et al. (1991) analyzed the difference between the passive range of motion of males and females and reported that females have slightly more neck mobility. Both studies reported the range of motion from the C1-C2 to the C6-C7 segment level (Table 3-2).

Table 3-2: Cervical Spine Segment Range of Motion in Degrees - Dvorak et al. 1991

	C2-C3	C3-C4	C4-C5	C5-C6	C6-C7
Active – Male [deg]	10	15	19	20	19
Passive – Male [deg]	12	17	21	23	21
Passive – Female [deg]	12	18	22	24	22

3.4 Biological Tissues in the Cervical Spine

The response of cervical spine segments is dependent on the mechanical properties of the biological tissues. There are two types of tissues: soft tissues, which include ligaments and the intervertebral discs, and hard tissues like the entire skeletal system, including the vertebrae. The shape of the vertebrae determines the types of motion permitted, such as flexion and extension and the coupled motion of lateral bending and axial rotation. The ligaments and the intervertebral discs are attached to the vertebrae. These soft tissues dictate the moment-rotation response. If the ligaments or the discs are injured, the cervical spine's ability to support the head is weakened.

3.4.1 Collagen

Collagen is a major building block of almost all of the biological tissues, and it is the most abundant protein found in the human body. Collagen molecules join and wrap around each to form fibrils, and these fibrils connect with each other to form collagen fibres. The alignment and the density of the collagen fibres determine the mechanical properties of the tissue, hard or soft (Fung 1993). Densely packed aligned fibres form cortical bone, and loosely packed fibres form fascicles which in turn create tendons and ligaments.

Collagen is a biological material that exhibits time dependent mechanical behaviour. Materials, like collagen, with time dependent properties are described as viscoelastic. One of the most important viscoelastic properties is the variation of the stress strain response due to strain rate. The stiffness is defined as the instantaneous slope of the stress strain curve, and the stiffness increases with increasing strain rate (Figure 3-6). The dependence of stress strain response on strain rate is not unique to viscoelastic materials; non-viscoelastic materials such as steel also exhibit strengthening with higher strain rate. The purpose of this thesis is to discover if this stiffening property seen in individual tissues is also applicable to a system like a cervical spine segment in flexion or extension.

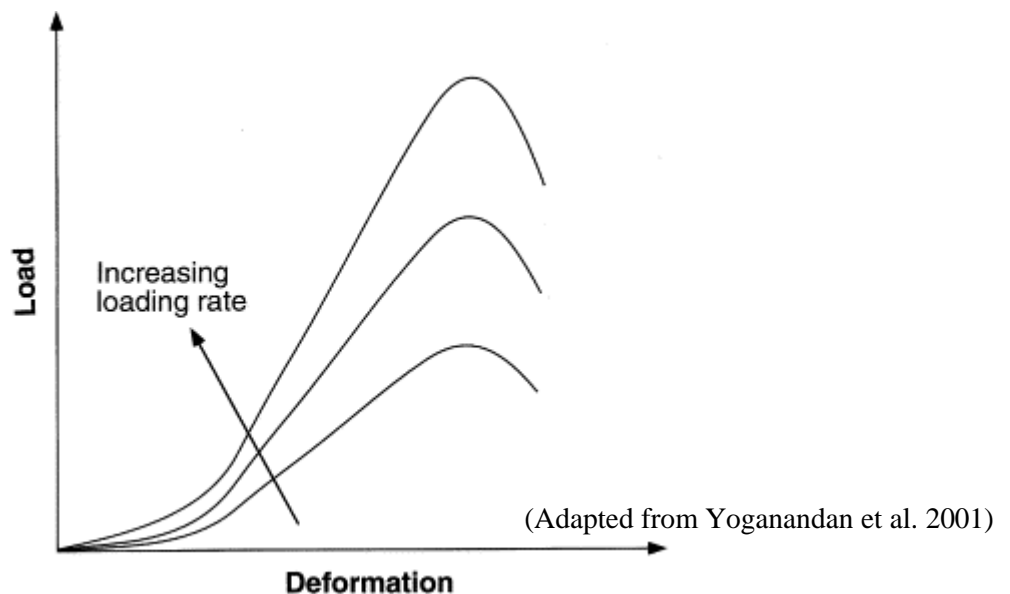


Figure 3-6: Strain Rate Sensitivity of Collagen

Three other important viscoelastic properties are hysteresis, creep, and stress relaxation. Hysteresis is defined as energy dissipation in the form of heat and it can be measured by the difference in the area under the loading and unloading curves on a stress strain plot. Hysteresis in collagen tissues like ligaments is caused by fibres bundles untangling and by individual fibre micro tears in the ligament that weaken the structure when it is unloaded. Elastin is a similar protein to collagen, except that it can stretch further and its loading and unloading cycle is almost perfectly elastic, meaning it does not exhibit hysteresis.

When a soft tissue is stretched and held at a certain strain, the initial stress will gradually decrease until it reaches steady state in a phenomenon called stress relaxation. Creep is similar to stress relaxation except instead of holding the strain constant, the stress is held constant. In creep, the strain will increase with constant stress until it reaches a steady state.

3.4.2 Bone

The human vertebrae comprises of two types of bone. Cortical bone is very hard and dense and it usually forms a shell around the exterior of all the bones in the body. Trabecular, or cancellous bone, is softer and more porous than cortical, but it can absorb more energy due to its higher failure strain. Bone tissue is comprised of collagen, minerals (primarily calcium), and water (Wainwright et al. 1976). On a macroscopic level, the strength of bone is influenced mainly by porosity, bone mineral density, and the direction of loading. However, the structure of bone can be broken down to the microscopic level. The primary building block of bone is collagen fibrils, which are short fibres surrounded by minerals. Thin sheets of aligned collagen fibrils stacked on top of each other form lamella, while randomly oriented fibrils create woven bone. Lamellar bone is much more common than woven bone, and an osteon is the most common structure formed by lamellar bone (Bartel et al. 2006). An osteon consists of several lamellae with varying orientations wrapped into a cylindrical shape with a hollow center, called the Haversian canal, which contains nerves and blood vessels (Figure 3-7). Osteons are the building block of cortical bone.

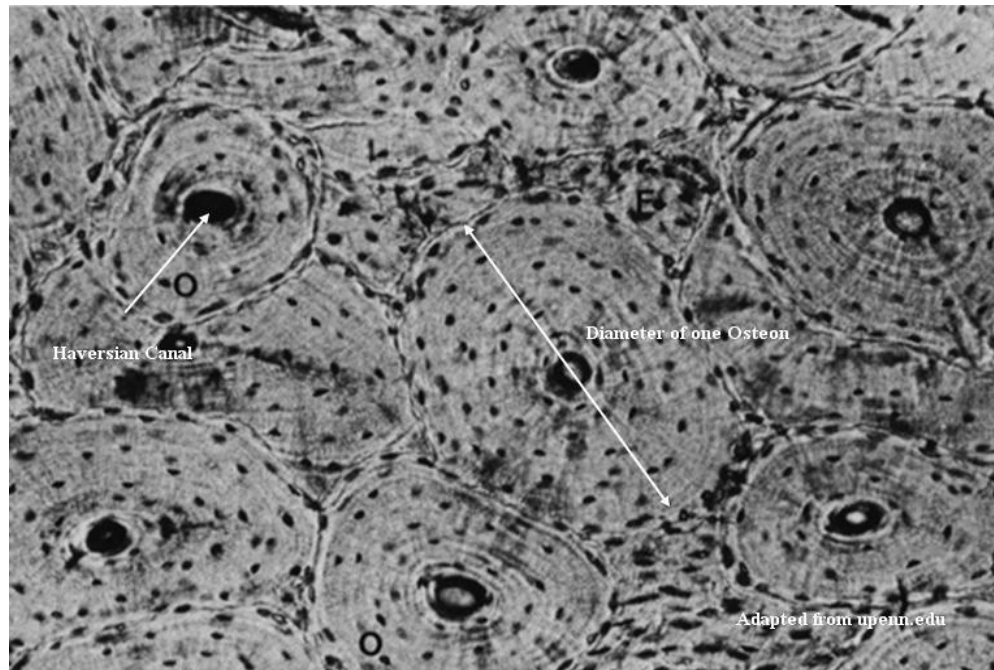


Figure 3-7: Osteons and the Haversian Canal

In trabecular bone, there are no osteons, the lamellae are not aligned with one another, and the resulting structure is a non-uniform matrix with high porosity. Cortical bone has a density in the range of 1.7 to 2.0 g/cm³, and trabecular bone density is between 0.1 and 0.3 g/cm³ (Cowin 1988). Trabecular bone can remodel much faster than cortical bone, allowing it to model itself to transmit load efficiently.

The mechanical properties of bone, such as elastic modulus and failure stress, vary greatly from one person to another and from one location to another. There is a strong negative correlation between age and failure stress, but there is no correlation between age and elastic modulus (McCalden et al. 1993). The same study also showed a negative correlation between bone density and age, but no link between bone mineral density and age. The correlation with stress, but not modulus indicated that the geometry varied with age and the mechanical properties do not. Researchers have found it easier to measure the properties of cortical bone instead of trabecular bone since its density remains relatively constant with age. Some studies have hypothesized that the strength of bone can be derived from its porosity and the properties of cortical bone since the elastic modulus of the bone material is

the same (Pugh et al. 1973, Townsend et al. 1975). However, this theory has been disputed by studies showing evidence that cortical bone is stronger than trabecular bone (Williams et al. 1982).

Due to the alignment of the osteons, cortical bone is anisotropic. Instead, studies have reported mechanical properties for the longitudinal axis (the long axis of the bone) and the transverse axis. There are two principle directions in the transverse plane, but the properties are close to identical in both, meaning that cortical bone is a transverse isotropic material. Several studies have reported the elastic modulus (Evans et al. 1976, Reilly et al. 1975, Yoon et al. 1984, Ashman et al. 1984), and the tensile and compressive strength (Evans et al. 1976, Reilly et al. 1975, Cezayirlioglu et al. 1985) of femoral or tibial cortical bone in the longitudinal and transverse directions.

Within the past decade, advancements have been made in modeling trabecular bone using geometry from CT and MRI scans with the goal of determining material properties and failure mechanisms. Morgan et al. (2003) concluded that the compressive modulus of trabecular is dependent on bone density and the location of the bone sample. Holding density constant, tibial bone was stronger than bone from the vertebrae and the femoral head. Fields et al. (2011) analyzed the microstructure of trabecular bone and the loading paths in compression. In the microstructure of trabecular bone, there are columns of solid bone that can be aligned in any direction. Fields et al. (2011) discovered that the density of columns aligned in the direction of loading had a higher correlation with strength than overall bone density measurements. The microstructure determines the strength and elastic properties, and the microstructure is highly variable.

While all the previous bone studies mentioned have dealt with static properties, McElhaney et al. (1966) found that the mechanical properties of bone are rate sensitive. As strain-rate increases, so does the elastic modulus and the failure strength of bone (Figure 3-8).

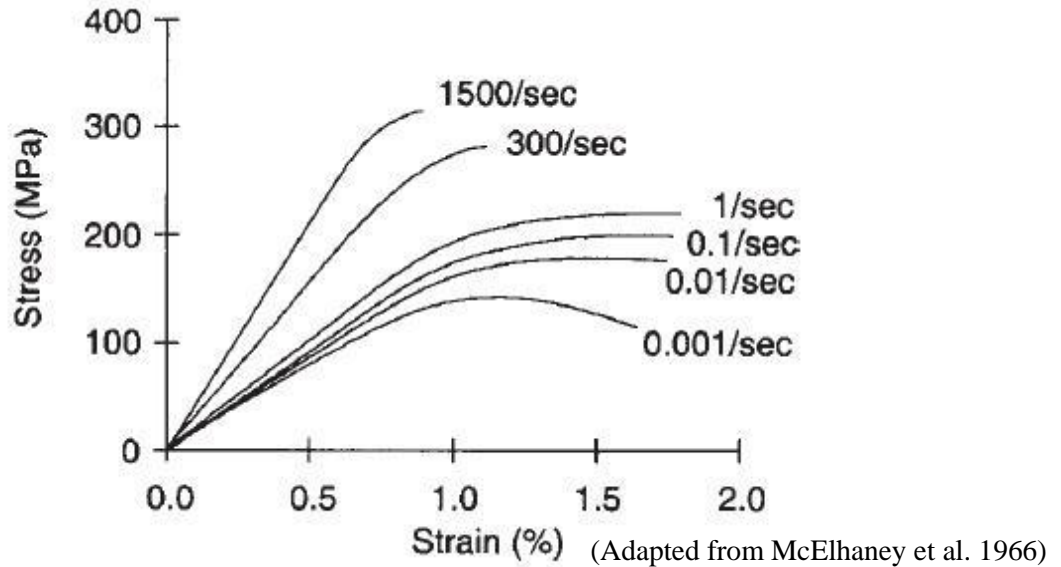


Figure 3-8: Strain Rate Sensitivity of Bone

3.4.3 Intervertebral Discs

During flexion and extension, the disc is put under a classical bending load. One side of the disc is under compression and the other side is in tension. Several studies have been performed in vitro to ascertain the mechanical properties of the disc. Some of the studies have focused on the properties of the disc as a whole, while others have been centered on the annulus fibrosus or the nucleus pulposus, the two building blocks of the disc. This section will first discuss the studies done on the annulus fibrosus or the nucleus pulposus, followed by the full disc studies.

Wagner et al. (2004) isolated the annulus fibrosus and tested this biological tissue separately from the intact disc. Six human lumbar spines were procured from donors aged 16 to 38 and rectangular specimens from the anterior portion of the annulus fibrosus were dissected and isolated. The samples were tested at quasi-static rates up to 0.4 MPa in tension and 0.04 MPa in compression. The stress-strain data was fitted with an exponential function with two constants A, B. The exponential function accurately represented the behaviour of the material; the annulus fibrosus has a significant toe region where the slope of the curve gradually steepens with increasing strain. The annulus fibrosus does not have much resistance to compression since the matrix is the only substance able to transmit load in

compression. The compression portion of the stress strain curve is considered to be linear. The values for A and B were reported to be 0.447 +/- 0.379 MPa and 31.9 +/- 12.2 MPa respectively in the circumferential direction in tension (Figure 3-9).

$$\sigma = A/B * [\exp(B\varepsilon) - 1]$$

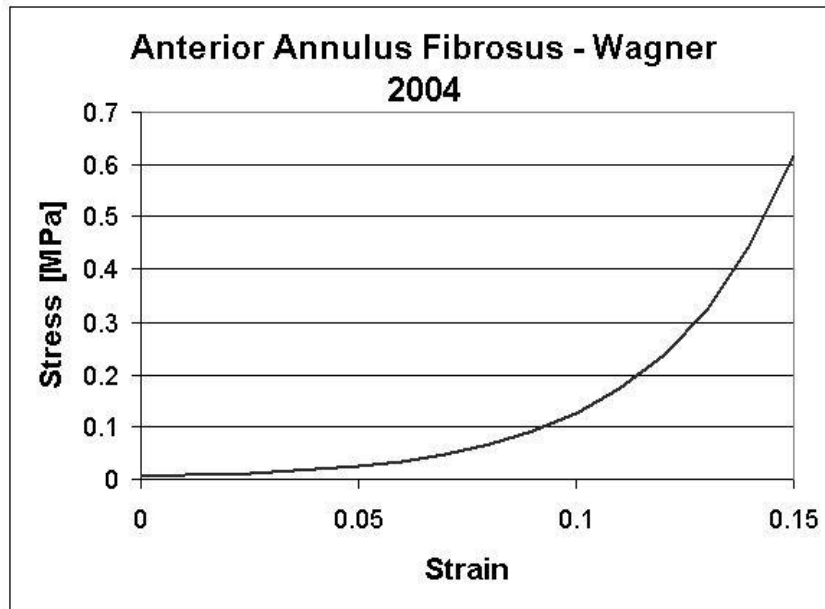


Figure 3-9: Circumferential Tensile Stress Strain Response of the Outer Annulus Fibrosus

Ebara et al. (1996) tested the annulus fibrosus of 15 lumbar spines, donor age 26 to 53, at various positions and orientation from the disc. The study found that the properties in the circumferential direction are not constant; specimens at the outer edge of the disc were significantly stronger than those closer to the center, and specimens from the anterior portion of the disc were stiffer than those from the posterolateral location (Figure 3-10). The study did not find a significant age effect, and concluded that the mechanical properties of the annulus fibrosus depend on the structure of the disc rather than the age. The stress strain data was fitted with a quadratic equation.

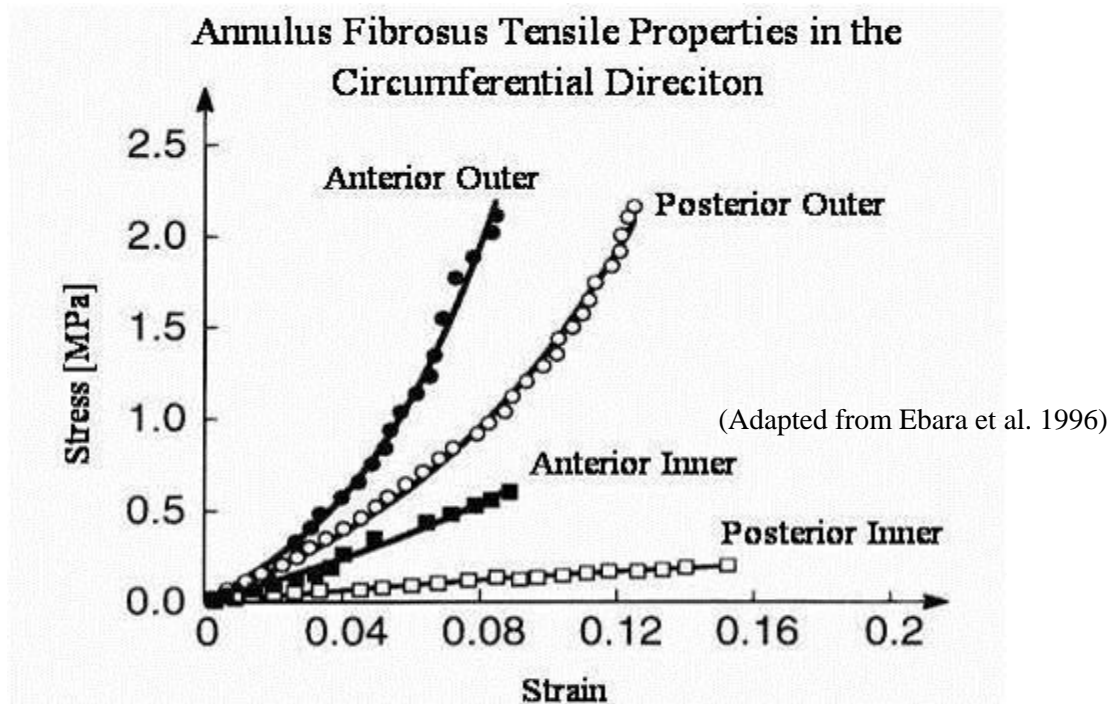


Figure 3-10: Site Specific Properties of the Annulus Fibrosus - Circumferential Direction

Elliot et al. (2001) tested the annulus fibrosus from 10 lumbar discs from seven donor spines ranging in age from 27 to 72. The annulus fibrosus was tested at several positions and orientations (circumferential, radial and axial). The results displayed a toe region followed by a quasi-linear region before failure. The data was fitted by two linear equations: one for the toe region and one for the “linear region.” Again, this study found that the response was dependent on position and orientation, but it did not analyze the age factor. Since the fibre orientation angle is smallest relative to the circumferential direction, the annulus fibrosus is strongest in that direction, followed by the axial direction, and finally the radial direction. The radial direction is much weaker because all the fibres are perpendicular to this direction and the matrix is the only substance resisting tension. The conclusions of this study are in agreement with those from the Ebara et al. (1996) study; however the values for elastic modulus are considerably weaker (Table 3-3).

Table 3-3: Site Specific Elastic Properties of the Annulus Fibrosus (Elliot et al. 2001)

	Modulus [MPa]	
	Outer	Inner
Circumference		
Toe-Region	2.52	1.7
Elastic Region	17.45	5.6
Axial		
Toe-Region	0.27	0.34
Elastic Region	0.82	0.96
Radial		
Toe-Region	0.19	
Elastic Region	0.45	

Fujita et al. (1997) focused on the radial properties of the annulus fibrosus. Fifteen discs from eight human lumbar spines with donor age ranging from 50 to 70 were tested. Specimens from the middle of the disc were stiffer than those from the outer and inner edges, and they failed at a smaller strain (Figure 3-11). There was no difference between specimens from the anterior and posterolateral portions of the disc.

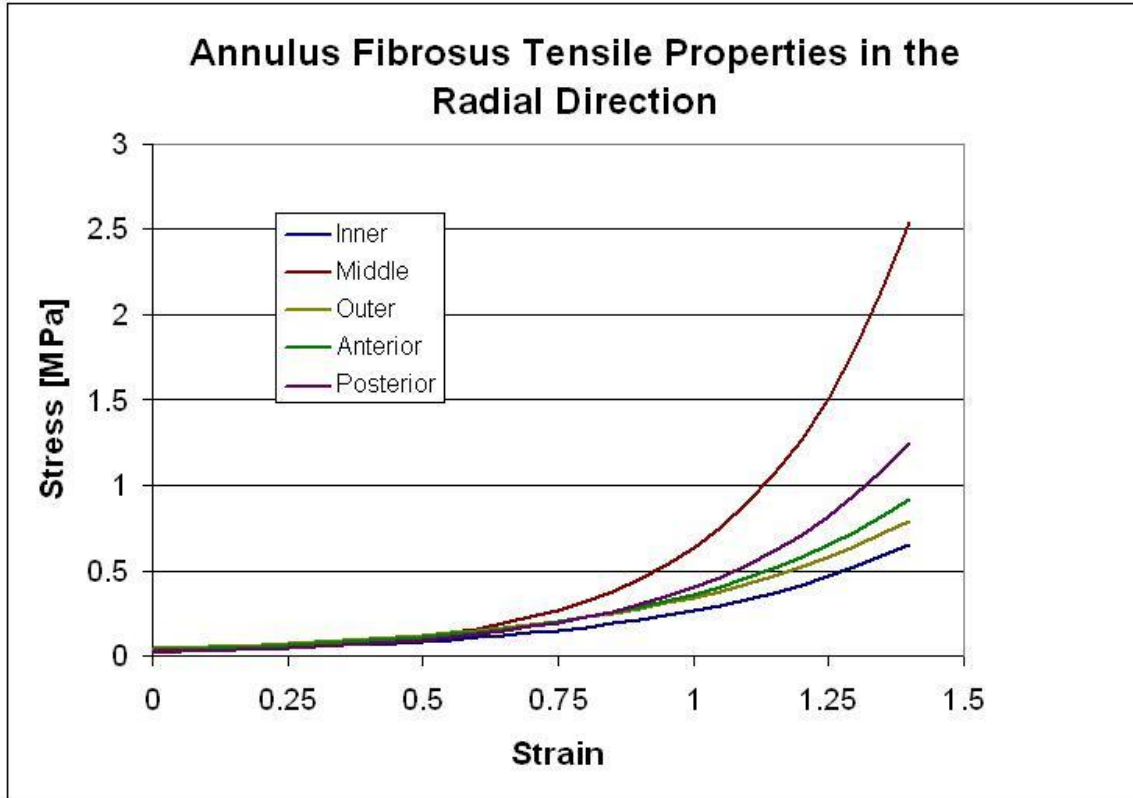


Figure 3-11: Radial Stress Strain Curve of the Annulus Fibrosus – Fujita et al. 1997

While all studies tested a large portion of the annulus fibrosus, which consisted of a multiple lamellae (although the exact number is not known), Skaggs et al. (1994) and Holzapfel et al. (2005) isolated a single lamella and reported its tensile behaviour.

Skaggs et al. (1994) and Holzapfel et al. (2005) reported the stress strain response of single lamella samples from the same four circumferential positions in the annulus fibrosus as Ebara et al. (1996): anterior inner and outer, and posteriolateral inner and outer (Table 3-5). Skaggs tested 11 human lumbar spines but did not report mean donor age while Holzapfel et al. (2005) also tested 11 human lumbar spine discs with the mean cadaver age being 58 years old. The findings of the two studies were very similar. In both studies, the lamellae from the anterior outer portion of the disc were strongest. The two studies used different approaches to calculate the elastic modulus. Skaggs reported the modulus of the sample when it was at 75% of its failure strain, while Holzapfel

calculated three different modulus values for three ranges of stress (Tables 3-4, 3-5): low (0 – 0.1 MPa), medium (0.1-0.5 MPa), and high (0.5-1 MPa).

Table 3-4: Elastic Properties of Single Annulus Fibrosus Fibre

	Skaggs et al. (1994)		Holzapfel et al. (2005)					
	Modulus [MPa]		E _{low} [MPa]		E _{medium} [MPa]		E _{high} [MPa]	
Position	Avg.	S.D.	Avg.	S.D.	Avg.	S.D.	Avg.	S.D.
Anterior - Outer	136	50	8.01	6.5	24.1	12.3	64.8	48.6
Anterior - Inner	76	50	3.8	5.02	14	8.63	31.2	19.8
Posterolateral - Outer	82	43	5.96	3.05	32.5	12.1	77.6	20
Posterolateral - Inner	59	41	3.79	2.61	13.9	8.13	27.5	12.8

Skaggs et al. (1994) also reported the failure stress and strain of the test samples (Table 3-5). As expected, the stiffer part of the annulus fibrosus, the anterior outer portion, failed at the highest strain stress and at the lowest strain.

Table 3-5: Failure Properties of a Single Annulus Fibrosus Fibre

	Skaggs et al. (1994)			
	Failure Stress [MPa]		Failure Strain	
Position	Avg.	S.D.	Avg.	S.D.
Anterior - Outer	10.3	8.4	9.2	3.4
Anterior - Inner	3.6	2.0	11.3	6.3
Posterolateral - Outer	5.6	3.2	12.7	2.7
Posterolateral - Inner	5.8	2.9	15.4	3.0

The annulus fibrosus has been studied in two ways. The first method is to isolate a small section of the disc consisting of a few layers, or lamellae, of the annulus fibrosus, and the second method is to isolate only a single lamella. Green et al. (1993) claimed that the stress strain response of multi-layer

samples was weaker than that of the whole disc because the fibres of multi-layer samples have been cut and shortened. Skaggs et al. (1994) and Hozlappfel et al. (2005) argued that the variation in orientation and number of lamellae in a multi-layer sample distorts the results and undervalues the strength of the annulus fibrosus. Ebara et al. (1996) noted that the multi-layer samples were weaker than single-lamella samples and claimed that both studies were important to determine the fibre and fibre-matrix interaction properties that are necessary for fibre reinforced finite element models.

Iatridis et al. (1997) studied the lumbar nucleus pulposus in shear and developed a linear viscoelastic solid model with five material constants. Thirteen disc specimens were harvested from eight spines ranging in age from 16 to 68 years old. The study applied an initial torsional shear strain to the samples and then monitored the stress relaxation behaviour. A dynamic frequency sweep test was also done with a frequency range of 1 to 100 rad/s. During the initial loading, the stress strain response of the nucleus was linear. For the static case, the stress relaxation saw the final stress drop to less than 3% of the initial peak stress, meaning that the nucleus pulposus is acting more like a fluid (cannot resist shear) than a solid. The dynamic frequency sweep testing found that the shear modulus increased along with the frequency, indicating a solid-like behaviour. At 1 rad/s, the shear modulus was 7.4 kPa and it rose to 19.8 kPa at 100 rad/s.

The results of the experimental testing of the annulus fibrosus and nucleus pulposus reached a consensus about the general behaviour of the materials. The strength of the annulus fibrosus specimens is dependent on the orientation and the source location of the sample. The annulus fibrosus is strongest in the circumferential direction at the outer edge of the anterior portion of the disc. The nucleus pulposus is made up of water mostly, but under dynamic conditions its behaviour resembles a viscoelastic solid instead of a fluid. However, the properties of these materials are difficult to quantify due to their small size, the variability from person to person, and the limited number of specimens. It is even more difficult to determine their properties in the cervical spine because all these studies have been done on lumbar spine samples.

Yoganandan et al. (1989b) analyzed the compression response of thoracic and lumbar intervertebral discs from eight male donors (age ranging from 25 to 86). The study reported the compression stiffness to be 2850 N/mm at the onset of failure with a displacement rate of 2.54 mm/s. The study

compared degenerative discs and healthy discs, and the results showed that the damaged discs are much weaker in compression (stiffness of 1642 N/mm).

Kemper et al. (2006) did compression testing on 11 lumbar spine segments (L1-L2 through L4-L5) harvested from 6 lumbar spines (donor age 18 to 56). The study used three loading displacement rates: 0.1, 0.2, and 1.0 m/s. The stiffness increased significantly with increasing loading rate. The load-displacement curves are quasi-linear and they do not have a “toe region” feature. It is possible that this study only analyzed the linear portion of the viscoelastic response, which is located after the toe region and before onset of failure. The stiffness values reported for the 0.1, 0.2, and 1.0 m/s loading rates were 1835 N/mm, 2490 N/mm, and 6551 N/mm respectively.

Markolf et al. (1972) tested 26 lumbar spine discs and 20 thoracic spine discs, dissected from 17 spines ranging in donor age from 21 to 55 years old. The discs were tested in flexion, extension, lateral bending, axial rotation, compression and tension. The compression tests were load controlled, and for loads between 220 and 670 N, the average stiffness was reported to be 2000 N/mm in compression and 900 N/mm in tension.

Yingling et al. (1997) compared the strength of the discs and the vertebral endplate by testing porcine spines in compression. This study also varied the testing rate to study dynamic effects. The study found that the failure in compression always occurred in the vertebral body and not the disc. At low strain rates, the failure was in the end plate, whereas at higher rates, the failure was more likely to be in the vertebral body. The stiffness and failure load increased with increasing loading rate (100N/s to 1000N/s) although it eventually reached a saturation limit (no significant change from 1000 to 16000N/s). At quasi-static loading rate, the stiffness was measured to be 1700 N/mm, and at saturation, the stiffness was 3000 N/mm.

3.4.4 Ligaments

Extensive testing has been done on ligaments at quasi-static and at dynamic strain rates. All of the studies used their own apparatus to define the ligament response in tension. Some studies reported the failure properties as stresses and strains while others reported the failure properties as force and displacement. A few studies have also quantified the stiffness of the linear portion of the typical ligament load-displacement curve. This section will discuss the quasi-static studies followed by the high-rate studies.

3.4.4.1 Quasi-Static

Chazal et al. (1985) tested, in tension, 43 ligaments from 12 human spines (donor age 30 to 80). The study was one of the first to present the typical ligament stress strain response curve. The instantaneous stiffness is defined as the slope of the stress strain curve. The toe region is the initial loading part of the curve where the stiffness starts close to zero and gradually increases. The second part of the curve is the linear region where the stiffness is fairly constant. The final section of the curve is where the stiffness gradually drops due to individual fibre failure in the ligament. The ultimate stress is defined as the maximum stress on the curve, and it is also the point on the curve where the instantaneous stiffness is zero. The study reported the stress and strain at three points in the curve for each ligament: the transition between the toe-region and the linear region, the end of the linear region, and the ultimate stress (Figure 3-12).

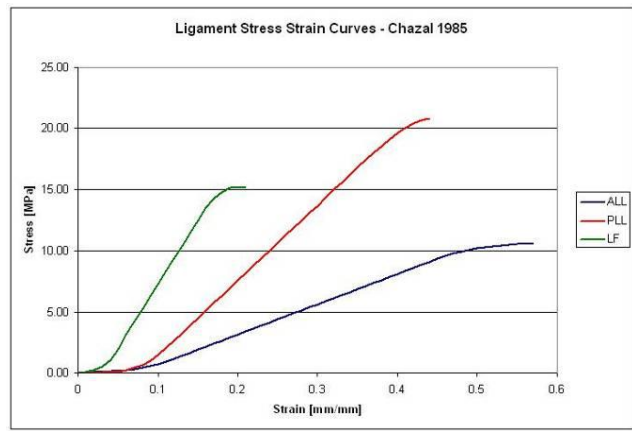


Figure 3-12: Stress Strain Response of the ALL, PLL, and LF – Chazel et al. 1985

Myklebust et al. (1988) harvested ligaments from 41 male cadavers with mean age 67 years (the majority of spines were between 60 and 80 years old). 402 ligaments were tested in total, and there were at least 3 ligaments of each type from each spinal level (from the C2 to the sacrum). The deformation rate was 10 mm/sec. The average failure force and displacement was reported for each ligament at each segment level (Table 3-6). The study noted that ligament failure displacement increased with distance from the vertebral axis of rotation.

Table 3-6: Failure Properties of the Cervical Spine Ligaments – Myklebust et al. (1988)

	ALL		PLL		LF	
	Force [N]	Elong. [mm]	Force [N]	Elong. [mm]	Force [N]	Elong. [mm]
C2-C3	207	8.7	84	9.6	86	5.8
C3-C4	47	4.2	82	7.4	75	3.7
C4-C5	47	4.8	47	3.4	56	12.8
C5-C6	59	5	85	4.8	89	8
C6-C7	176	13.7	102	5	160	7.7
C7-T1	97	7.6	95	6.4	221	9.9

Pryzbylski et al. (1996) tested anterior and posterior longitudinal ligaments from 20 cervical spines that ranged in age from 58 to 95 years old (average 80). The same characteristic response was reported as before showing a toe-region, a linear region, and a failure region (Table 3-7). The tests were done at a deformation rate of 0.33 mm/s.

**Table 3-7: Failure and Elastic Properties of the Cervical Spine Ligaments
(Pryzbylski et al. 1996)**

	C2-C3	C3-C4	C4-C5	C5-C6	C6-C7
X area [mm²]					
ALL	11	38	34	33	28
PLL	28	43	35	33	28
Stiffness [N/mm] of the linear region					
ALL	43	37	54	57	48
PLL	78	54	90	65	55
Ult. Load [N]					
ALL	66	104	106	104	105
PLL	150	111	102	89	95
Elongation [%]					
ALL	33	43	42	36	39
PLL	41	45	33	33	43
Modulus [MPa]					
ALL	75	13	42	51	48
PLL	98	8	48	22	21

Yoganandan et al. (2000) measured the length and cross sectional area of the ALL, PLL, capsular ligaments, LF, and ISL from C2 to T1. Twenty five spines were tested (average age 68) at 10mm/s and the force-displacement relationship was recorded. The force-displacement curves did not include a toe-region. The stiffness, failure load, and failure elongation were reported (Table 3-8).

**Table 3-8: Properties of the Middle and Lower Cervical Spine Ligaments
(Yoganandan et al. 2000)**

Ligament	Sample Size	Stiffness [N/mm]	Maximum Load [N]	Failure Elongation [mm]
C2-C5				
ALL	10	16	93	5.8
PLL	7	25.4	71	3.5
FJ	8	33.6	239	10.2
LF	12	25	121	6.5
ISL	8	7.74	39	6.3
C5-T1				
ALL	7	17.9	145	6.5
PLL	10	23	188	6.1
FJ	11	36.9	364	7.8
LF	11	21.6	129	9.4
ISL	8	6.36	39	6.7

3.4.4.2 High Rate Studies

Yoganandan et al. (1989) tested 54 ALL and LFs from donors ranging in age from 46 to 88 years old. Four loading rates were used: 8.8, 25.0, 250.0, 2500.0 mm/sec. The study reported the failure force, failure displacement, linear region stiffness and failure stiffness (failure force divided by failure displacement). These values were plotted against the logarithm of the loading rates (Figures 3-13, 3-14). Failure force and stiffness increased with higher loading rates, while the failure displacement did not show any trends.

Shim et al. (2005) performed Hopkinson bar testing on three spines (age 40, 65, and 69) and reported the stress strain curves for several ligaments. Shim found a major difference between the quasi static and dynamic responses for all ligaments tested (Figures 3-15, 3-16).

Bass et al. (2007) tested at high strain rates (627mm/s) the ALL, PLL and LF from six male (average 60 +/- 8 years) and five female (average 58 +/- 6 years) spines at the C3-C4, C5-C6 and C7-T1 levels. 47 male ligaments and 42 female ligaments were successfully harvested. The objective of the study was to compare the failure force and elongation of the ligaments and test the differences between ligament, gender, and segment level (Figures 3-13, 3-15, 3-16).

Ivancic et al. (2007) tested 97 ligaments (six spines average age 80.6, range 71 to 92) at high speed only (~700 mm/s). The results were compared against older, quasi-static studies and found that at higher strain rates, the failure force increases, and the failure strain (elongation) decreases (Figures 3-13, 3-14).

Mattucci et al. (2012) tested 261 human cervical spine ligaments from 16 spines (8 male and 8 female). The average spine age was 44 years old and no spine was older than 50. Ligaments were tested to failure at three strain rates: slow (0.5 s^{-1}), medium (20 s^{-1}), and high ($150\text{-}250 \text{ s}^{-1}$). Failure force, failure strain, failure stress, linear stiffness, and linear modulus were reported for all cervical spine ligaments (Figures 3-13, 3-14, 3-15, 3-16). The study also analyzed the effect of spinal level and gender, and it also compared the effect of age against previous studies that tested older spines.

Failure Force for High Rate Ligament Testing

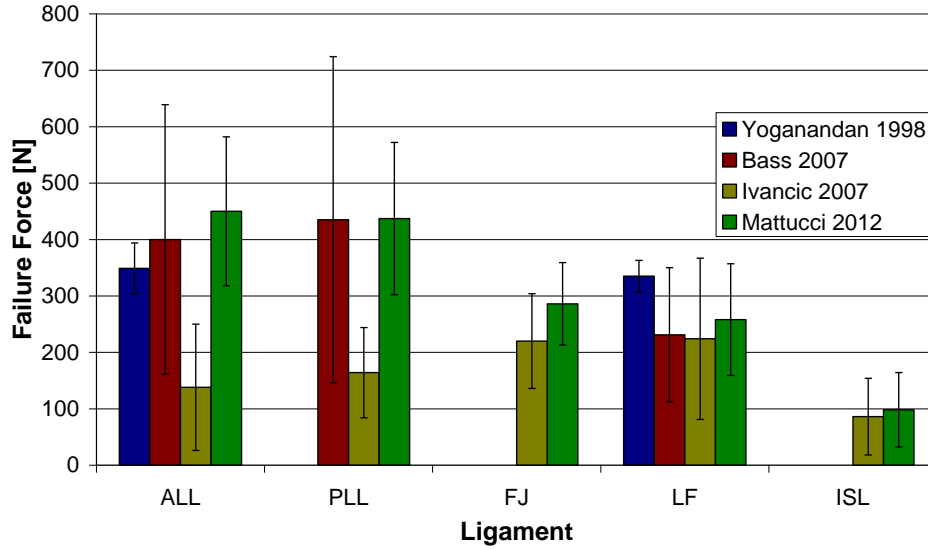


Figure 3-13: Summary of High Rate Ligament Testing - Failure Force

Elongation at Failure for High Rate Ligament Testing

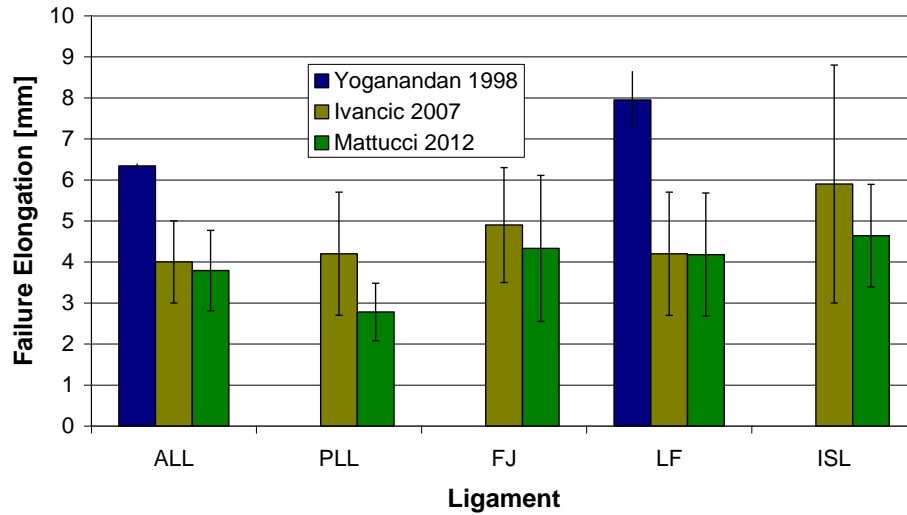


Figure 3-14: Summary of High Rate Ligament Testing - Failure Elongation

Failure Stress for High Rate Ligament Testing

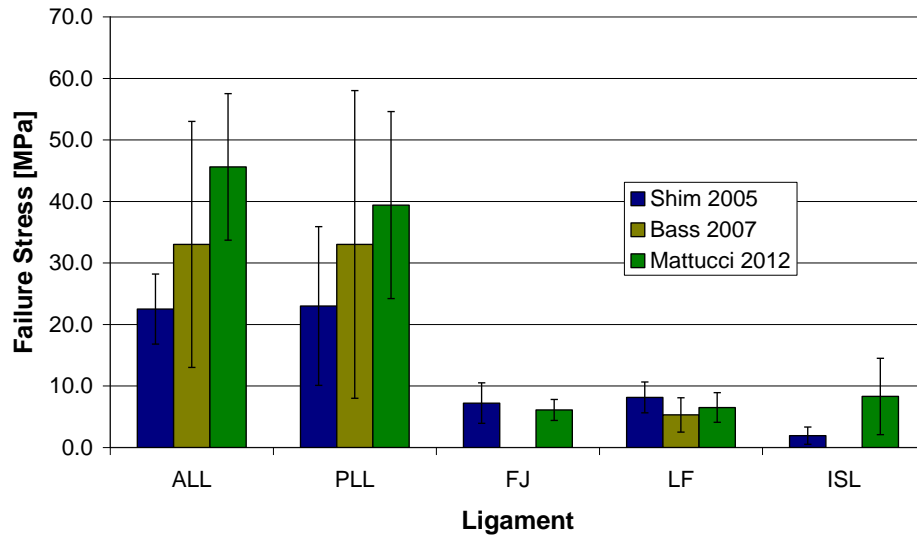


Figure 3-15: Summary of High Rate Ligament Testing - Failure Stress

Strain at Failure for High Rate Ligament Testing

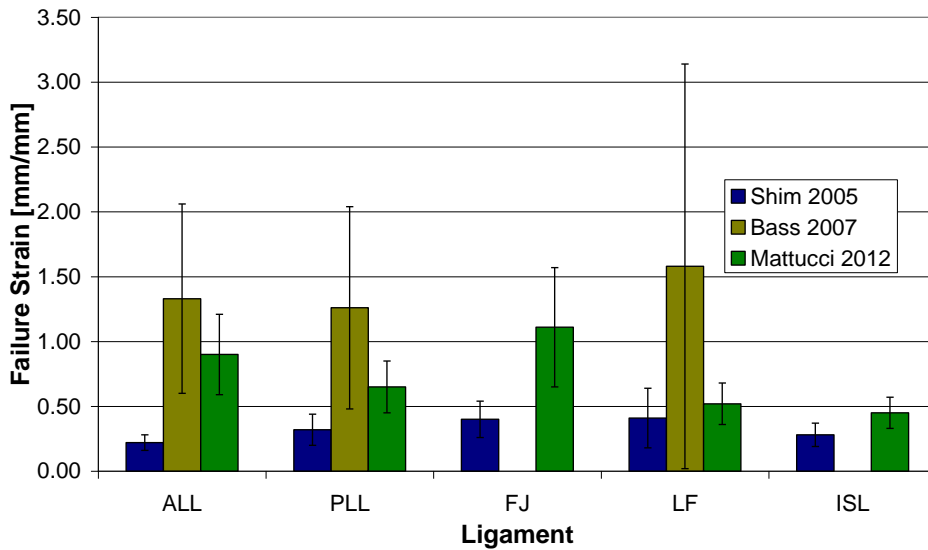


Figure 3-16: Summary of High Rate Ligament Testing - Failure Strain

3.5 Age Related Properties

An important challenge with in vitro testing of human cervical spines is donor age. Older spines are generally more available for testing than younger spines. In the case of developing a model of a 50% male for car crash simulations, the material properties should be more reflective of the average age of the occupant, which is 35 years old (Table 1114, United States Census Bureau, 2009). Studies that have used older spines are still useful for justifying the results of young spines by ensuring that general trends, like stiffness decreasing with age, are apparent in studies of younger samples. A few studies have analyzed the age effect on the mechanical properties of soft tissues, but not necessarily tissues from the cervical spine.

Noyes et al. (1976) tested 26 anterior cruciate ligaments in tension. Six ligaments were dissected from donors aged 16 to 26 years, and 20 ligaments were harvested from donors aged 48 to 86 years old. The study found significant differences between all the mechanical properties. The average maximum force and stiffness of the young ligaments was 1730 N and 182 kN/m respectively, and only 734 N and 129 kN/m respectively for the older ligaments. The strain at failure for the younger ligaments was 0.44 and 0.30 for the older ligaments.

Iida et al. (2002) found a negative correlation ($p = 0.02$) between age and the tensile strength of interspinous ligaments at the L4-L5 level from human lumbar spines. Twenty four spines were tested ranging from 18 to 85 years old. These specimens all had a history of lumbar degenerative disease. The study was limited by the fact that the majority of the spines tested were between 60 and 80 years old, and only two were younger than 50.

Stemper et al. (2010) compared two groups of thoracic disc segments: group A (donor age 28 +/- 8) and group B (donor age 70 +/- 7). The study found major differences between the tensile and compressive properties of the two groups. The younger group was much stiffer than the older group. The tensile stiffness of the younger discs was 486 N/mm and it was 397 N/mm for the older discs. The compressive stiffness was also higher for the younger discs; 3300 N/mm versus 2527 N/mm.

3.6 Numerical and mathematical models of the cervical spine

The purpose of the experimental research is to provide high rate segment response data in flexion and extension for validating a new finite element model of the human cervical spine. Numerous models of the cervical spine have already been developed using the material properties of discs and ligaments from older specimens. These models have been analyzed in all modes of loading, and the results have been compared against the experimental data of various studies.

The finite element method (FEM) is an approximate numerical technique for analyzing structural, fluid flow, or heat transfer problems. In this thesis, the FEM is applied to the human cervical spine to find the loading response due to the complexity and nonlinearity of the structures. The FEM begins with the discretization of the large bodies, like the vertebra and the ligaments, into smaller building blocks called elements. The process of discretizing the geometry into elements is called meshing. Elements can have one, two or three dimensions depending on the geometry and the nature of the material; for example 3D solid elements are used to represent cancellous bone and 1D spring elements are used to simulate ligaments. The material properties are controlled by the equations governing the force displacement response. The governing equations are applied to each element in the mesh, and the force and displacement values are calculated at every node. A node is a point at the corner or at the end of an element and it is the connection point for adjacent elements. Three dimensional brick elements have eight nodes (one at each corner) while 1D spring elements have only two nodes.

A finite element analysis requires an initial loading condition, which is generally a force applied to nodes on the surface of the mesh or a rigid body rotation. The governing equations calculate the resultant forces and displacements at every node. The displacement of the whole body and the localized strains can be measured by the relative movement of the nodes, and the summation of all the nodal forces results in the force response of the entire system.

Kumaresan et al. (1999) developed a C4-C5-C6 model and tested the response with varying material properties. This was a very interesting parametric study because it clearly showed that the disc and ligament properties have the largest influence on the moment-rotation response of the C4-C6 functional spinal unit in all four modes of loading. The properties of the bone and endplate did not have any significant effect. The study used three sets of properties for each test run: the first was the

average properties found in literature, and the other two sets were the upper and lower bounds of the average properties. This finding was important because it showed the importance of the disc and the ligaments in the segment response, and it provided a rationale for further research into the mechanical properties of these soft tissues.

Halldin et al. (2000) developed a finite element model of the neck to predict compression injury to the vertebra. The purpose of the investigation was to further the research into occupant safety during rollover accidents where the head hits the roof of the vehicle. The muscles were omitted from the model because they did not have a significant effect on the compression response of the spine. The ligament properties were derived from the work of Myklebust et al. (1988). Additional work has been done with this model by adding different muscle types and analyzing the kinematic response in frontal, rear and lateral impacts (Hederstierna et al. 2008, 2009). These studies found that solid element muscles increased the stiffness of the spine compared with single beam element muscles.

Van der Horst (2002) developed a multibody model of the cervical spine for her Ph.D. thesis. The purpose of the multibody model was to predict the kinematic and dynamic response of the system with a focus on whiplash injury. The intervertebral discs were not modeled as actual discs; instead they were modeled as a spring damper system in all six axes of motion. The properties of the spring damper system were derived from experimental studies that analyzed the stiffness of the disc in all six directions. The ligaments were modeled as single spring elements with three separate linear force displacement regions: one for the toe-region, another for the linear region, and a third nearing failure. For flexion and extension testing, the moment was applied at T1 and the relative rotation of each segment was measured. The results of the model were compared to the published data from Camacho et al. (1997), revealing good agreement in extension. However, in flexion, the multibody model was stiffer than the experimental response.

Meyer et al. (2004) constructed a FEM to try to determine why people experience neck pain during low speed rear impacts. The model included the skull and the whole cervical spine. Since it was a low intensity impact, the study did not consider damage to the bone, so they modeled the surface with rigid shell elements. The ligaments were modeled as a set of three 2D springs that simplify the ligament tensile response to three separate linear regions: toe-region, linear, and failure. The intervertebral disc was modeled with brick elements as a single material with a modulus of 100 MPa

and a Poisson's ratio of 0.30. Only passive muscles were modeled, and they were represented with brick elements. The model simulated rear, frontal, lateral, and oblique (combination of frontal and lateral) impact and there were mixed results when compared against the volunteer testing data. The test results plotted the head acceleration against time for the various loading conditions.

Zhang et al. (2006) developed a full cervical spine model (head plus C0-C7). The head was only meshed with shell elements to recreate the head inertia during impact. The geometry was obtained from a 68 year old cadaver. The vertebrae and the discs were meshed with hexahedral elements, while the ligaments were modeled with springs. The model was compared against the experimental testing of Panjabi (1998 and 2001). The study was in good agreement in flex/ext, and axial rotation, but not very good in lateral bending.

Panzer et al. (2009) validated the C4-C5 segment from their cervical spine model, developed at the University of Waterloo. The model was analyzed using commercial FE software LS-Dyna. The annulus fibrosus properties were derived from the experimental testing of Holzapfel et al. (2005), the nucleus pulposus was assumed to be a fluid with a bulk modulus of 1720 MPa, and the ligament properties were obtained from the testing of Chazel et al. (1985) and Yoganandan et al. (2000). The model was compared against Nightingale et al. (2007), Wheeldon et al. (2006), and Camacho et al. (1997) studies. The model was a bit stiffer than the Nightingale study in flexion, and less stiff than the experimental data in extension. Wheeldon and Camacho data was in good agreement with the model in flexion, but the model was stiffer in extension.

Panzer et al. (2011) analyzed the whole spine model that was developed earlier by the authors (Panzer et al. 2009). Although it was a whole spine study, the results were broken down into segment and compared against experimental studies (Nightingale et al. 2002, 2007 and Wheeldon et al. 2006). In flexion, the model was stiffer than the experimental data at every spinal level except for C6-C7, where the model was stiffer than Wheeldon et al (2006) but weaker than Nightingale et al. (2007), and C7-T1, where the model was weaker than both experimental studies, but still within one standard deviation. In extension, the model was weaker than the two studies at every level except at C4-C5.

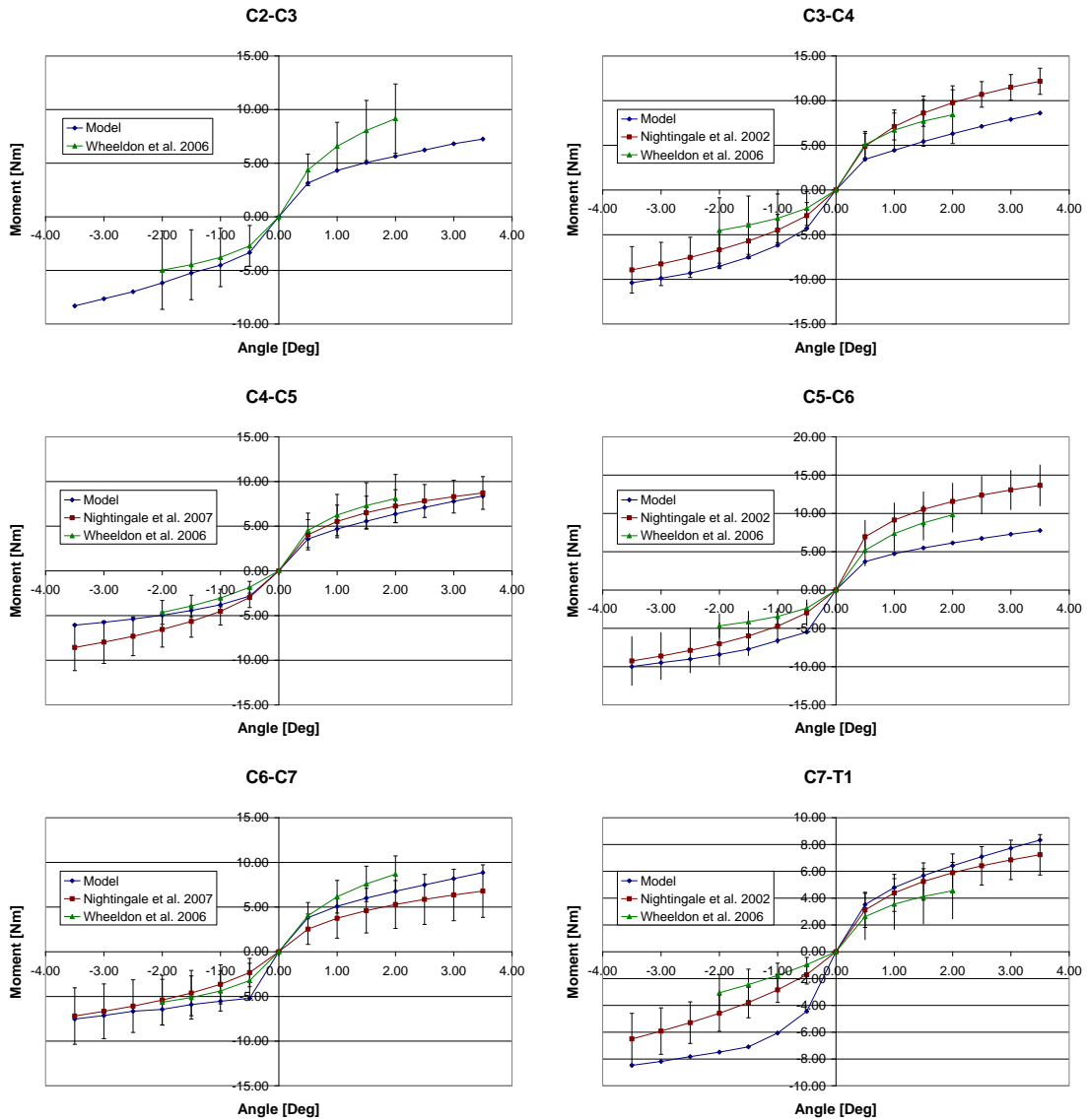


Figure 3-17: Comparison of Cervical Spine Finite Element Model with Flexion Extension Segment Studies (Adapted from Panzer et al. 2011)

Kallemeyn et al. (2010) created a model from C2-C7 and validated it against the testing on one full spine only. Model geometry came from a 74 year old cadaver. The finite element software ABAQUS was used to conduct all the analyses. The intervertebral discs were assumed to be one-

third nucleus pulposus by volume, and the annulus fibrosus fibres were assumed to be at a 25 degree angle relative to the transverse plane. The ligaments were modeled with 3D truss elements and a hypoelastic material model was used to reflect the ligament tensile behaviour. The cortical bone and cancellous bone were given an elastic modulus of 10 GPa and 0.45 GPa respectively, and hexahedral elements were used to mesh the vertebrae. The whole spine model was only tested up to 1.0 Nm in all four modes of loading. The C2-C3, C4-C5, and C6-C7 model segments were analyzed against their own experimental work and against previously reported data (Panjabi et al. 2001, Wheeldon et al. 2006). The segment models, and the experimental specimens, were tested with all the ligaments attached first, and then they were run again with the interspinous ligament, ligamentum flavum, and capsular ligaments cut one at a time. In extension, the model did not predict any change to the response (measured the rotation under a 1.0 Nm moment), while the experimental testing showed that the range of motion increased after each ligament was cut. In flexion, the experimental testing response demonstrated that the range of motion increased each time a ligament was cut except at the C6-C7 level. The model and experimental response were in good agreement with each other. The ligament dissection effect was much more significant at the C4-C5 level than the other two levels tested.

Chapter 4

Low and High Rate Experimental Testing Procedure

4.1 Cadaver Morphology

The research methods used in this study were approved by the Office of Research Ethics at the University of Waterloo. All specimens procured for testing were under the age of 50. Research has shown that the mechanical properties of ligaments (Iida et al. 2002) and intervertebral discs (Stemper et al. 2010) decline with age. As a person ages, the tensile and compressive properties of soft tissues in the spine weaken due to degeneration. Fifty years of age was chosen as a cut off point for spine procurement because it was a compromise between wanting spines close to the average age of a car crash victim (35 years old), and cadaver availability. Eight out of nine spines tested were between 40 and 50.

A total of nine fresh-frozen cadaver cervical spines (six male, three female) were acquired for testing. The average age of the specimens was 45 with the youngest spine being 29 years old and the oldest spine 50 years old. The average weight was 85 kilograms with a standard deviation of 33, and the average height was 1.78 metres with the standard deviation being .08. The cervical spines were frozen within 24 hours of death. The spines were procured from ScienceCare (Phoenix, AZ) and National Disease Research Interchange (NDRI, Philadelphia, PA). The spines from ScienceCare were sectioned from the T1-T2 disc up to and including the base of the skull. The spines from NDRI were only sectioned from C1 to T1. Table 4-1 shows the age, weight, height, procurement source and cause of death of each spine donor.

Table 4-1: Cervical Spine Donor Morphology

Spine #	Spine ID	Age	Sex	Weight (kg)	Height (m)	Provider	Cause of Death.
1	C090022	49	M	80	1.83	Science Care	Not Specified
2	C065494	29	F	66	1.68	NDRI	Brain Cancer
3	C100386	50	M	55	1.80	Science Care	Lung Cancer
4	C080914	48	M	109	1.88	Science Care	Heart Attack
5	C100800	46	F	136	1.65	Science Care	Heart Disease
6	S101442	49	M	55	1.75	Science Care	Colon Cancer
7	C066985	49	M	70	1.78	NDRI	Colon Cancer
8	C111141	48	F	136	1.75	Science Care	Cancer
9	C111187	37	M	59	1.83	Science Care	Colon Cancer

4.2 Testing Preparation

After thawing, the spines were dissected into segments. A segment consists of two adjacent vertebrae, the intervertebral disc that separates the vertebrae, and the ligaments that connect the two vertebrae. Each spine was dissected into C2-C3, C4-C5, and C6-C7 segments or C3-C4, C5-C6, and C7-T1 segments (Figure 4-1). Therefore it took two spines to acquire one sample for each segment level. Once the segments were sectioned, they were carefully cleaned to remove the spinal cord and non-ligamentous soft tissue, which included muscle, blood vessel, nerves, and fat.

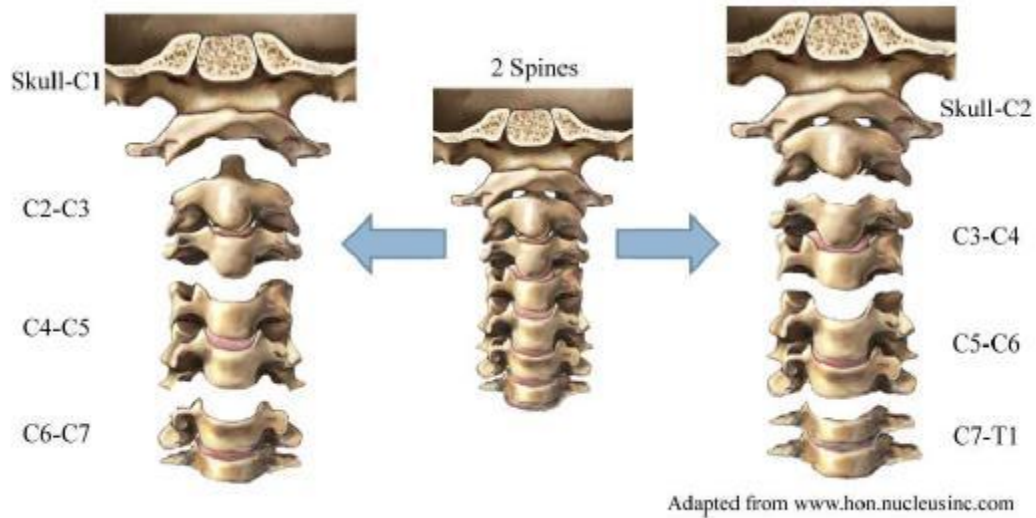


Figure 4-1: Spine Dissection

For each segment, the height and width of both vertebral bodies and the thickness of the intervertebral disc were measured with calipers (Table 4-2). The height was defined as the distance between the superior and inferior surfaces of the vertebral body, and the width was defined as the distance between the anterior and posterior surfaces of the vertebral bodies. These measurements were used to determine the instantaneous axis of rotation (IAR) of the segment. In flexion and extension, the IAR of the superior vertebra about the inferior vertebra intersects the vertebral body of the inferior vertebra. In the sagittal plane, the position of the axis is defined as a percentage of the width (x axis) and height (y axis) of the vertebral body with the origin located at the posterior, inferior corner (Amevo et al. 1991).

Table 4-2: Average Dimensions (with Standard Deviation) of Donor Vertebral Bodies

Vertebra	Height [mm]	Width [mm]	Inferior Disc Thickness [mm]
C2	21.12 (3.69)	17.05 (1.68)	4.88 (1.76)
C3	17.33 (3.06)	18.85 (2.04)	4.53 (1.51)
C4	15.41 (2.84)	19.18 (1.77)	2.97 (0.84)
C5	20.22 (2.91)	20.22 (2.91)	5.02 (2.06)
C6	14.64 (2.63)	20.35 (2.13)	4.31 (1.05)
C7	16.43 (2.66)	19.69 (1.31)	3.83 (0.93)
T1	18.31 (3.48)	19.83 (2.24)	

Eight screws in total were inserted into each segment. Two screws were inserted into the superior face of the superior vertebra and the inferior face of the inferior vertebra, and another screw was put into the exposed faces of each articular process. The screws were inserted into the bone, but they did not penetrate the disc or the cartilage of Steel wire was wrapped around one of the vertebral screws, fed through the transverse foramen, and then twisted around one of the screws in the articular process (Figure 4-2). The steel wire and screws were necessary when the vertebrae were placed into plastic cups and the cups were filled with liquid resin. Testing on isolated cervical spine ligaments showed that the resin holds better against dry surfaces, such as screws and steel wires, than against wet surfaces like human ligaments. The screws and the steel wire also gave the resin more surface area to resist against the bending tensile force that tried to pull the specimen out of the resin.



Figure 4-2: C6-C7 Segment Ready for Potting

The vertebral bodies were potted into separate plastic cups (Spaenaur, Kitchener, #317-052). The cups had an 87 mm diameter, and a 25.4 mm height. The inferior vertebra was potted first so the IAR of the segment can be centered at the top edge of the cup. The location of the IAR was defined as a ratio of the width (x coordinate) and height (y coordinate) of the vertebral body with the origin located at the posterior, inferior corner of the vertebral body (Amevo et al. 1991).

A small hole was made in the center of the cup to locate the segment IAR in the proper horizontal position. A 1.6mm hole was drilled into the inferior surface of the lower vertebra at the reported distance in the x direction from the posterior edge of the vertebral body (Amevo et al. 1991). The IAR also had to be located in the vertical direction (y axis). The position of the IAR in the y axis was marked by making a small horizontal incision to non-ligamentous tissue on the anterior face of the

vertebral body. The end of a 1.58mm pin was inserted into the hole at the bottom of the inferior vertebra, while the other end of the pin was placed into the hole that was made in the center of the plastic cup. The height of the vertebral body was adjusted so that the small incision in the tissue on the anterior face of the vertebral body was aligned horizontally with the top edge of the cup. The pin ensured that the x and y position of the IAR was aligned with the axis of rotation on the machine (Figure 4-3).

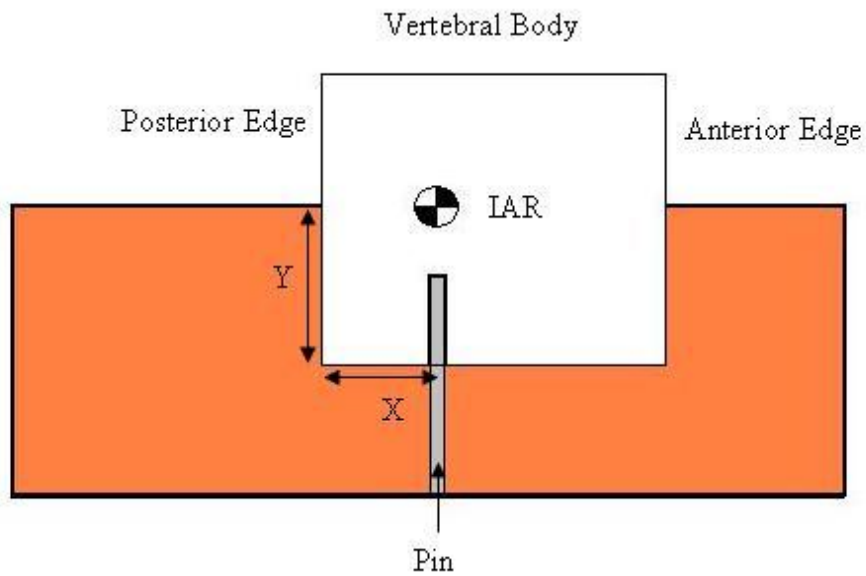


Figure 4-3: Potting Procedure

Once the lower vertebra was in position in the plastic cup, liquid resin (R1 Fast Cast #891, GoldenWest MFG., Inc. California, USA) was poured into the cup. The resin consisted of two separate liquids that, after being mixed together in even amounts, solidified after one or two minutes (Figure 4-4). The segment was flipped upside down and then the superior vertebra was potted into a second plastic cup. A jig was built to position the cups so that they were aligned vertically.

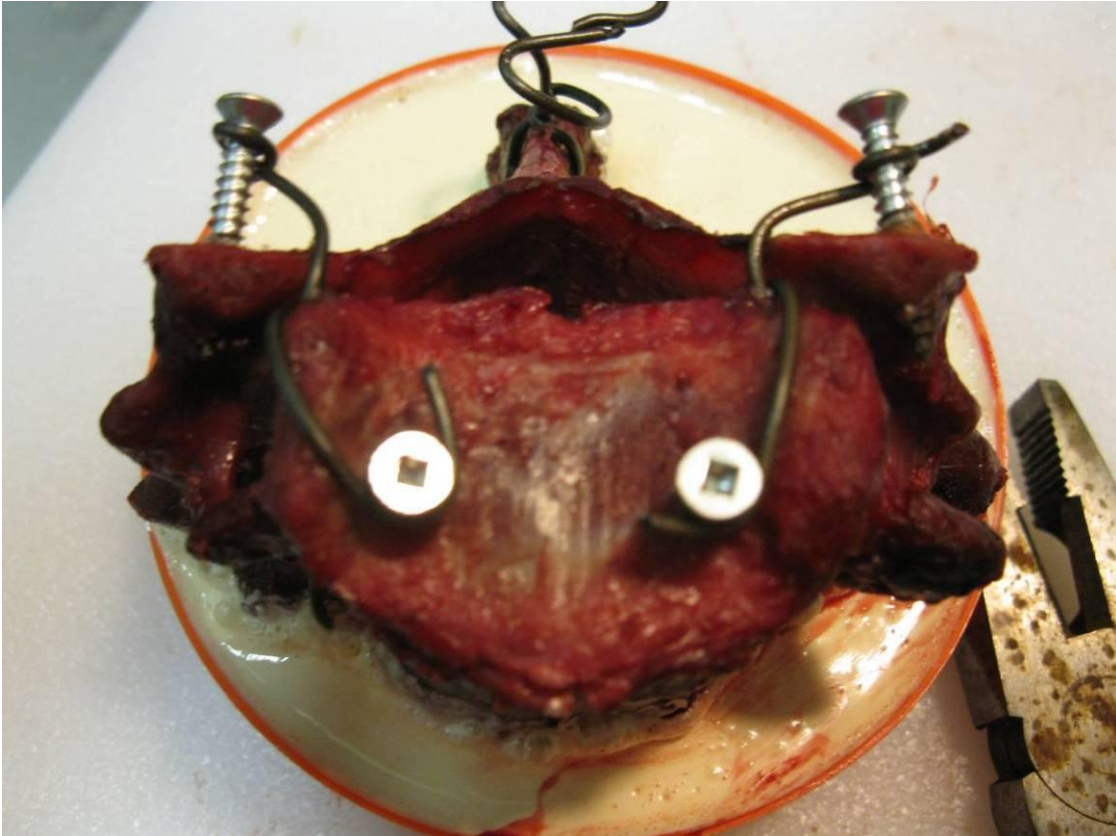


Figure 4-4: Half Potted Specimen

4.3 Testing Apparatus

The flexion/extension testing apparatus, which was custom designed and built for this research, employed a fixed axis concept. The inferior vertebra of a cervical spine segment was fixed to a six-axis load cell (Model 45E15A4 1000N, JR3, California, USA), while the superior vertebra was connected to a Danaher Motion servomotor (Electromate, Ontario, Canada). Since it's important that the segment rotated naturally, the axis of rotation of each segment had to match the axis of the servomotor. If the axes did not coincide, then the segment would have rotated about an unnatural axis, and it would have produced artificial forces and moments. The vertical position of the load cell was adjustable, so the axis of rotation of the machine did not always intersect with the top edge of the cup (Figure 4-5).

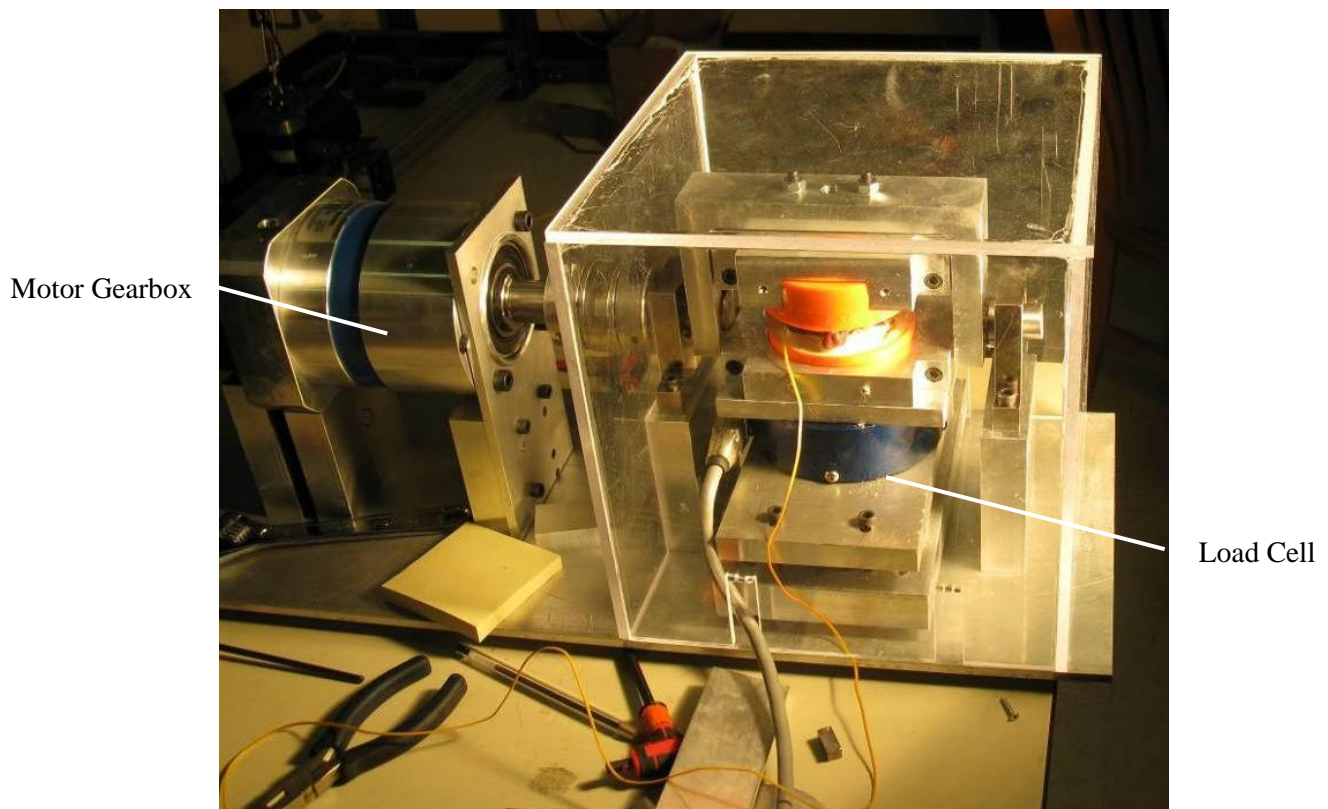


Figure 4-5: Fixed Axis Machine

The inferior vertebra was securely attached to the load cell via an aluminum block cup holder (Figure 4-6). The cup holder was essentially just a block with a hole cut out in the center for the cup to sit in. After the hole was cut out with a lathe, the block was cut into two parts. The first part was the base and it was fixed to the load cell with four screws. The second parts acted like a clamp and gripped the bottom cup. The clamping force was not strong enough on its own to hold the cup firmly, so four screws were inserted into the solid resin. The superior cup was secured to the machine by another two-piece holder. The larger piece was connected to a machined bracket, and the second smaller piece clamped the plastic cup.

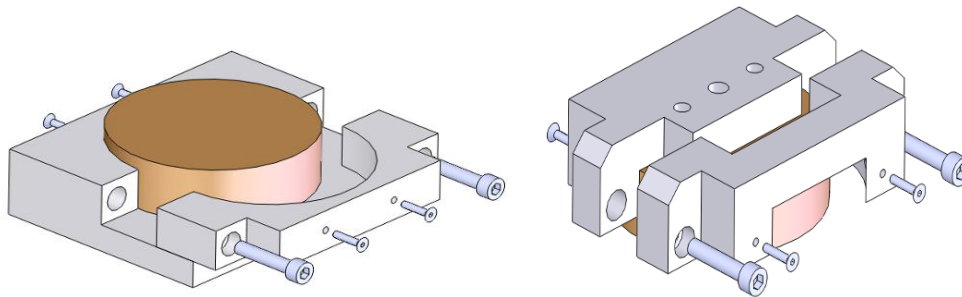


Figure 4-6: Upper and Lower Pot Holders

The machined bracket was U-shaped so that the instantaneous axis of rotation of the segment was in line with the axis of the servomotor (Figure 4-7). The design of the bracket allowed for adjustment in the distance between the bracket and the superior cup holder. Motion from the servomotor was transferred to a steel shaft via a coupler, and then the shaft was coupled to the bracket with a keyway. The angular velocity of the servomotor was reduced by a 7:1 ratio GAM gear reducer (Electromate, Ontario, Canada).

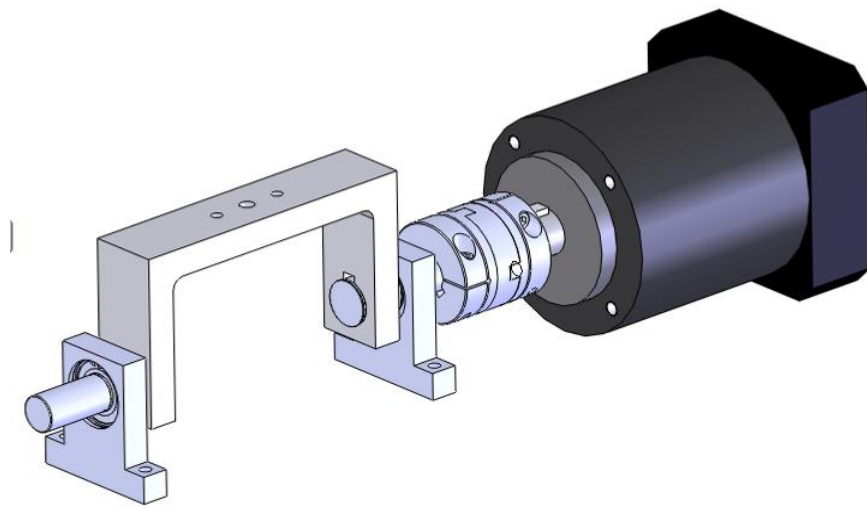


Figure 4-7: Servomotor and Rotating Bracket

4.4 Testing Procedure

The cup holding the inferior vertebra was fixed to the machine first, followed by the superior cup. The load cell measured the loads before and after the specimen was loaded into the machine to check the compressive preload. In order to recreate in vivo conditions, the specimen was sprayed with saline solution to maintain 100% humidity and a thermocouple was placed in contact with the segment soft tissue to measure temperature. The segments were tested at 100% humidity and at 37 °C. An atmospheric chamber surrounded the machine (not including the coupler, the gear reducer and the motor), and a heating coil was placed inside the chamber. A heat lamp was positioned just outside to speed up the heating process, but not too fast or else the specimen temperature distribution would have been uneven.

4.4.1 Reporting of Results

The six-load cell outputted the force and moment in all three axes. The load cell was positioned in the fixture such that the z axis was aligned with the superior inferior axis of the segments (normal to the transverse plane). Instead of having the x and y axis aligned normal to the frontal and sagittal planes, they x and y axis were rotated 45 degrees (Figure 4-8). The 45 degree rotation of the axis provided a quick visual check to see if the specimen was properly centered because the x and y forces and moments of every flexion or extension should have been identical. In flexion, the M_x and M_y moments and the F_y force were positive and the F_x force was negative, and in extension the opposite held true. The F_z force was positive in tension and negative in compression and the M_z moment indicated axial rotation, which should have always been zero in flexion and extension.

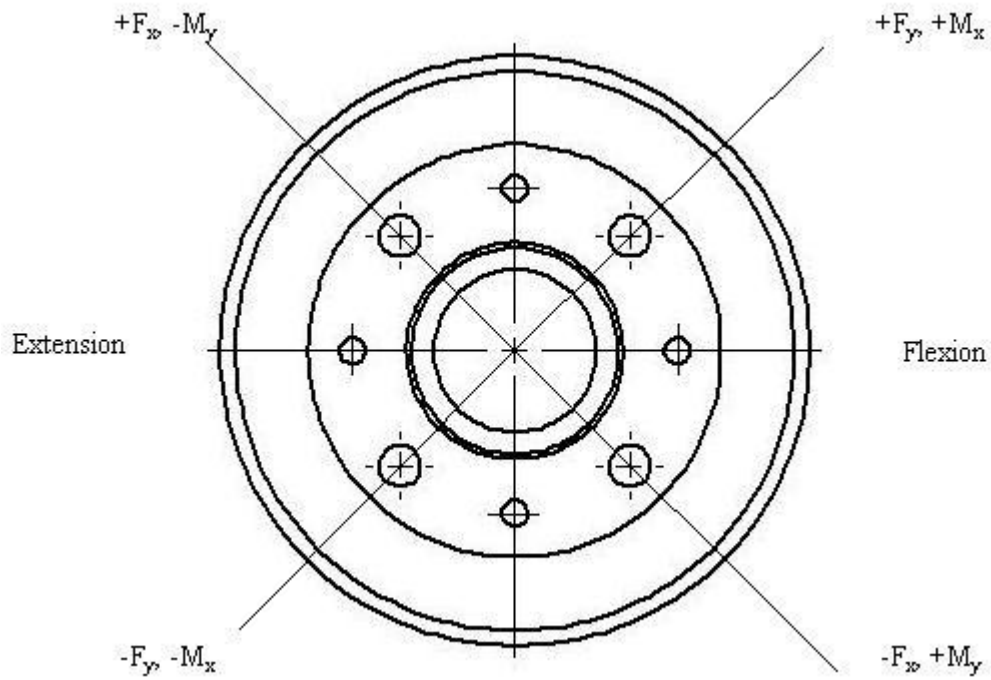
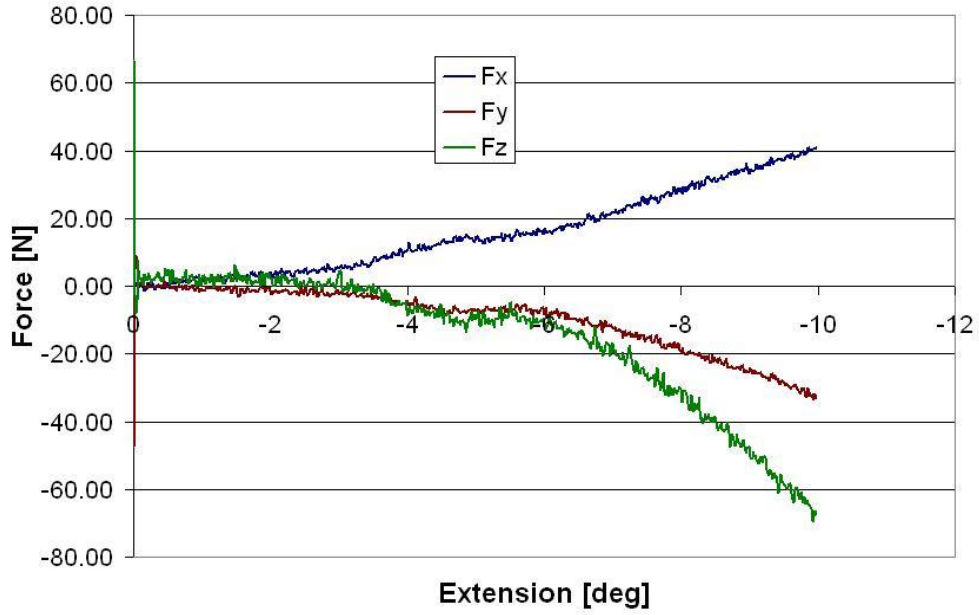


Figure 4-8: Load Cell at 45 degree angle

In the literature, the flexion/extension response has always been defined as the relationship between the resultant moment of the segment and the angle of rotation. Therefore, in this research project, the data from the six axes had to be manipulated in order to determine the resultant moment. The three force curves and the three moment curves were plotted on different graphs for each test run (Figure 4-9). The forces and moments do not pass through the origin because of an offset in the load cell that varied depending on the torque of the screws attaching the lower cup holder to the load cell. Instead of adjusting the electronics of the load cell, the six curves were shifted to account for the offset (the moment and force at zero degrees of rotation) and to calculate the resultant moment.

Force Data - C111141 C5C6 1 DPS Ext3



Moment Data - C111141 C5C6 1 DPS Ext3

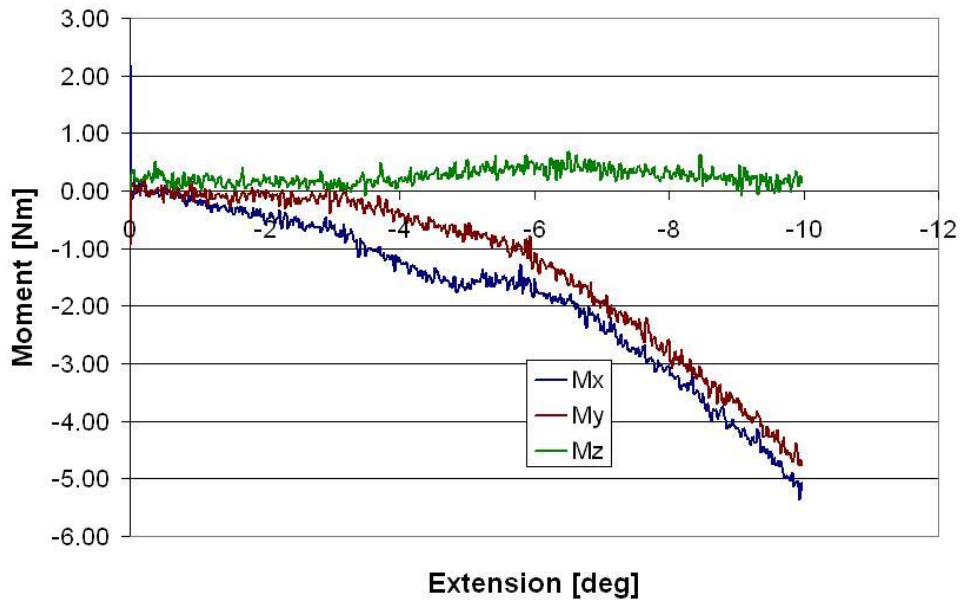


Figure 4-9: Raw Data - Forces and Moments

The resultant moment was defined as the moment about the neutral axis in the disc where the compressive and tensile forces were zero. The neutral axis could not be accurately located because the forces in the disc cannot be directly measured, so the resultant moment was assumed to be at the mid-height of the disc directly above the instantaneous center of rotation. The moment recorded by the load cell had to be transposed to the center of the disc and the shear forces had to be included too since there was a lever arm distance from the center of the disc to the measuring point of the load cell (Figure 4-10).

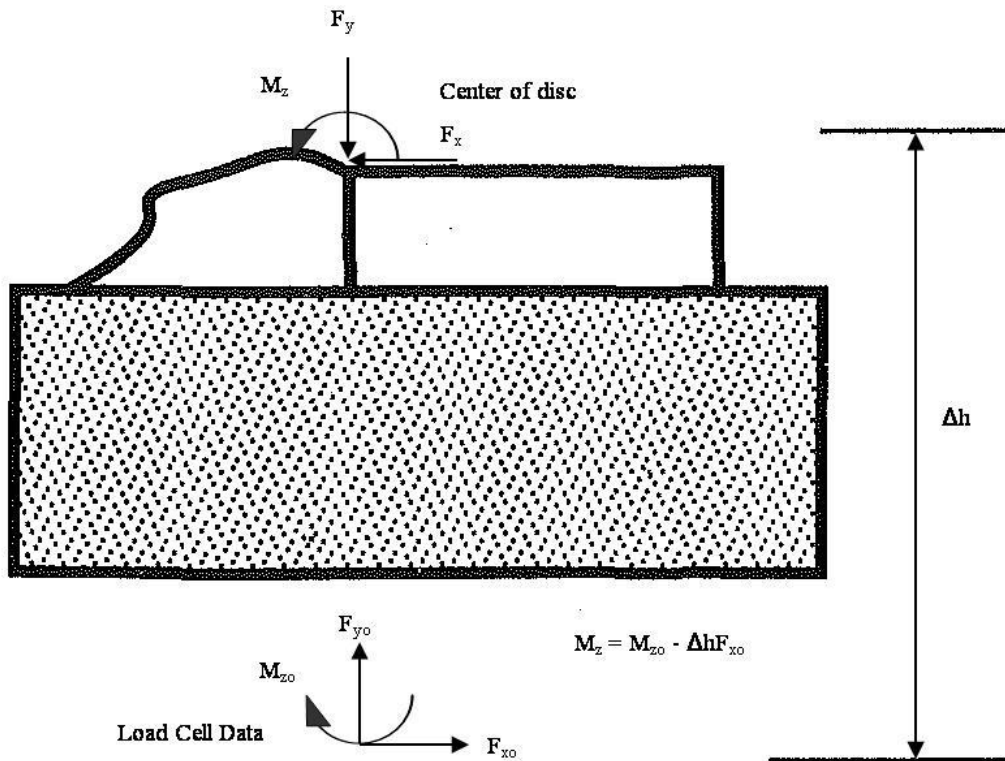


Figure 4-10: Adjustment of Force Moment Reading

Once the resultant moment was found, it was plotted against rotational angle to produce the desired graph (Figure 4-11).

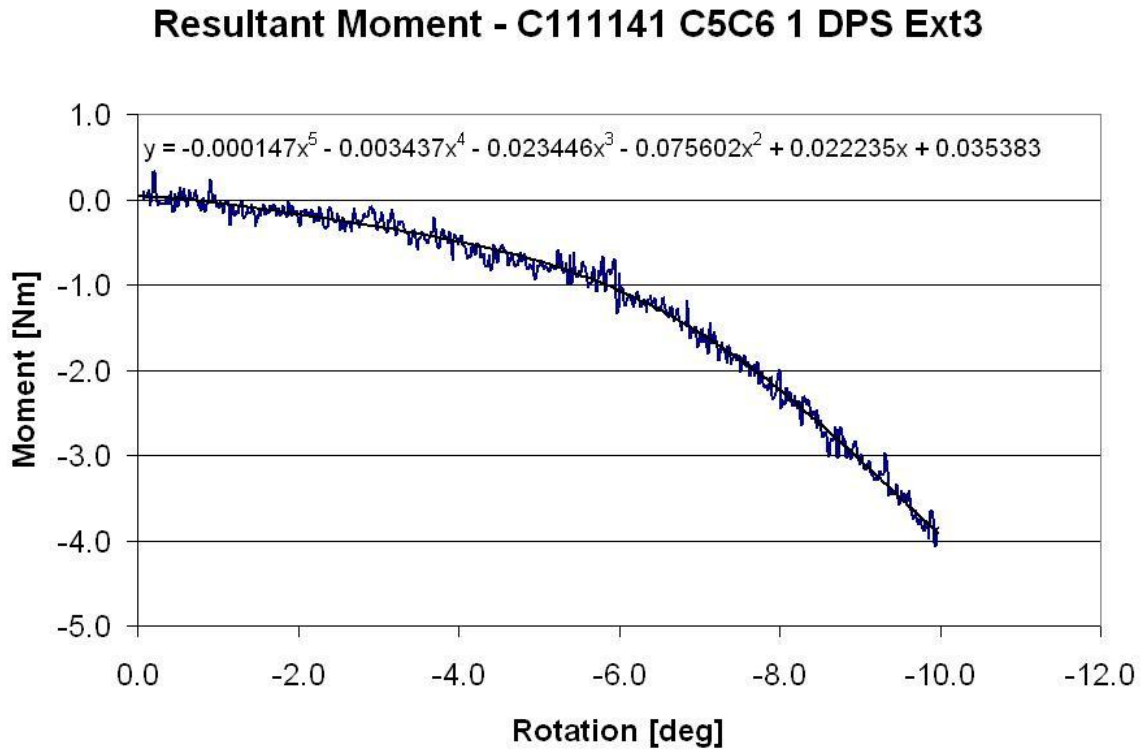


Figure 4-11: Sample Resultant Moment Graph

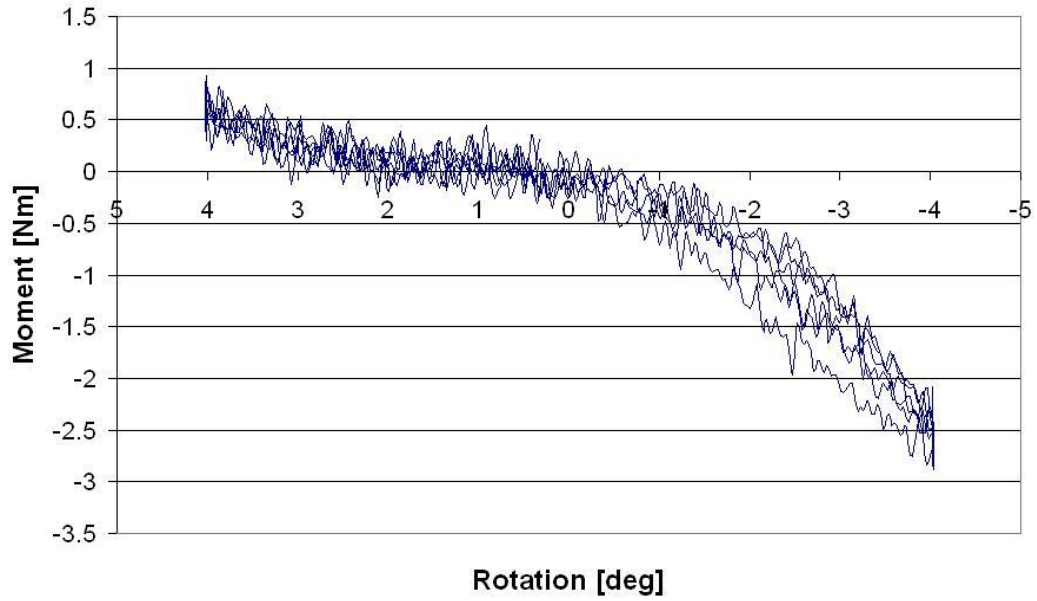
4.4.2 Preconditioning

Samples were preconditioned to four degrees in flexion and extension for ten cycles at an angular velocity of one degree per second. The objective of preconditioning is to untangle the collagen and elastic fibres, and align them in the direction of loading (Fung 1993). After being unloaded for a long period of time post-mortem, the fibres need to be loaded and unloaded to reestablish in vivo properties. It has been shown that as the fibres altered their alignment to match up with the direction of loading, the material properties of the ligament weakened (Quinn et al. 2011). After preconditioning cycle, the stiffness of the tissue dropped until it reached a steady-state. The drop in stiffness between the 1st and 2nd cycles was greater than the drop between the 2nd last and the last cycle.

Determining the preconditioning strain and the number of cycles is a compromise between sufficient preconditioning and damage to the tissue. Cheng et al. (2009) reported that different preconditioning procedures affected test results, even if the testing procedure after preconditioning remained constant. The preconditioning procedure has not been reported well by previous segment level studies; only Nightingale et al. (2002, 2007) documented their procedure, which consisted of 30 cycles up to 1.5 Nm in flexion and extension.

Preconditioning made it possible to find the point of transition between flexion and extension. It is important to find this point because if the rotation does not begin at zero moment, zero rotation, the data will be skewed and it cannot be properly compared against finite element models or previous experimental studies. The segments were potted with care to align the axis of rotation and ensure that the segments are in their natural position. However, after loading the segments into the test apparatus, the center point where the moment is zero (transition between flexion and extension) had to be located. After a few cycles of preconditioning, the data was analyzed to find the offset of the center point. The machine was then rotated to adjust for this offset to determine the actual center point of the segment, and then the 10 cycle preconditioning procedure commenced. Figure 4-12 shows how the initial preconditioning found that the motion transitioned from flexion to extension at 1.5 degrees. After the machine was shifted by 1.5 degrees, the absolute flexion and extension moment curves mirror each other about the origin, indicating that the motion does transfer from flexion to extension at zero degrees.

C111141 C3C4 Preconditioning1



C111141 C3C4 Preconditioning2

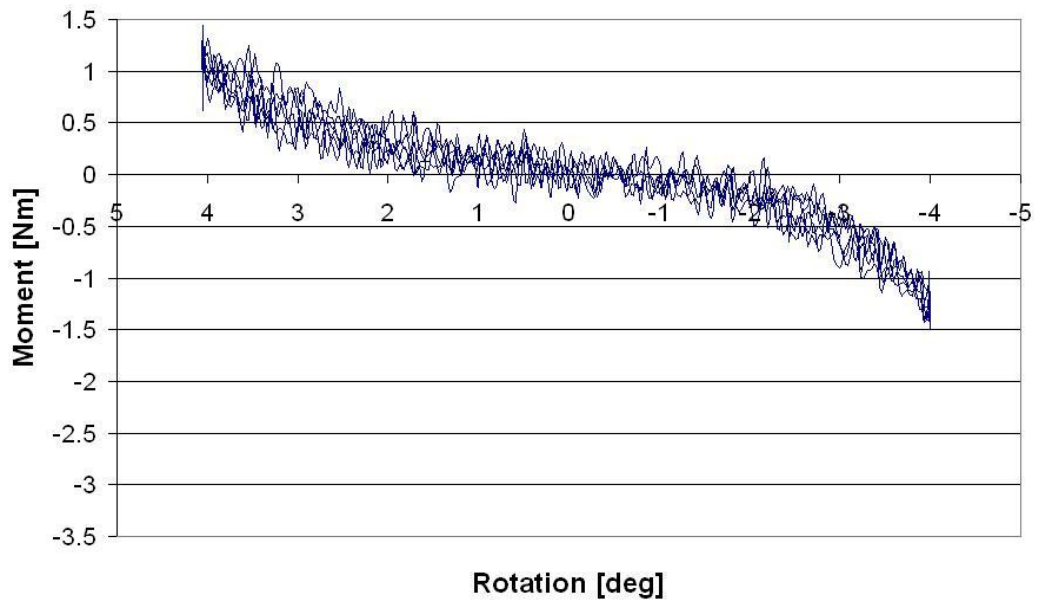


Figure 4-12: Precondition - Finding the Center Point

4.4.3 Preload

Numerous studies have debated the need for a preload and the effect it has on spine stiffness. This debate has been mostly concerned with moment-controlled apparatuses. Cripton et al. (2000) proved that the actual moment applied may not be the desired moment due to variances in the way the preload was applied and how the machine was built. Cripton et al. (2000) altered the preload application method with a system of guides and wires to change the line of action of the preload during flexion or extension. The difference between the actual moment applied and the desired moment was called an “artifact” moment because it was due to machine setup. As for the preload itself, Patwardhan et al. (2003) found a positive correlation between spine stiffness in flexion and extension, and preload. As the preload was increased, the stiffness of human lumbar segments also increased. Stokes et al. (2002) reported the same trend with porcine lumbar spine segments. Thompson et al. (2003) hypothesized that increasing the preload compresses the disc (possibly beyond in vivo conditions), and the stiffness will increase in flexion and extension if the disc has been pre-compressed.

Ideally, the preload would match in vivo conditions; however there has not been any research that has reported the in vivo load on the disc. It is possible that the preload is equal to the weight of the head, but this ignores any musculature effects. Therefore the preload was set to zero for all tests.

4.4.4 Flexion and Extension Tests

Each segment was tested at one degree per second and 500 degrees per second in flexion and extension, and each test was repeated three times to verify repeatability. The C2-C3, C3-C4, C4-C5, and C5-C6 segments were tested up to 10 degrees (except for the C5-C6 segment from the S101442 donor spine, which was tested to 8 degrees) and the C6-C7, and C7-T1 segments were tested to 8 degrees. The rotation was limited to avoid damaging the segment after only one test. The first C2-C3 segment tested was damaged because the strain was too large, and some of the ligament fibres failed. One C7-T1 segment was also damaged during testing, and no data was obtained. The maximum rotation was also derived from studies that documented the range of motion of spinal segments, in vivo and in vitro.

The angular acceleration of the servomotor was 56,250 degrees per second, so it took the machine 8.8 milliseconds to accelerate from zero to 500 degrees per second, and another 8.8 milliseconds to decelerate at the end of the test (Figure 4-13). During the initial acceleration phase of 8.8 milliseconds, the servomotor rotated 2.2 degrees.

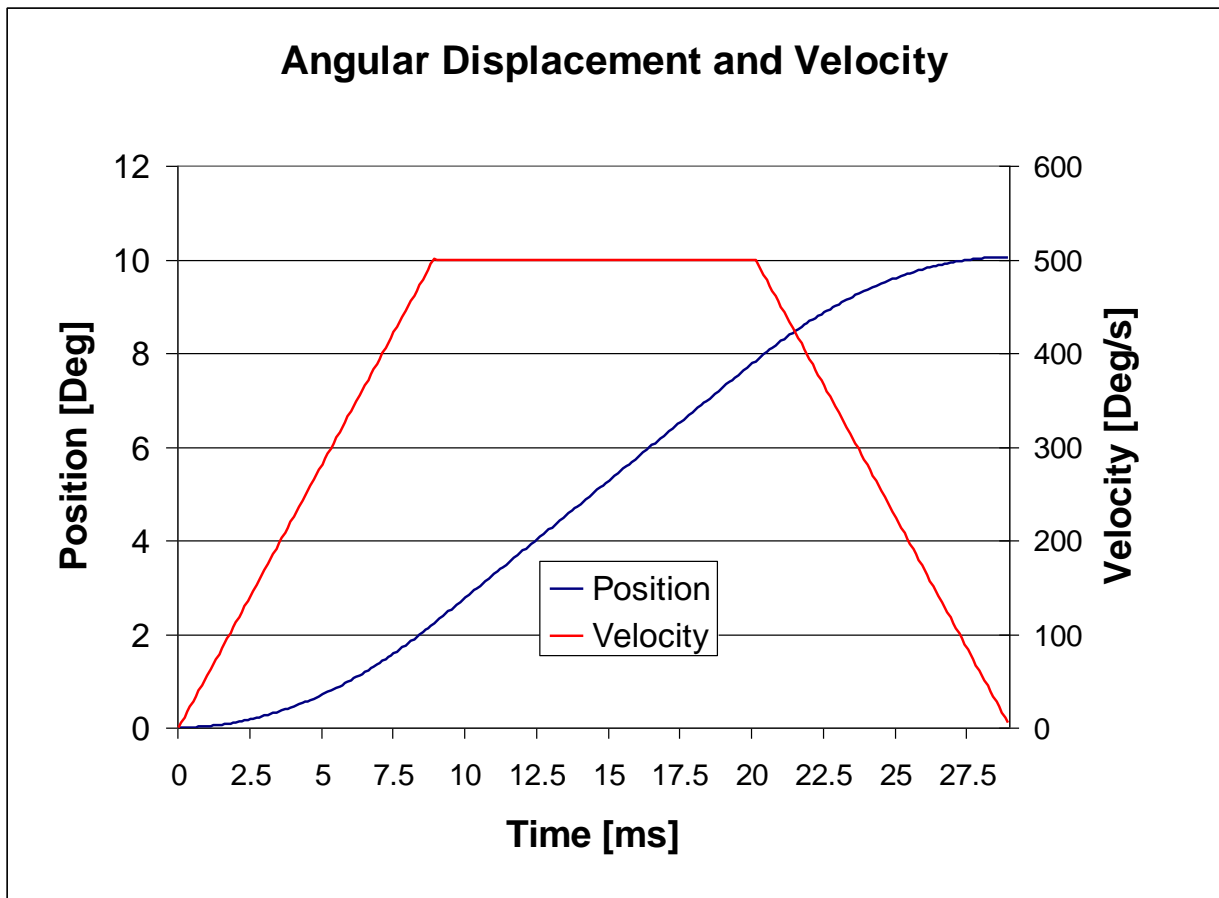


Figure 4-13: Angular Rotation and Velocity versus Time

4.5 Data acquisition

The force and displacement data was recorded with LabView using a data acquisition card (National Instruments, Model 6216). The sampling rate of the low and high speed tests were 100 Hz and 10 kHz respectively. A fourth order Butterworth filter with a 926 Hz cutoff frequency was installed in the electronics of the load cell, which introduced a seven millisecond delay, defined as the time offset between the maximum moment and the maximum rotation of the test. The delay affected the high speed tests only. The delay was equal to 70 data points on average, so the force and moment data had to be shifted accordingly to align it with the displacement data. The displacement and force data was matched up by aligning the peak force and peak rotation. A 5th order polynomial was fit to each test run to eliminate the oscillatory component from the test data and each test was repeated three times to establish repeatability.

4.6 Statistical Analysis

The purpose of the experiments was to determine if there is a significant difference between the response of the segment at low and high rotation rates. Blocking is an effective statistical tool for evaluating the significance of the difference between two means because it compares the average difference against a zero difference instead of comparing the two means on their own. The variability was large from one segment to another at the same level, but blocking essentially negated this variability and focused on the difference between the low and high speed results of each segment.

A fifth order polynomial was fit to every test run, and at least three tests runs were done for each segment at low and high speed. Typically, the second and third curves were almost identical, and the first test run was much stiffer because the preconditioning only went up to four degrees. The second or third curve was chosen for the statistical analysis since it was a better representation of the segment response. Therefore, there was one representative curve for the low speed test, and one for the high speed test at each segment level. There were four samples for each segment level (except for C7-T1 which only had a sample size of three).

For each segment, in flexion and extension, the difference between the resultant moment at low speed and high speed was calculated at each degree of rotation. If there was no rotation rate effect, there should have been no difference between the resultant low and high speed moments, and a paired t-test, or a paired difference test, was used to test for the significance of the rotation effect.

Chapter 5

Segment Finite Element Model Description

The cervical spine model used in this thesis was developed at the University of Waterloo for the Global Human Body Models Consortium (Fice et al. 2009). The explicit finite element model had already been developed by the GHBMC group at the University of Waterloo before the experimental work in this thesis was conducted. The segment models were taken from the whole spine model and compared with the experimental segment results. The model was representative of a 50th percentile male. This section will only focus on the body parts included in the segment models: the vertebrae, the intervertebral discs, and the ligaments (including the facet joints). The muscles and cardiovascular tissues were removed from the segment models. The material properties and mechanical models were derived from the experimental research that was reviewed earlier in this thesis. The model was developed for the LS-DYNA explicit finite element software (LSTC, Livermore, CA) and the test runs were done with version R4.2.1. The full cervical spine model, including skin tissue and the skull, consists of 4,458 beam elements, 95630 shell elements, and 204,180 solid elements for 304,268 elements in total (Figure 5-1).

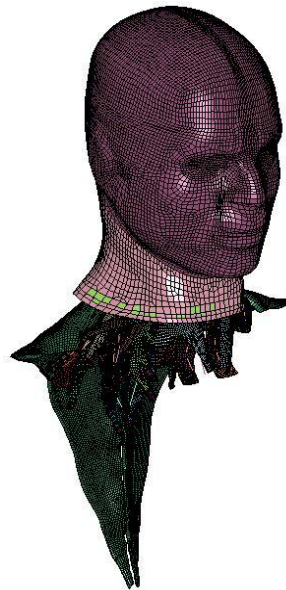


Figure 5-1: Full GHBMC Neck Model

5.1 Vertebrae

GHBMC performed CT and MRI scans on a 50th percentile male cadaver (Gayzik et al. 2011) in the seated position to obtain the whole body geometry, including the geometry of the individual vertebral bodies (Figure 5-2, 5-3). The T1 and the skull were modeled by other institutions involved in the GHBMC project, but their detailed models were not available earlier on. Therefore, a course mesh of the skull and the T1 were made and added to the cervical spine model so that full spine impact and C7-T1 segment simulations could be run.

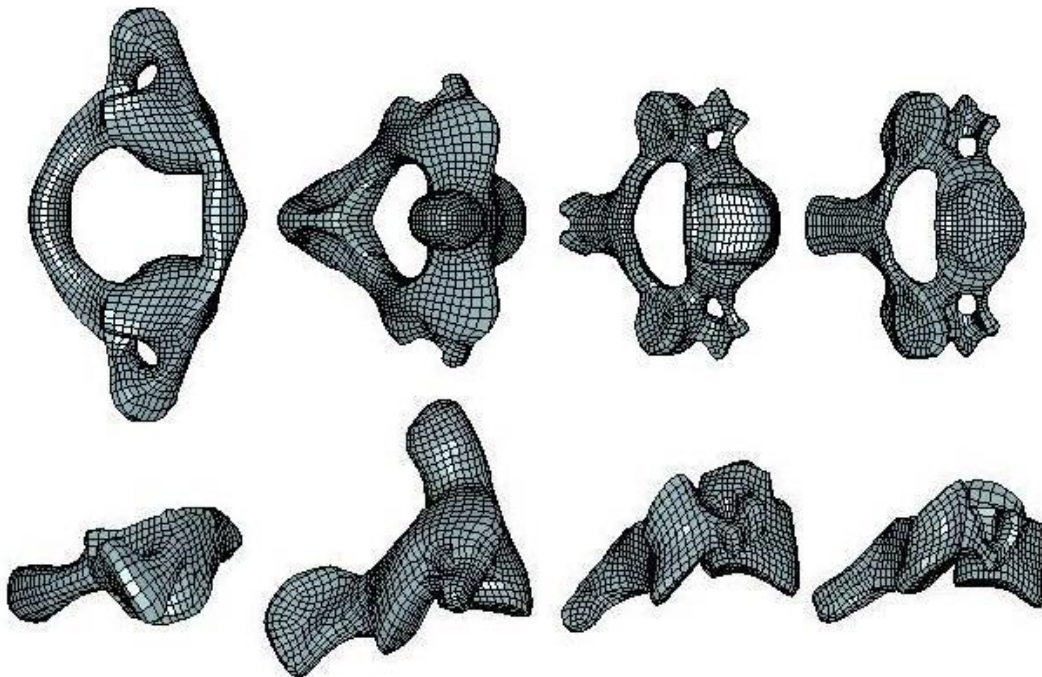


Figure 5-2: Top and Side View of C1 through C4



Figure 5-3: Top and Side View of C5 through T1

The minimum element edge length was approximately 1mm in order to accurately predict loading and vertebral fractures. Whereas the previous UW model used a rigid body model for the vertebral (Panzer 2006), which did not allow failure, the GHBMC model used a plastic kinematic material model for the cancellous and cortical bone (Table 5-1). The plastic kinematic material model is very simple: the elastic region is linear with the slope being the elastic modulus, and the plastic region is also linear with a slope called E_{plastic} . The two linear regions are separated at the yield stress (σ_y), and the bone finally fails in the plastic region once it reaches the failure strain. The mechanical properties inputted into the model are compressive (Reilly et al. 1975, Cowin et al. 1988).

Table 5-1: Mechanical Properties of Cortical and Cancellous Bone in the Model

	Cortical	Trabecular
E [GPa]	18.44	0.442
σ_y [MPa]	190	2.83
E_{plastic} [GPa]	1.2489	0.0301
Failure Strain	0.0178	0.095

The vertebrae are composed of cortical and cancellous bone, and these two bone types were modeled with separate element types. Cortical bone was represented by solid elements, and the cortical exterior of the vertebrae was represented by shell elements (Figure 5-4).

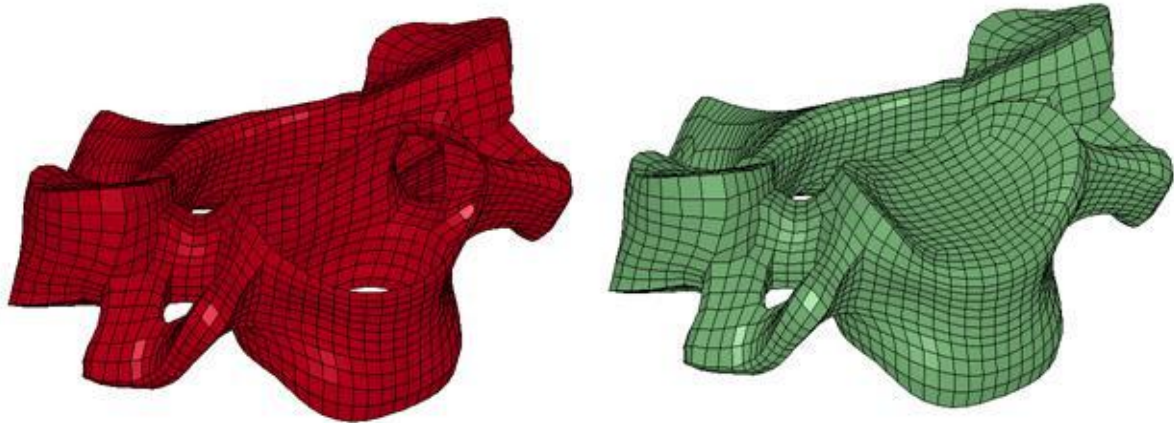


Figure 5-4: Vertebra Cortical Shell [red] and Cancellous Interior [green]

5.2 Intervertebral Discs

The annulus fibrosus was modeled by five pairs of concentric rings of shell elements. The concentric rings allowed for material property variance in the radial direction, but not in the circumferential direction. The shell elements were placed inside the ground substance which was modeled by solid elements. The ground substance had a thickness of four solid elements in the radial direction, and a pair of annulus fibrosus ring shell elements shared every node at each level in the radial direction (Figure 5-5).

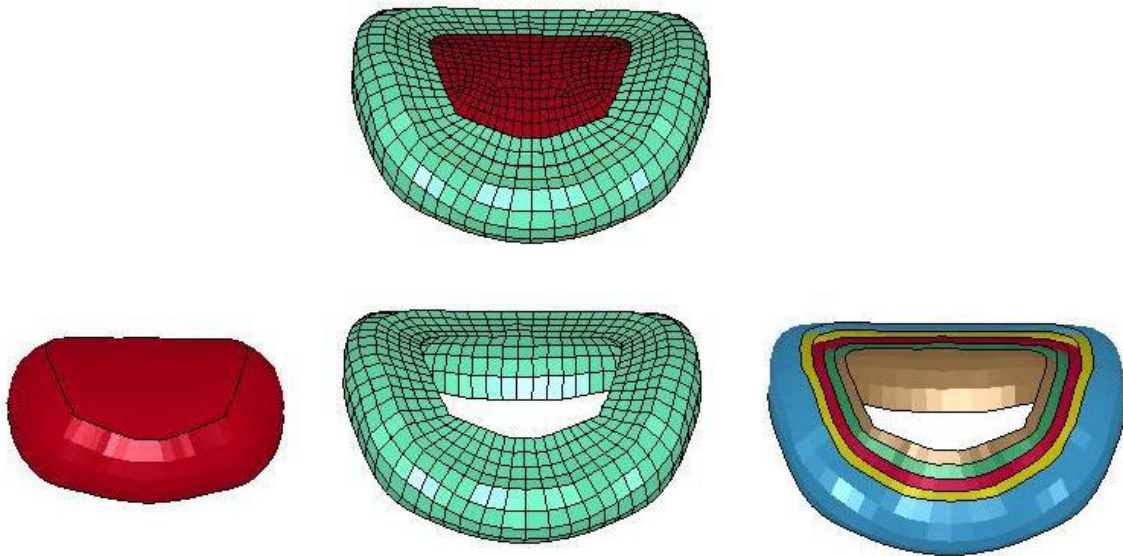


Figure 5-5: Nucleus Pulposus [left], Ground Substance [center], Annulus Fibrosus Layer [right]

The nucleus pulposus was modeled as an elastic fluid with a bulk modulus of 1.72 GPa and a density of 1.36 g/cm^3 . These values were based upon the experimental work done by on the nucleus pulposus in shear (Iatridis et al. 1996).

The properties of the ground substance were derived from the work of Fujita et al. 1997 and Elliot et al. 2001, who studied the strength of the annulus fibrosus in the radial direction. The fibres were all perpendicular to the radial direction and had no influence on the results, so the materials properties from these studies were for the ground substance alone. The Hill constitutive foam model (Hill 1978) model was used for the ground substance, and the experimental data was fit to the material model (Panzer et al. 2006). Although the properties of the ground substance were site dependent (Fujita et al. 1997), this model did not take that into account since the differences were not that significant and the fibres played a much more important role in the strength of the annulus fibrosus than the ground substance. Another important feature of the disc model was the number of solid elements through the thickness of the disc; the GHBMC model used small enough elements to have a thickness of four solid elements, which improved the model accuracy (Panzer et al. 2009).

The model material properties for the fibres of the annulus fibrosus were derived from the research of Holzapfel et al. 2005. It was also reported by Holzapfel that the strain rate effect was not significant for the annulus fibrosus fibres. This study published stress strain curves for the inner and outer fibres of the disc, and these curves were interpolated to get five separate stress strain curves for each pair of concentric fibre rings in the model (Figure 5-6). These curves were input into a fabric model in LS-DYNA. The fabric model allowed for the angle of the fibre, relative to the transverse plane, to be varied from 25 degrees at the inner layer to 45 degrees at the outer layer.

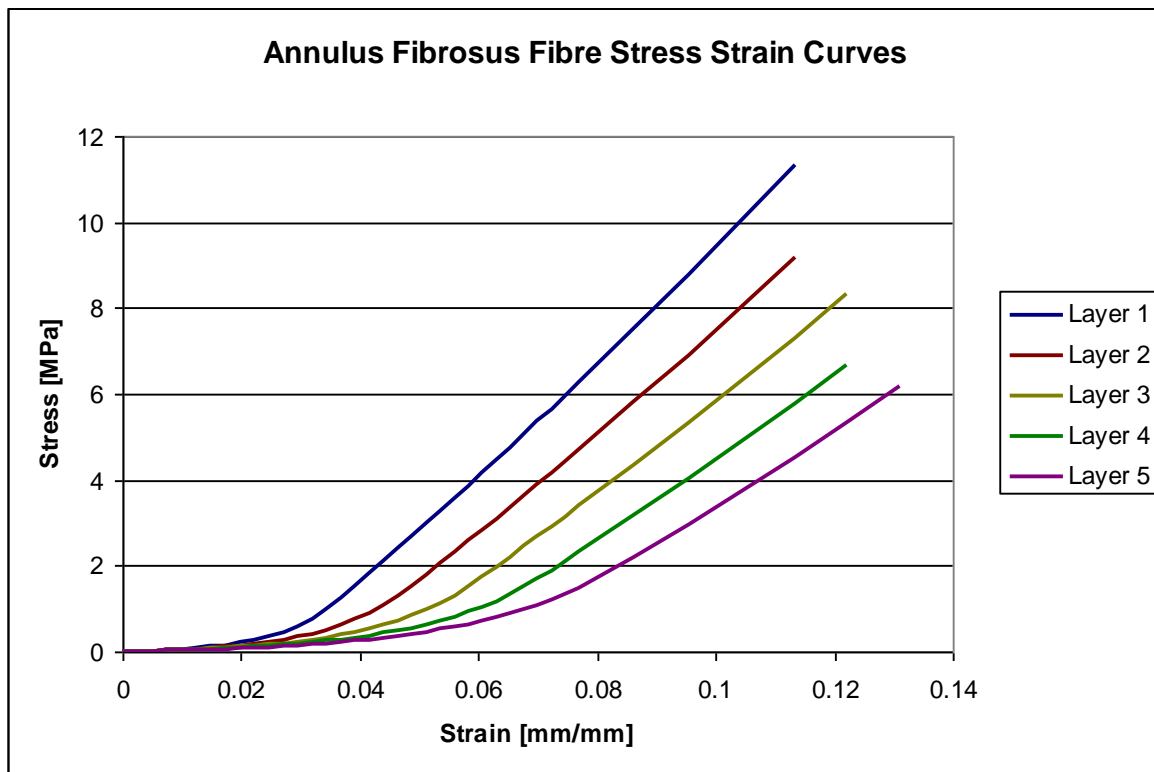


Figure 5-6: Stress Strain Curves for each Annulus Fibrosus Layer

5.3 Ligaments

One of the largest improvements of the GHBMC model over earlier model developed by the University of Waterloo (Panzer et al. 2006) was the ligament material properties. The material properties of the earlier model were derived from an experimental ligament study where the mean cadaver age was 68 (Yoganandan et al. 2000). The ligament properties used in the GHBMC model were from the research of Mattucci et al. (2012), where the average donor age was 44 years old. The younger population had much stiffer ligaments and this was more representative of the target 50th percentile male for the GHBMC project.

The ligaments were modeled by one-dimensional beam elements that can only carry load through tension. Multiple beam elements were used to represent each elements and the force was spread evenly between the elements. The extra elements also made it possible to institute progressive failure by deleting each beam element after it reached a certain displacement (failure displacement). For example, the anterior longitudinal ligament was modeled with seven beam elements across the anterior surface of the disc and the two vertebrae (Figure 5-7). There were three pairs of symmetric beam elements and the seventh beam element was in the center. The outside pair of elements had a lower failure displacement and failed first while the center beam had the highest failure displacement and it failed at the end.

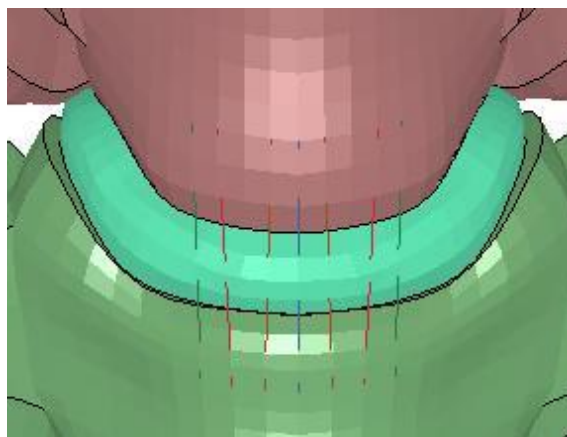


Figure 5-7: 7 Beam Elements Representing the ALL

The force displacement curves were derived from the research of Mattucci et al. (2012). The study developed generic load curves for each ligament and it can be scaled depending on the spinal level. Once the beam element hit the ultimate force of its load curve, the force stayed constant until the element failure displacement is reached (Figure 5-8). Since there were multiple beam elements representing each ligament, progressive failure of the ligaments was instituted by varying the failure displacement of each beam element (Mattucci 2011). The material properties of the ligaments are not represented by a model, but instead the properties are defined by the load curves in the input file.

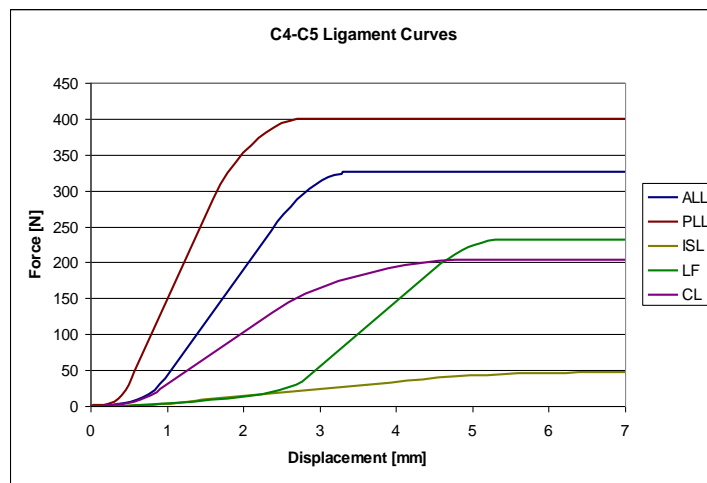


Figure 5-8: Quasi-static Load Curves of each Ligament

Another improvement in the GHBMC model over the older UW model was ligament strain rate sensitivity. The force-displacement response of ligaments was dependent on the strain rate (Yoganandan et al. 1989, Shim et al. 2005, Bass et al. 2007, Ivancic et al. 2007, Mattucci et al. 2012), and the beam elements were modified to accommodate the influence of strain rate. Based on the experimental results of Mattucci et al. (2012), two extra load curves were added to the material properties to modify the original force displacement curve: one curve scaled the force values depending on the strain rate, and the other curve scaled the displacement to alter the shape of the curve and made it fit with the experimental results.

5.4 Facet joints

The facet joints in the model were made up of solid elements, representing the cartilage on the surfaces of the articular processes, and beam elements surrounding the joint, representing the capsular ligaments (Figure 5-9). The synovial fluid contained within the facet joint was not modeled due to a lack of experimental research into its material properties and model instability when the volume between the joint is compressed to zero. In the previous UW model, the synovial fluid was modeled by air bag segments in the space between the cartilages (Panzer et al. 2006), but it was omitted from the GHBMC model.

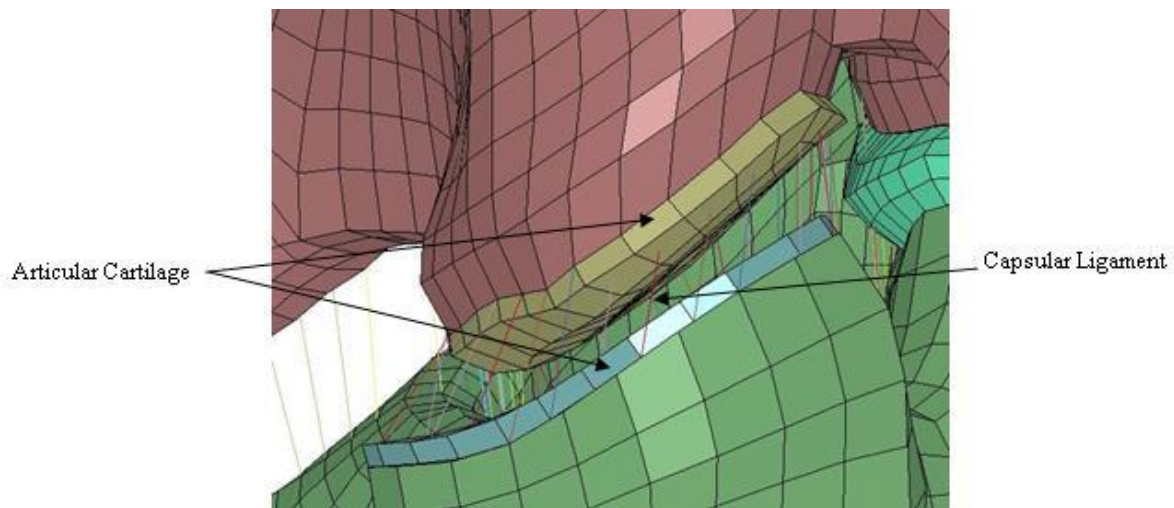


Figure 5-9: Closeup of Model Facet Joints

The articular cartilage was modeled by a single layer of solid elements with a quasi-linear viscoelastic material model. Cartilage is a porous material dependent on its permeability during compression. However the permeability was ignored in the model because it was assumed that the total compression and compression rates seen by the cartilage during automobile accidents were not large enough to cause fluid loss. There was also a lack of data on the material properties of human articular cartilage and so the properties used in the model were derived from bovine testing (DiSilvestro et al. 2001). The properties in the GHBMC model were the same as the older UW model (Panzer et al. 2006). The older UW model used a quasi-linear viscoelastic (QLV) model formulation to represent

the cartilage (Table 5-2). The QLV model consisted of a stress relaxation summation equation containing two variables: G_i (the stress relaxation term) and β_i (the stress decay term). The strain rate sensitivity was accounted for by a convolution integral.

Table 5-2: Mechanical Properties in the model of the Articular Cartilage

i	G_i [MPa]	β_i [1/s]
1	0.2100	1E-06
2	0.0243	3.0300E-03
3	1.0824	8.0807E-02
4	1.9984	1.2927E-02
Bulk Modulus - 2 GPa		

The capsular ligament was modeled with four groups of seven beam elements evenly distributed around the facet joint. Once again, each group of beam elements followed the same force displacement curve, but the displacement to failure was staggered to model progressive failure of the ligaments. The capsular ligament had a much lower failure force than the other ligaments, but it also had a higher range of motion than all the ligaments except for the ligamentum flavum.

5.5 Application of Flexion and Extension Moments

The purpose of the modeling was to investigate the segment in flexion and extension and compare the predictions with the experimental data. To accurately compare the model and the experimental tests, the boundary conditions had to be identical. The most important boundary condition of the experimental testing was the fixation of the axis of rotation of the machine about the instantaneous axis of rotation of each segment (Amevo et al. 1991, Bogduk et al. 2000). In previous experimental studies, the moment was applied to the superior segment and it was free to displace or rotate about any given point (Nightingale et al. 2002, 2007, Wheeldon et al. 2006). This situation was easy to replicate in a model because a pure moment was applied to the top of the superior segment and that segment was unconstrained in all six degrees of freedom. (Panzer 2006).

In order to apply the moment, a rigid body of shell elements was attached to the exposed surfaces of the vertebral bodies. This rigid body shared the top layer of nodes with the solid elements of the vertebral body since there were no shell elements representing cortical bone on the superior and inferior surfaces of the vertebral bodies (Figure 5-10). For simulating the experimental testing, the inferior rigid body was fixed, and a rotation was applied to the superior rigid body. For the low speed tests, the model parameters that considered strain rate sensitivity were deleted, and for the high speed tests, the rotation versus time curve was identical to the experimental testing (Figure 4-13).

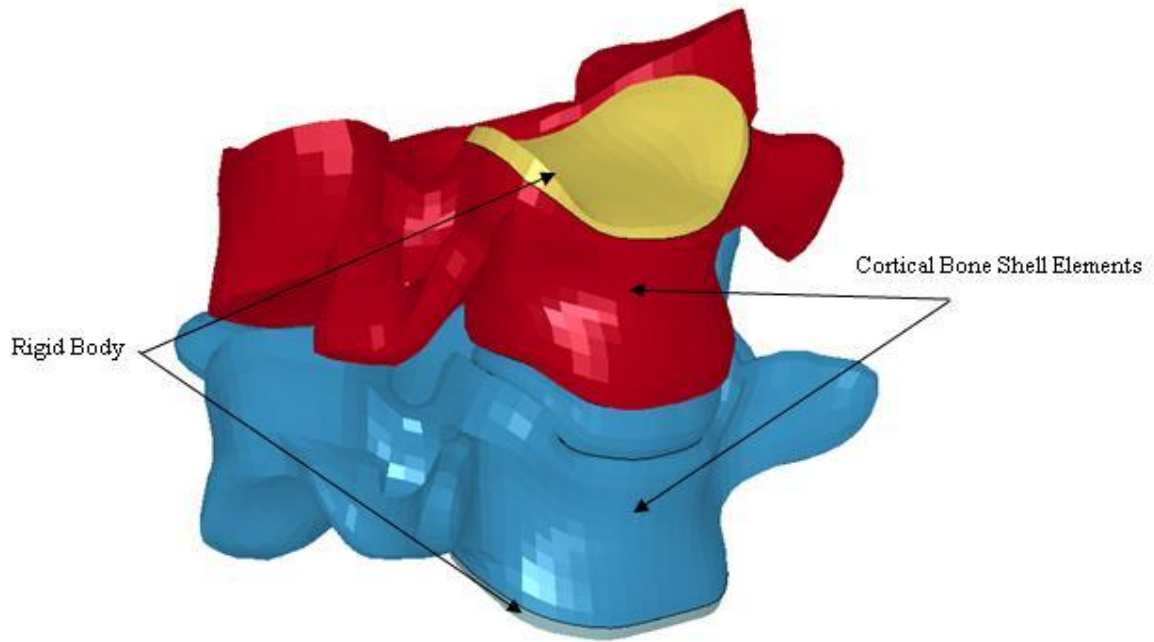


Figure 5-10: Rigid Bodies attached to the Vertebrae for Moment Application

The key to the modeling was fixing the axis of rotation of the moving rigid body. The rigid body was defined in LS-DYNA by a PART_INERTIA card, which gave the rigid body its mass, density, and moment of inertia about six axis. The model code can calculate its own center of mass, or the center of mass can be defined and since it was a rigid body, the code automatically constrained the axis of rotation about the center of mass.

Chapter 6

Experimental and Model Results

6.1 Experimental Results

For ten degrees of rotation in flexion at one degree per second, the average moments (with standard deviation) for the C2-C3, C3-C4, C4-C5, and C5-C6 segments were 7.2 Nm, 5.1 Nm, 5.2 Nm, and 5.5 Nm, respectively. At the higher rotation rate of five hundred degrees per second, the average moments for these segments were 9.2 Nm, 6.2 Nm, 6.2 Nm, and 7.6 Nm respectively. The C6-C7 and C7-T1 segments were only rotated to eight degrees in flexion. For C6-C7, the average moment was 8.8 Nm and 10.0 Nm at one degree and five hundred degrees per second, respectively. The moment at one degree per second was 12.2 Nm for the C7-T1 segment, and the moment for the same segment was 19.0 Nm at the higher loading rate.

For ten degrees of rotation in extension at one degree per second, the average moments for the C2-C3, C3-C4, and C4-C5 spines were 12.3 Nm, 11.2 Nm, and 8.7 Nm, respectively. At five hundred degrees per second, the moments for these segments were 13.7 Nm, 13.5 Nm, and 10.4 Nm respectively. The C5-C6, C6-C7 and C7-T1 segments were only rotated to eight degrees in extension. The measured moments for the C5-C6 segment were 5.0 Nm and 6.7 Nm for the low and high loading rates, respectively. For C6-C7, the moments were 8.2 Nm and 9.1 Nm at one degree and five hundred degrees per second, respectively. The maximum moment at one degree per second was 13.2 Nm for the C7-T1 segment, and the maximum moment of the same segment 14.5 Nm at the higher loading rate. The average response curves for low and high rate testing in flexion and extension are shown for each segment level (Figures 6-1, 6-2). The blue and red curves are the one and five hundred degree average response curves respectively. The error bars show one standard deviation from the average.

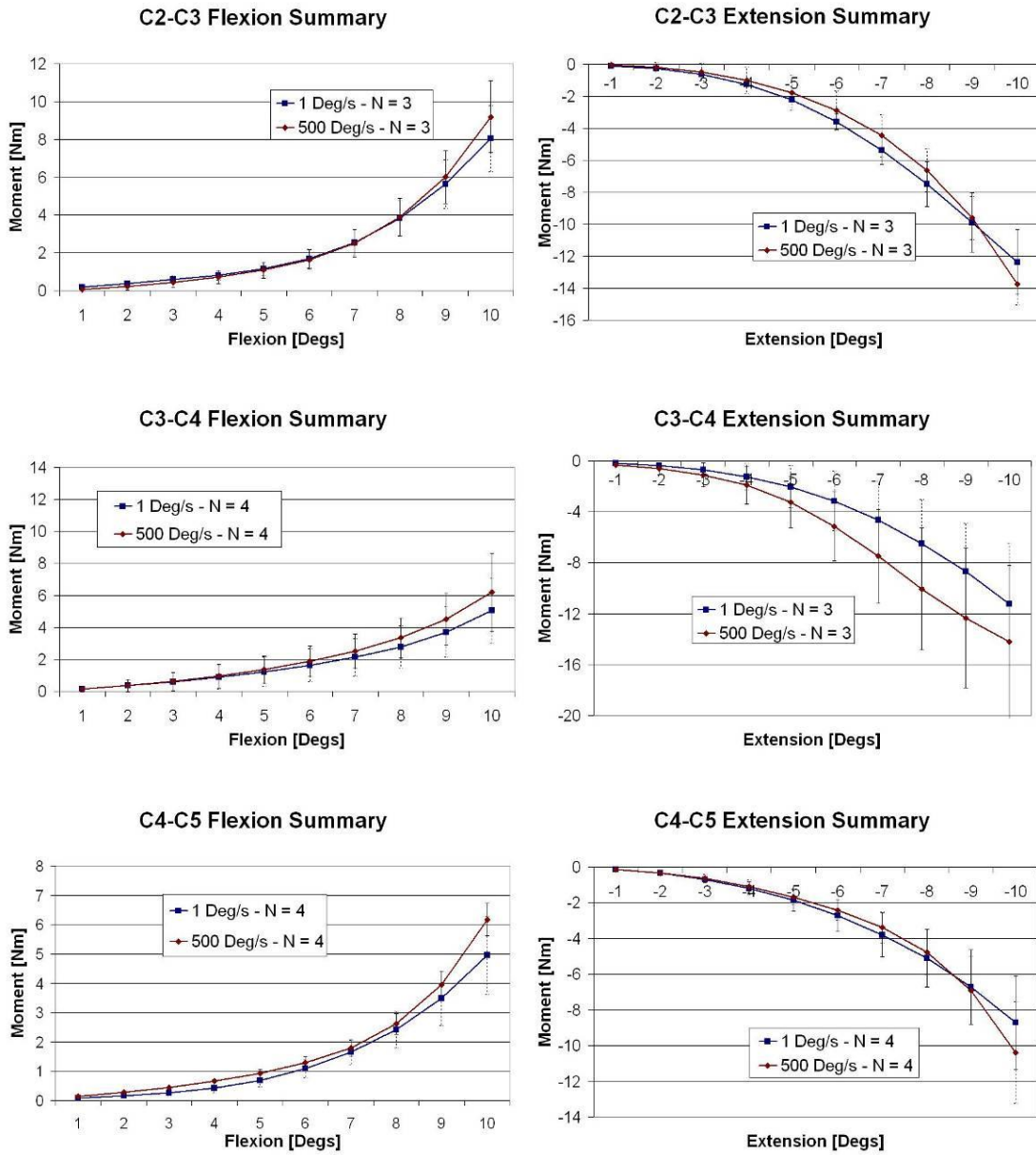


Figure 6-1: C2-C3, C3-C4, C4-C5 Experimental Results – Low and High Speed Tests

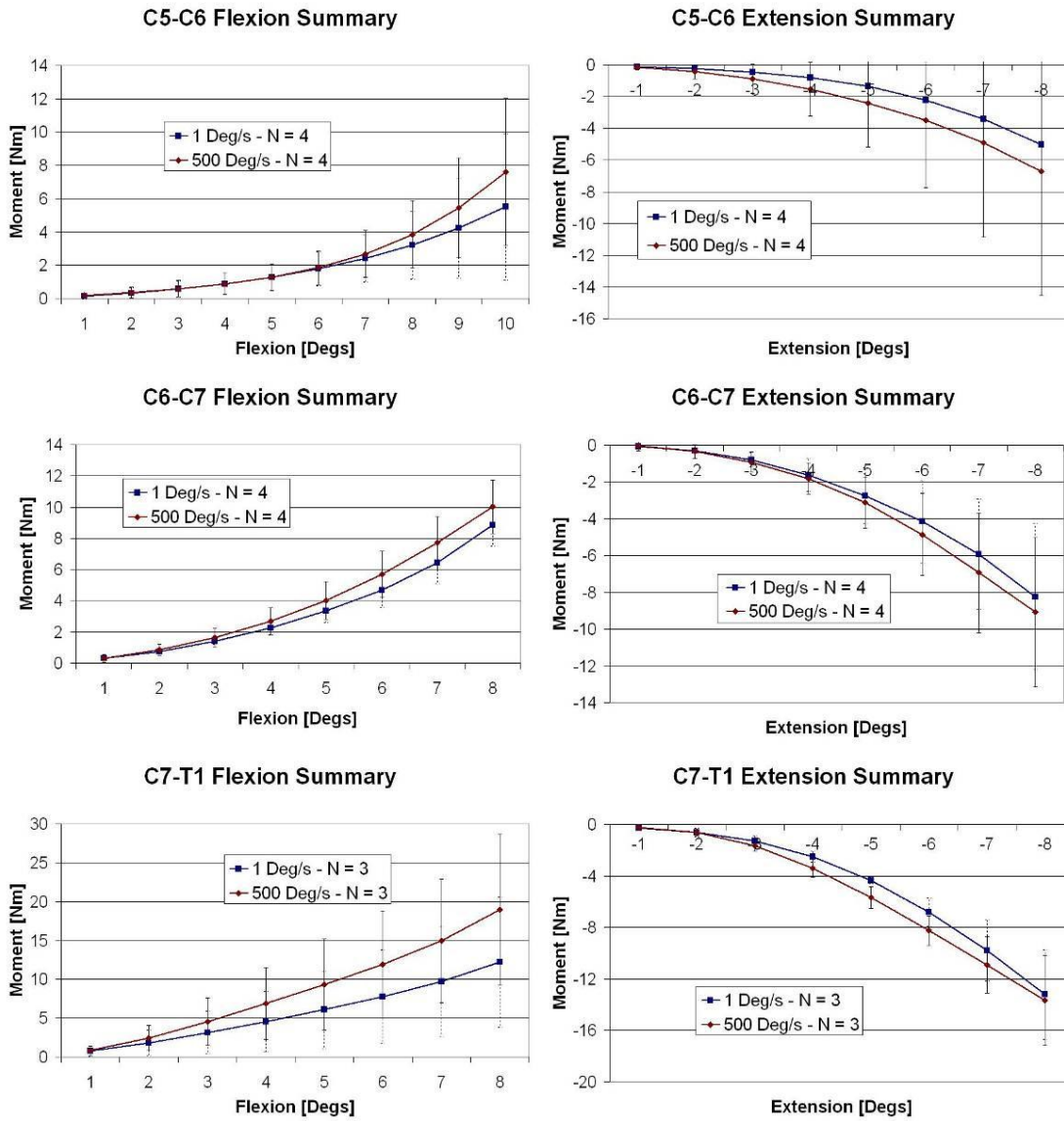


Figure 6-2: C5-C6, C6-C7 & C7-T1 Experimental Results - Low and High Speed Tests

Table 6-1 shows the results of the statistical test comparing the difference between the maximum moment of the low and high rate tests for each segment level. At each segment level, there were three or four test specimens, and each specimen was tested at one and five hundred degrees per second. A paired t-test is used to calculate the significance between the two means. Instead of comparing the average of the slow rates tests and the average of the high rate tests, the difference between the slow

and high rate tests of each segment was examined. The results in the table show the p-value of each test, which indicates the significance of the test. P-values below 0.05 (green shaded cells in Table 6-1) indicate that there is significant evidence of a difference between the low and high rate tests, values less than 0.10 (yellow) indicate marginal evidence, and values above 0.10 (red) reveal no evidence of a significance difference between the two means.

Table 6-1: P-value of the Statistical Test Comparing Low and High Rate (Maximum Rotation)

Summary	C2-C3	C3-C4	C4-C5	C5-C6	C6-C7	C7-T1
Flexion	0.11	0.04	0.05	0.03	0.01	0.11
Extension	0.21	0.07	0.05	0.04	0.03	0.07

6.2 Model Results

The experimental results were compared against the model. Figures 6-3 and 6-4 show the comparison between the results of the low and high speed experimental and model tests. The blue curves represent the experimental results, and the red curves are the model results. The darker colour shades denote the low speed tests, while the lighter red and blue are the high speed test curves. The solid black errors bars represent one standard deviation from the mean for the low speed experimental testing, and the dotted errors bars represent one standard deviation from the mean for the high speed experimental testing. The comparison shows that there were significant disagreements between the baseline one degree per second tests of the model and the experiments, and there were differences between the actual and predicted strain rate effect.

In flexion, the model was stiffer than the experimental results at the C2-C3 through C5-C6 levels. The model results were outside of one standard deviation from the low and high speed experimental mean at these levels except for the low speed C2-C3 response. From C2-C3 through C5-C6, the strain rate effect (the difference between the low and high speed curves) was more significant in the model than the experimental testing. At the C6-C7, the model and the experimental results were in close agreement and the model results fell within one standard deviation from the mean of the low and high speed experimental results. The low speed curves and the high speed curves matched up together, indicating that the model conformed to the strain rate sensitivity shown by the segment testing. At the C7-T1 level, the experimental testing was stiffer than the model, although the difference between

the strain rates was similar and the model results at both angular displacement rates fell within one standard deviation from the mean.

In extension, the model and the experimental testing were in better agreement than in flexion. At the C2-C3 level, the experimental results were stiffer and the model was outside the error bars, but the predicted strain rate effect was similar to the actual strain rate effect. The model matched up closely with the low speed experimental results at the C3-C4 and C5-C6 levels since the model fell within the experimental error bars. However, the model predicted a smaller difference between the angular rotation rates than found in the experimental results. The model and experimental results were nearly identical at the C4-C5 and C6-C7 level, but at the C4-C5 level, the shape of the model and experimental curves were different. The model toe region is less stiff than the testing. At the C7-T1 level, the experimental results were significantly stiffer than the model outcome.

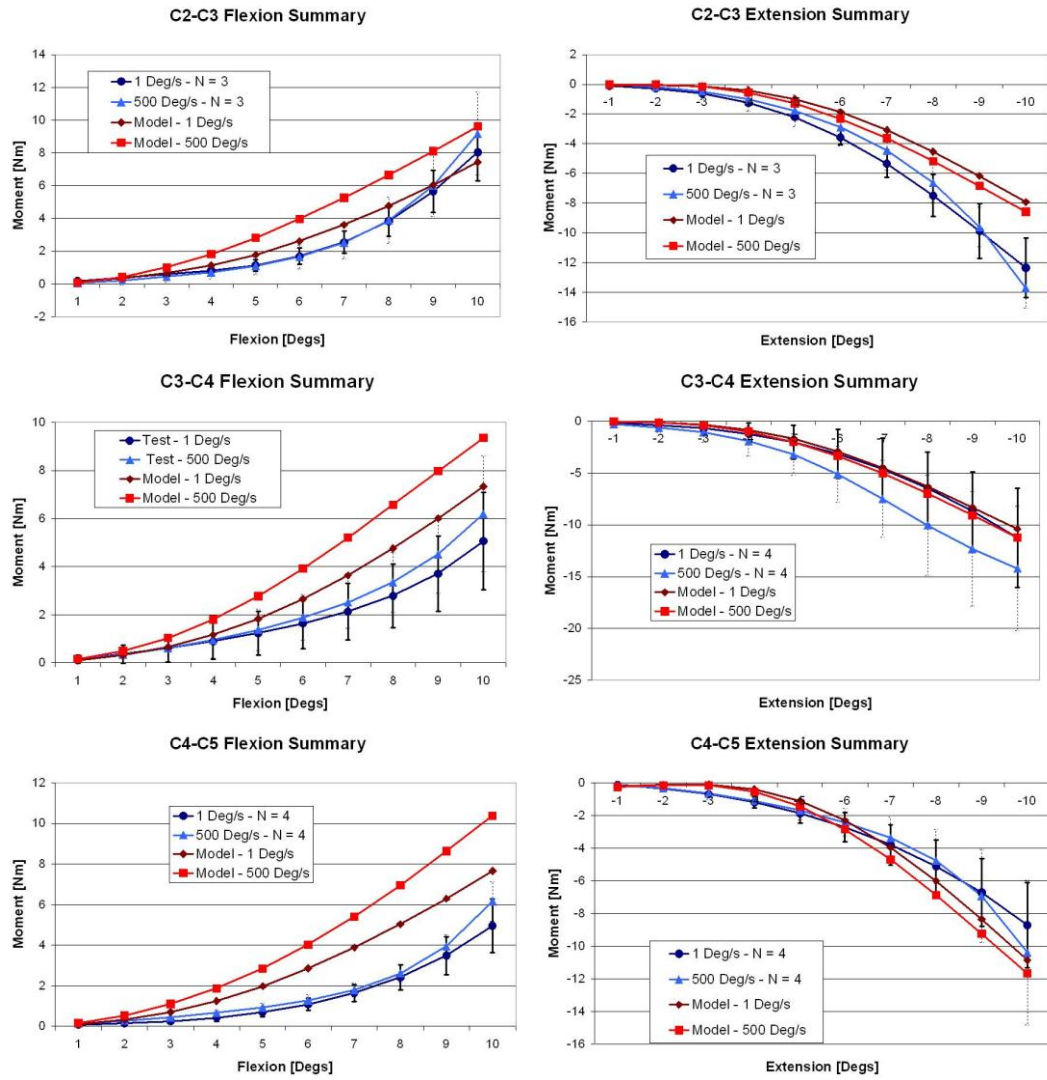


Figure 6-3: C2-C3, C3-C4 & C4-C5 Experimental Testing vs. Model Results

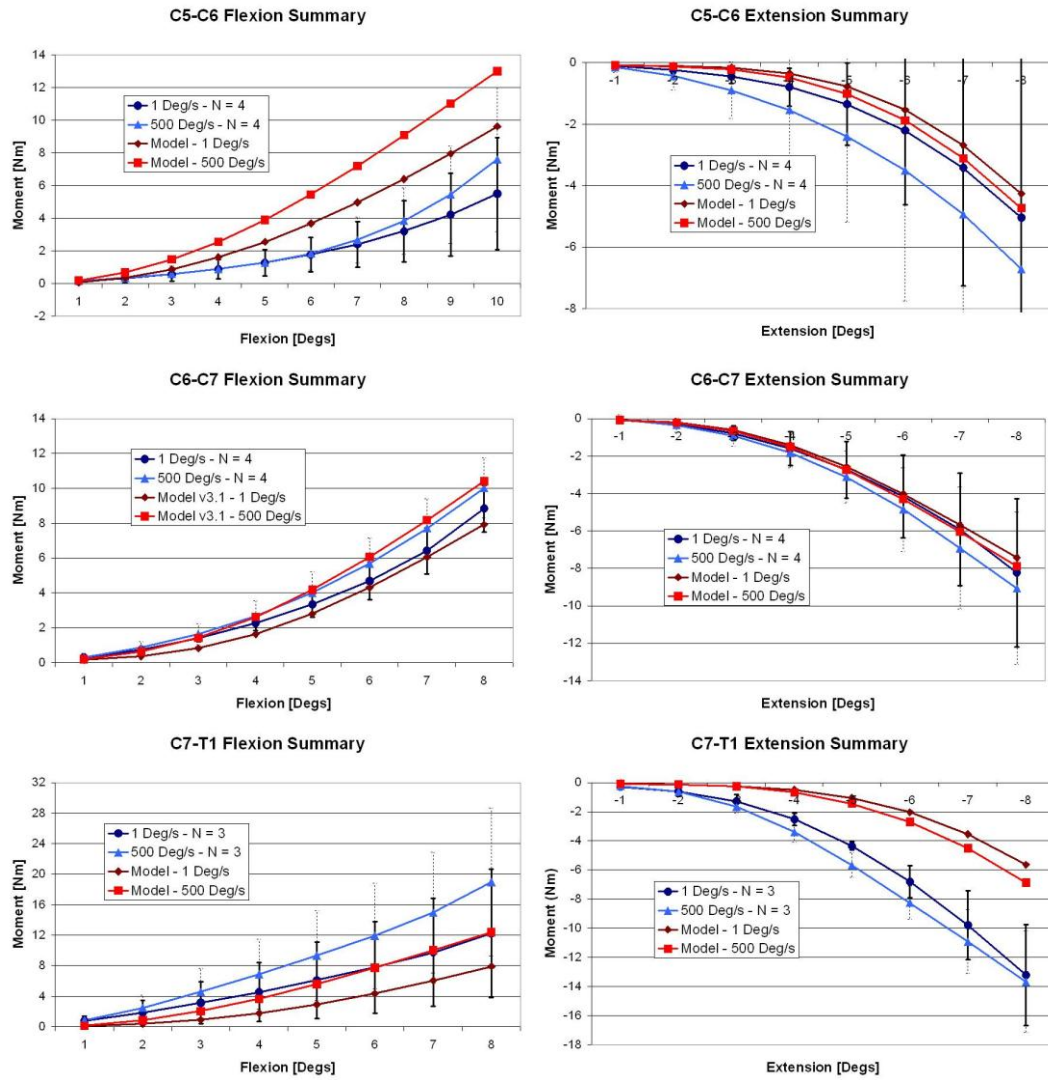


Figure 6-4: C5-C6, C6-C7 & C7-T1 Experimental Testing vs. Model Results

6.3 Discussion

The purpose of this research was to provide segment level validation data for the GHBMC cervical spine finite element model at each segment level from C2-C3 through C7-T1. The GHBMC model represents a younger 50th percentile male, and all nine spines tested in this study were under the age of 50 with the mean age of 45 years old. A major goal of the GHBMC project was to develop a detailed finite element model of the human body that is capable of predicting tissue injury.

The experimental work was conducted because there was a lack of published literature on the response of the neck to high rate loading in flexion and extension. The existing studies were deficient in at least one of the following aspects of model validation: the mean donor age was too high to be representative of a young 50th percentile male (Wen et al. 1993), only quasi-static response was studied (Wheeldon et al., 2006), not all segment levels were tested (Voo et al. 1998), and the range of motion was too low (Panjabi et al. 2001). This study addressed all of these issues. The mean donor age was 45 years, the spines were tested at a quasi-static rate and a high rate, all segment levels were tested from C2-C3 through C7-T1, and the range of motion went up to the physiological limit (Dvorak et al. 1988, 1991).

6.3.1 Strain Rate Effects

There was almost no difference between the low and high speed curves at low rotations (less than six degrees). Tables 6-2, 6-3, and 6-4 show the p-value of the blocking statistical test of the moment at two, four and six degrees respectively. The majority of the p-values were greater than 0.10, which suggested there was no evidence to support the conclusion that the strain rate had an effect on the response. However, Table 6-1 illustrated that the strain rate did play a significant role at 10 degrees of flexion or extension (eight degrees for the C6-C7 and C7-T1 segments and C5-C6 in extension).

Table 6-2: Statistical Comparison for Rotation Rate Effects (2° Rotation)

Summary	C2-C3	C3-C4	C4-C5	C5-C6	C6-C7	C7-T1
Flexion	1.00	1.00	0.03	0.41	0.26	1.00
Extension	1.00	0.08	1.00	0.23	0.36	0.18

Table 6-3: Statistical Comparison for Rotation Rate Effects (4° Rotation)

Summary	C2-C3	C3-C4	C4-C5	C5-C6	C6-C7	C7-T1
Flexion	1.00	0.34	0.08	1.00	0.14	0.31
Extension	1.00	0.06	0.06	0.14	0.08	0.16

Table 6-4: Statistical Comparison for Rotation Rate Effects (6° Rotation)

Summary	C2-C3	C3-C4	C4-C5	C5-C6	C6-C7	C7-T1
Flexion	1.00	0.07	0.12	0.42	0.04	0.18
Extension	1.00	0.10	1.00	0.13	0.07	0.14

The reason for the lack of evidence at low angle of rotations could be explained by the ligament stress strain curve. At low strains, the ligament response was in the toe region. The ligament strain rate effect did not become significant until the response exited the toe region and entered the linear region where the stress was much higher than it was in the toe region. In flexion and extension, the ligament strain increased with increasing rotation. At low rotation, the ligaments were in the toe region, and their contribution to the segment response was small compared to higher rotations. In the toe region, the ligaments were not strained significantly and the force was low relative to the failure force. At higher rotations, the ligament entered the linear region and the ligament strain rate effect was seen in the segment response. The lack of statistical significance also suggests that there may be modest intervertebral disc rate effects at low rotations. However, the contribution of the ligaments and the disc to strain rate effect at low rotations cannot be quantified.

In the model response, there was clearly a greater strain rate effect in flexion than in extension. At relatively low rotations of 10 degrees, it was assumed that the moment arm from the center of rotation to the ligament tensile force remained constant. Therefore, the model strain rate effect in flexion and extension was solely due to the ligament strain rate sensitivity. The annulus fibrosus did not have any high rate properties in the model. In flexion, the posterior longitudinal ligament, the ligamentum flavum, the capsular ligaments, and the interspinous ligament were in tension and in extension only the anterior longitudinal ligament was engaged. The high rate ligament properties in the model were derived directly from ligament experimental testing (Mattucci et al. 2012). In flexion, the model was

more sensitive to the strain rate because there were more ligaments engaged than there were in extension. The horizontal distance of the axis of rotation was closer to the PLL than the ALL in the upper cervical spine, but the axis moved closer to the center of vertebra as one moved down the spine (Amevo et al. 1991). These two ligaments had very similar loading curves, so if they were the only ligaments being considered, the response in flexion and extension should have been the same. However, in flexion there are the CL, the LF and the ISL that also influenced the response, and these ligaments, although significantly weaker than the PLL and ALL, were farther from the axis of rotation and were sensitive to the strain rate. These extra ligaments were the reason that in flexion, the high rate response was so much stiffer than the quasi-static response than it was in extension.

However, in the experimental testing, a difference in strain rate effect between the flexion and extension tests was not observed. This discovery indicated that the model was still lacking in its ability to predict the strain rate effect. The only aspects of the model that took the deformation into account were the ligaments. Since the ligaments alone did not capture the full effect, there must be other factors involved that influenced the dynamic response of the segments. One possibility was the intervertebral discs. As mentioned earlier, the center of rotation of the any cervical spine segment was closer to the posterior face of the vertebra rather than the anterior face. Therefore, in flexion the majority of the disc was under compression (the rest of the disc was in tension) and the opposite was true in extension. It was reported that the disc was stiffer in pure compression at higher strain rates (Kemper et al. 2006), so it was possible that the disc did play a role in the segment stiffening at 500 degrees per second of rotation.

6.3.2 Comparison with Existing Studies

Due to the differences in the testing apparatuses, the moment rotation response of the segments in this thesis was generally stiffer than the segment response reported by previous studies (Nightingale et al. 2002, 2007, Wheeldon et al. 2006). None of these studies tested the C2-C3 spine segment. Figures 6-5 and 6-6 show the moment rotation relationship of the quasi-static experimental tests and the results from the Nightingale and Wheeldon studies. In flexion, the results from this thesis were much stiffer at every segment level except C4-C5 where both Nightingale and Wheeldon studies were within one standard deviation. In extension, the Wheeldon study was stiffer than these results at

every level except for C6-C7 while the Nightingale response was weaker at every level. At the C5-C6 and C6-C7 levels, Nightingale was within one standard deviation.

The Nightingale and Wheeldon studies used a rotation controlled machine, applied the moment in a step wise fashion, and held the load for at least 30 seconds before recording the rotation. The 30 second delay allowed for creep which reduces the apparent stiffness of the segment since the rotation after 30 seconds would have been greater than the actual rotation right after load application. The Wheeldon study applied a maximum moment of 2 Nm and the Nightingale maximum moment was 3.5 Nm. In most cases in this thesis, the maximum moment was much higher, which was the reason why the Nightingale and Wheeldon curves did not extend to the full rotation of the experimental study. The average age of the donors in the Wheeldon study was 33 years old, and the average age for the Nightingale studies were 51 (2002 study) and 66 (2007). The difference in age could explain why the Wheeldon results were stiffer than the Nightingale data at every segment level except for C4-C5 and C6-C7 in flexion.

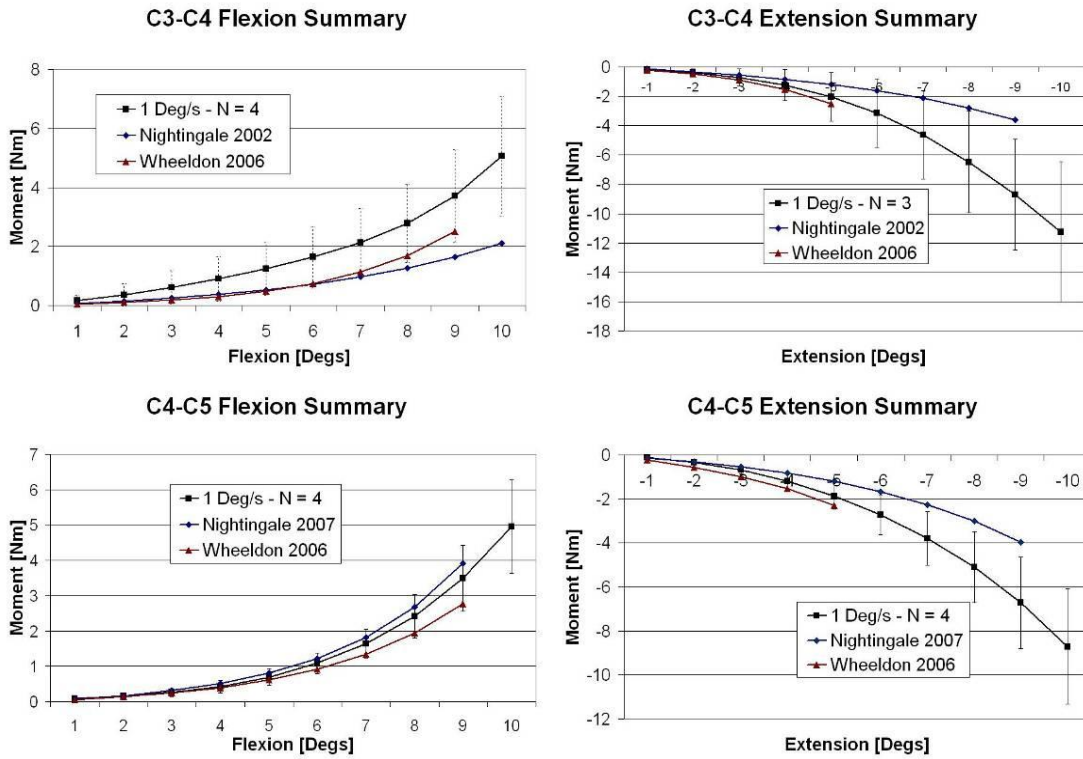


Figure 6-5: C3-C4 & C4-C5 Comparison with results from Nightingale et al. (2002, 2007) and Wheeldon et al. (2006)

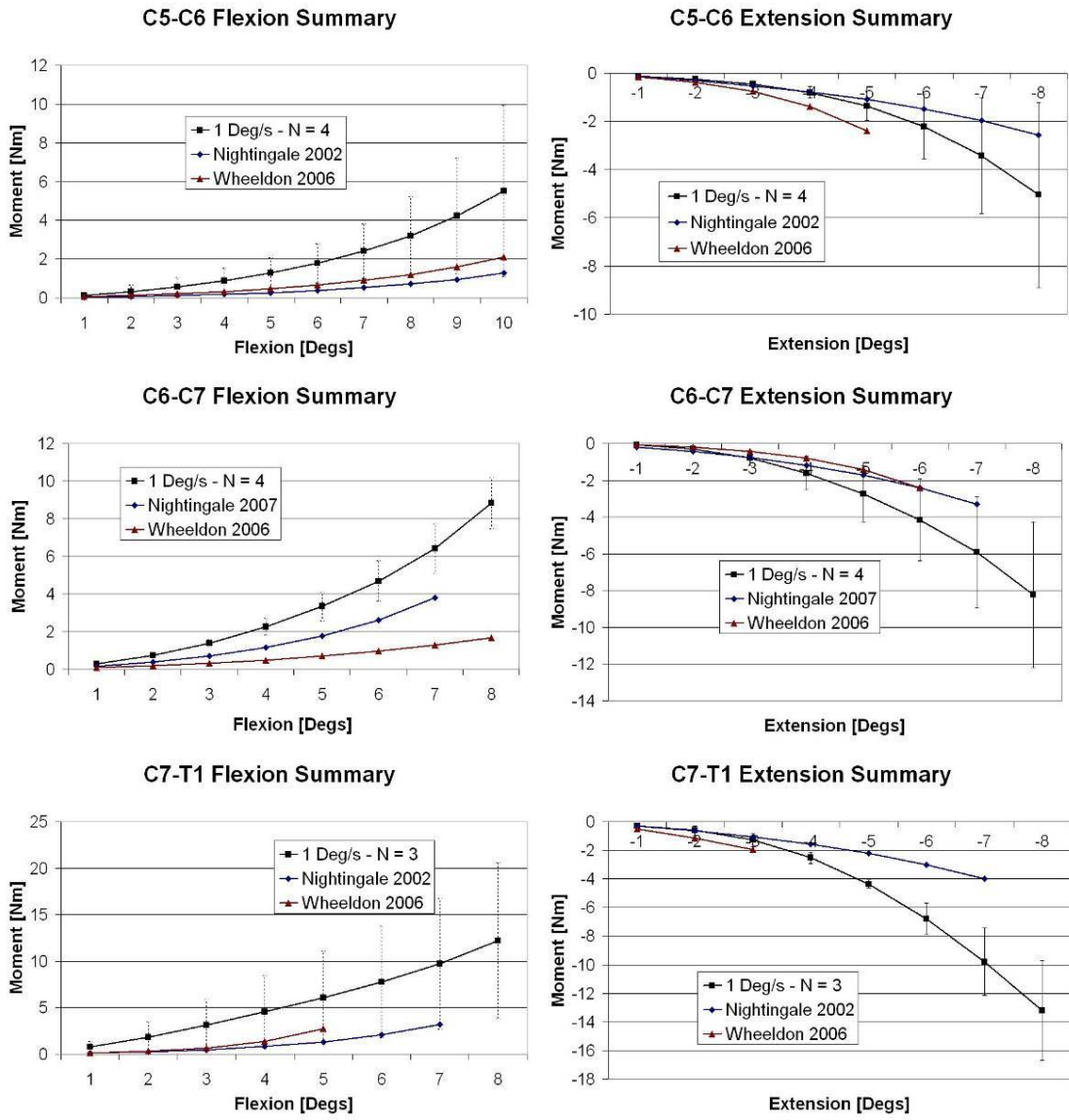


Figure 6-6: C5-C6, C6-C7 & C7-T1 Comparison with results from Nightingale et al. (2002, 2007) and Wheeldon et al. (2006)

6.3.3 Influence of the Fixed Axis Machine

The machine used in this thesis to flex and extend the samples fixed the axis of rotation of the segment. The axis of rotation was intended to be in-line with the average instantaneous axis of rotation of the segment, but due to experimental error and segment variability, the two axes were not perfectly aligned. One way to monitor the effect of the fixed axis machine was to look at the resulting shear (which was incorporated into the resultant moment) and compressive forces. The two shear forces and the compressive force were plotted against the angle of rotation to see if the shear forces were too high (selected segments shown in Figure 6-7). For the figure title, the first alphanumeric number indicates the donor spine ID followed by the spinal level, the rotation rate (1DPS equals 1 degree per second), and the test run (i.e. flex2 means the second flexion test). Several studies have looked into the response of the spine to shear and compression, and the data from this thesis was compared against their results to see the severity of the shear and compression forces generated by the testing apparatus.

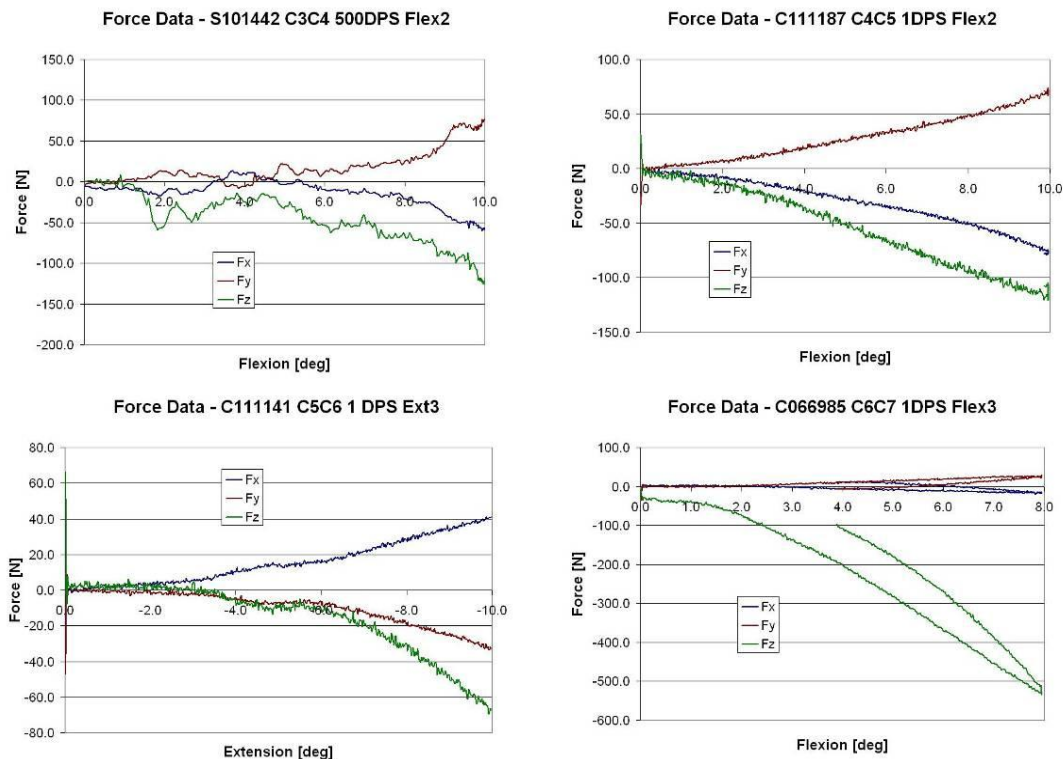


Figure 6-7: Sample Shear and Compression Force Curves Plotted against Rotation

Yingling et al. (1997), Gallagher et al. (2010) and Howarth et al. (2012) studied the response of porcine cervical spine segments in shear under various loading conditions and found that the segment failure shear load (anterior or posterior) was a minimum of 2000 N. Moroney et al. (1988) and Shea et al. (1991) tested human cervical spine segments (Shea tested C2-C5 units) in anterior and posterior shear, and found that the spine was stronger in anterior shear than posterior shear. This was somewhat expected due to the angle of the facet joints. In anterior shear, the facet joints were trying to slide over each other, but in posterior shear they were being pulled apart. Moroney et al. (1988) reported the shear force required to displace the superior vertebra 1.0 mm was 91 N and 40 N in the anterior and posterior directions respectively. Shea produced a load versus displacement curve which showed that it took 200N of anterior shear to displace the superior vertebra 2 mm and 150N of posterior shear to move the top vertebra almost 4 mm. Stemper et al. (2007) investigated various neck injury criterion for the lower cervical spine and found that the threshold for capsular ligament injury due to shear was 636 N and 384N for men and women respectively. The study also reported that the shear forces in the neck increased with increasing impact velocity.

Panzer et al. (2009) studied the response of their model to anterior and posterior shear and found that the stiffness varied on the spinal level. At the C2-C3 level, it took 100 N and 75 N of anterior and posterior shear force respectively to displace the superior vertebra 2 mm. At C4-C5, the shear load for 2mm of displacement was 200 N in anterior and posterior shear. At C6-C7, the segment was much stiffer in the anterior direction. It took 400 N of shear to displace the top segment 3mm anteriorly, but only 100N for the same displacement in the posterior direction.

Yoganandan et al. (2001) tested the compressive strength of cervical spine segments in the axial direction. The study reported the failure force and displacement for each segment (from C2-C3 to C7-T1) and found that the weakest segment, C2-C3, failed at 600 N, and the strongest segment, C7-T1, failed at 910 N. The failure displacement of all segments was between 1.4 mm and 1.7 mm. Panzer et al. (2006) ran model simulations in compression and reported that at every segment level, the force required to displace the superior vertebra 1.5 mm was greater than 1000 N.

None of the previous experimental studies in flexion and extension reported the shear or compression forces. Table 6-5 shows the average shear and compression forces from the experimental results of this thesis. In all cases, the shear and compression forces were greater at the higher rotation rate. At

all segment levels except C7-T1, the shear forces were higher in extension than in flexion, and the opposite was true for compression. In flexion, the compression forces were stronger at every level except for the C2-C3 segment level.

	Flexion		Extension		
	Shear force (N)	Comp. force (N)	Shear force (N)	Comp. force (N)	
C2-C3	Quasi	52	179	91	236
	High	82	234	107	243
C3-C4	Quasi	36	296	50	150
	High	54	354	72	188
C4-C5	Quasi	51	176	92	133
	High	72	232	114	163
C5-C6	Quasi	52	310	61	164
	High	82	322	100	214
C6-C7	Quasi	47	377	107	87
	High	74	433	148	119
C7-T1	Quasi	63	607	78	131
	High	103	733	97	124

Table 6-5: Shear and Compressive Average Forces for Flexion and Extension at every Segment Level

From the review of the shear force experimental and modeling studies, the shear force should be below 100 N to avoid any injury to the segment (Moroney et al. 1998, Shea et al. 1991, Panzer et al. 2009, Howarth et al. 2012). This is more important for the upper cervical spine because those vertebrae are smaller and less resistant to shear. In extension at the C2-C3 level, the shear force average was close to 100N and at risk of failing due to shear. The C6-C7 segments in extension also averaged a shear force above 100 N. In compression, all the segments were safely below the failure load published by Yoganandan et al. (2001) and the theoretical load simulated by Panzer et al. (2009).

Chapter 7

Summary and Recommendations

The purpose of this thesis was to investigate the high strain rate effects of the human cervical spine in flexion and extension at the segment level. The hypothesis was that the stiffness of the spine will increase at higher rates of rotation, and it was tested using a paired t-test, which isolated the strain rate effect at each segment level from the variability from segment to segment. This study was one of the first to analyze the dynamic response of cervical spine segments experimentally.

The rationale for this study was the need for high rate experimental data to validate a new, detailed finite element model of the cervical spine for the prediction of soft tissue injury during automobile crashes. The project was led by the Global Human Body Models Consortium (GHBMC), an organization of automotive manufacturers and part suppliers who wanted to develop a better human body model for use in car crash simulations. Physical car crash testing with dummies is an iterative, expensive, and time consuming process, so the development of better finite element models can help reduce the cost and time required to design a safe vehicle.

There are several validation cases for the GHBMC finite element model, and one of these cases is segment level testing in flexion and extension. Some of the other validation cases include tension and compression of the spine, whole spine impacts from the front, back and side, as well as off center and oblique impacts where the head is not at the neutral position at impact. Since the model will be used for high speed impacts, the model should be validated against experimental data done at strain rate typical in such impacts.

There were numerous studies looking into the segment response to bending moments in flexion and extension; however the majority of these studies were limited to quasi-static rates. These studies applied the load in steps instead of continuously, and it has been shown that this reduces the stiffness since creep is allowed to set in while holding a constant load. These studies were controlled by the load and measured the displacement, while the experimental work in this thesis did the opposite so that the strain rate could be controlled. Previous studies have also been limited by the age of the donor spines and the segment level tested.

Two rotation rates were selected for the flexion and extension tests in this thesis: one degree per second, representing quasi-static conditions, and 500 degrees per second. The 500 degree per second rate was chosen because it was close to the maximum rotation rate of all segment levels from C2-C3 to C7-T1 during a 22g frontal impact simulation with the old UW model (Fice, 2010). The C2-C3 through C5-C6 segments were rotated up to ten degrees and the C6-C7 and C7-T1 segments were rotated to eight degrees. These rotation limits were derived from published in vitro and in vivo range of motion studies (Dvorak 1988, 1991). The segments were tested inside an atmospheric chamber which was maintained at 37 degrees Celsius and 100% humidity. Before low and high rate testing, each segment was preconditioned: ten cycles to four degrees in flexion and extension

The full cervical spine FE model was broken down into segments and simulated in flexion and extension. Rigid bodies were attached to the superior surface of the superior vertebra and the rotation was applied to this body. Another rigid body was added to the inferior surface of the inferior vertebra, and it was fixed in all six degrees of freedom. The model was run at 500 degrees per second, and the ligament strain rate effects were deleted from the model in order to simulate the quasi-static test case.

This study was limited by the sample size due to the low supply of young post mortem human subjects. There appears to be a stiffening trend at the higher rotation rate, but since the sample size was only four, there was not any moderate evidence of the stiffening trend except at the C5-C6 and C6-C7 levels. Another approach could have been to test the C2-C3, C4-C5 and C6-C7 levels only and use every spine for those segment levels. The sample size would double to eight and the evidence would have been stronger, but the scope of the study would have been limited to those three spinal levels only, leaving the segment level validation incomplete. Six out of the nine spines procured were male; therefore the gender effect was not explored.

The experimental results were analyzed to see if there was any strain rate effect, and then they were compared against the model simulations. This study found varying degrees of statistical significance, but only the C5-C6 and C6-C7 segment experiments showed moderate to strong evidence of increased stiffness at the higher rotation rate in flexion and extension. There was weak evidence of a strain rate effect in flexion and extension at C3-C4 and C4-C5. There clearly was a strain rate trend at every segment level, but the evidence was only significant at high degrees of rotation (>8 degrees)

due to the low sample size of the study, and the high variability between spines. Although there were only four cases out of twelve showing moderate evidence of increased stiffness, every segment level in flexion and extension demonstrated the same trend, leading to the conclusion that had the sample size been larger there would have been stronger proof of a rotation rate effect in the cervical spine under flexion and extension loading conditions.

There were mixed results for the comparison between the testing and the model. At some segment levels, the two matched up closely, while in other instances there were significant disagreement between model and experimental results. The model also predicted that the rotation rate effect would be much more significant in flexion than in extension because there were more ligaments activated in flexion. However, the experimental results showed no significant differences between the flexion and extension strain rate effects. In the FE model of the spine, the only tissues with high rate mechanical properties were the ligaments; therefore the discrepancy between the rotation rate effect in the model and the experiments was most likely due to the rotation rate effects in the intervertebral discs.

7.1 Recommendations

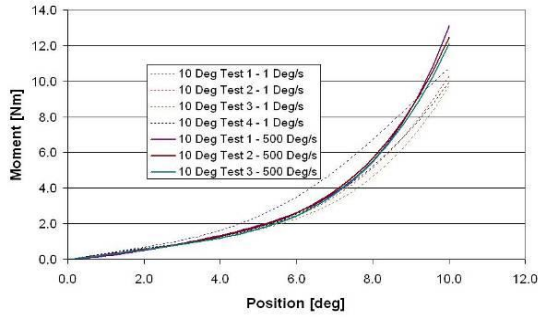
This thesis focused on the dynamic response of the segment by reporting the resultant moment and rotation relationship. The dynamic response of the experimental testing was used to validate the segment models. Ideally, the validation could be improved with translational kinematic experimental data. With the current flexion extension setup, the specimen could only rotate about a single point and translational displacement was constrained. The setup could be improved by allowing the segment to rotate freely and still control the displacement instead of the moment. The machine would be similar to the one used by Voo et al. (1998) for high rate testing, except that there would be another piston applying a force on the other side of the segment to induce a pure moment on the segment. The rotation rate could be easily calculated by multiplying the velocity of the piston and the moment arm to the center of rotation. Although the center of rotation could move, the displacement would be small compared to the moment arm and the error in the rotation rate calculation would be acceptable. The kinematics (rotational as well as translational) of the free vertebra would be measured with motion capture technology and the force response would once again

be recorded by a six axis load cell. The experimental data could be compared against the model results to verify that the model does capture the full kinematic response of the spine along with the dynamic response.

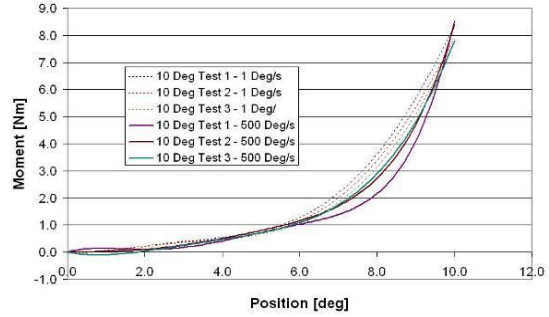
The material properties of the intervertebral discs in the model were derived from the experimental testing of lumbar spine discs. All the studies analyzing the compression of the disc and the tensile properties of the annulus fibrosus used human lumbar spines or equivalent porcine cervical spines. Experimental testing should be done on cervical spine segments to verify that the data from the lumbar spines is comparable to the cervical spine.

Appendix – Individual Segment Test Results

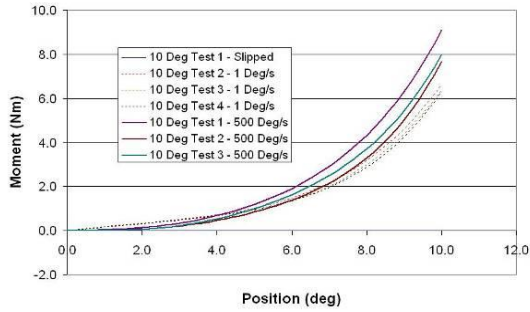
C066985 C2/C3 Flexion Tests



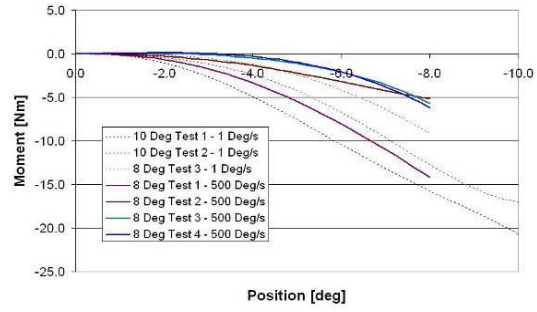
C111187 C2/C3 Flexion Tests



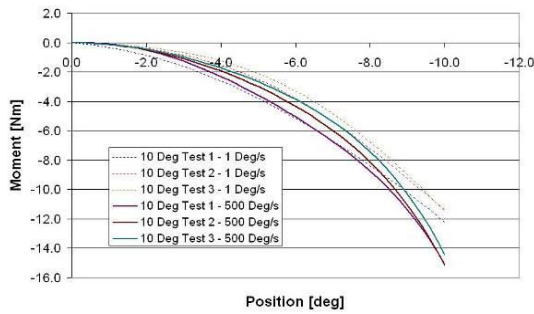
C100800 C2/C3 Flexion Tests



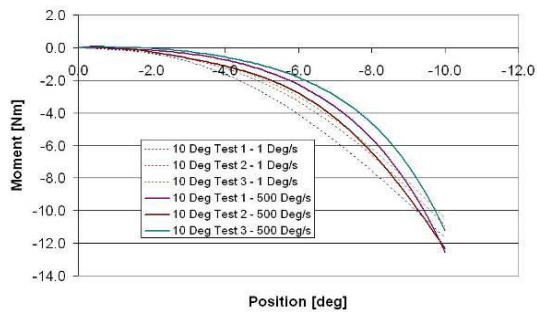
C066985 C2/C3 Extension Tests



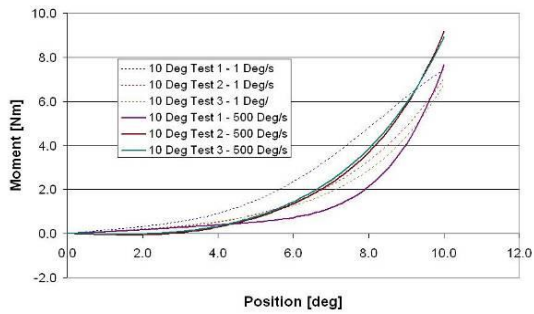
C100800 C2/C3 Extension Tests



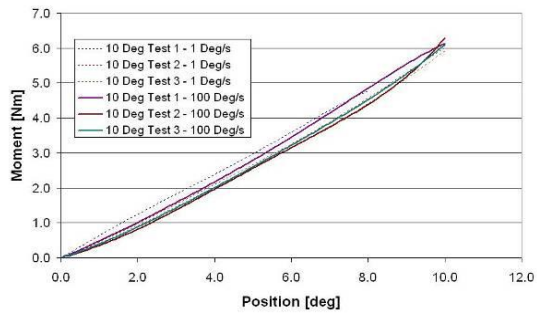
C111187 C2/C3 Extension Tests



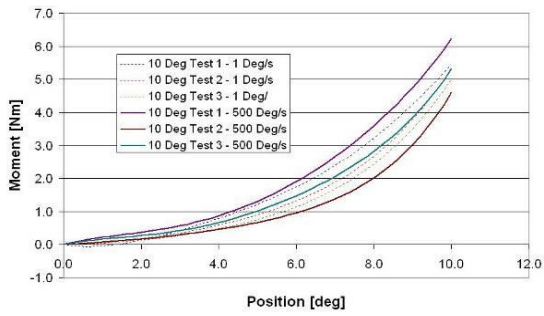
S101442 C3/C4 Flexion Tests



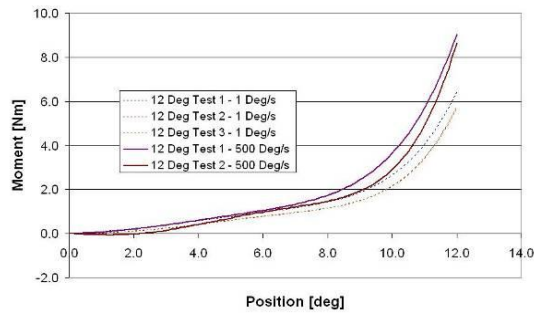
C0065494 C3/C4 Flexion Tests



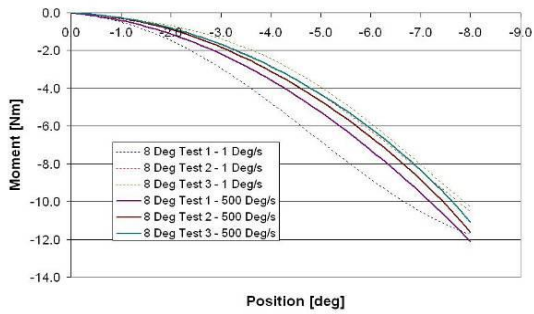
C111141 C3/C4 Flexion Tests



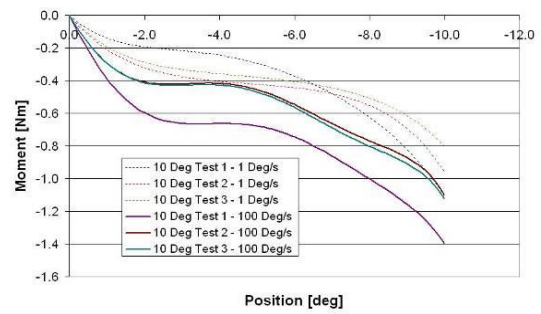
C080914 C3/C4 Flexion Tests



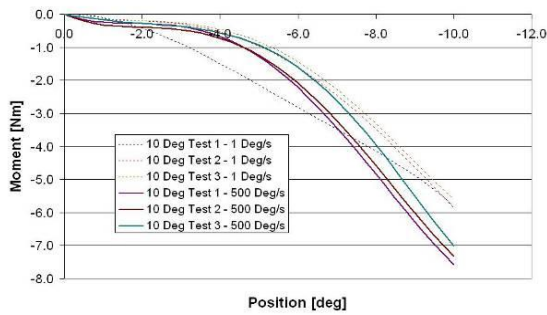
S101442 C3/C4 Extension Tests



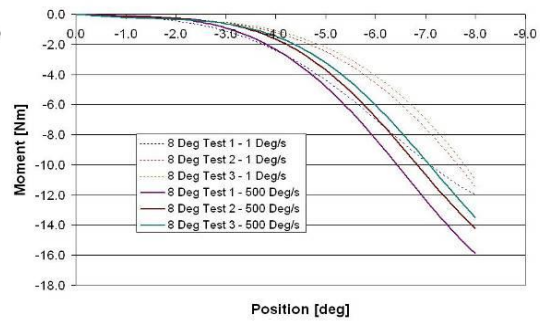
C0065494 C3/C4 Extension Tests



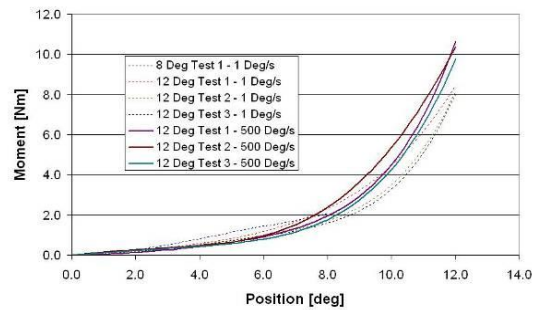
C111141 C3/C4 Extension Tests



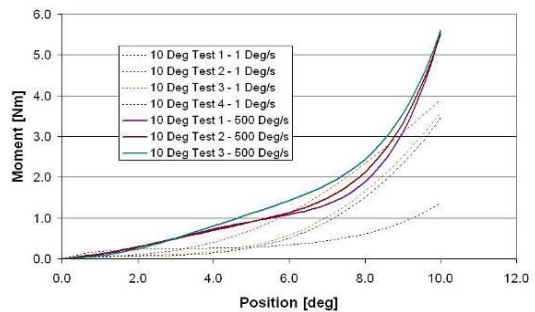
C080914 C3/C4 Extension Tests



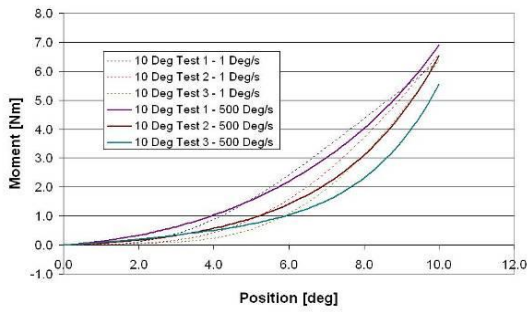
C100800 C4/C5 Flexion Tests



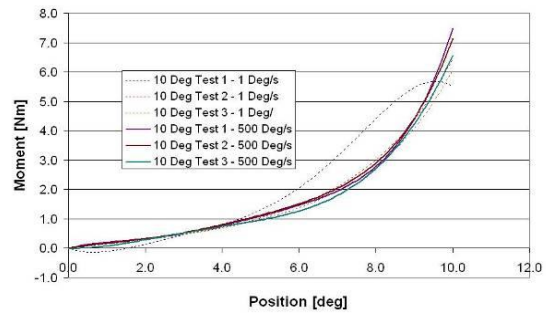
C066985 C4/C5 Flexion Tests



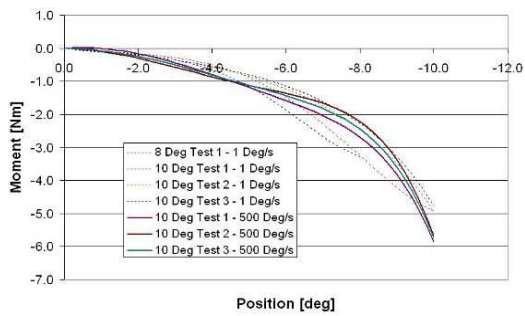
C100386 C4/C5 Flexion Tests



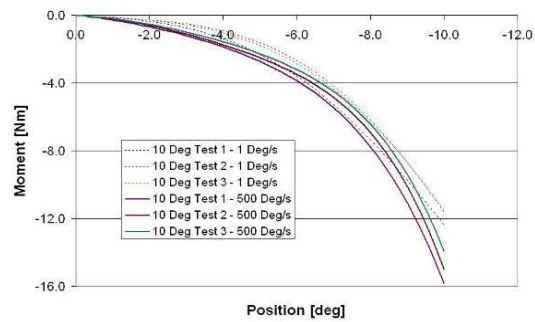
C111187 C4/C5 Flexion Tests



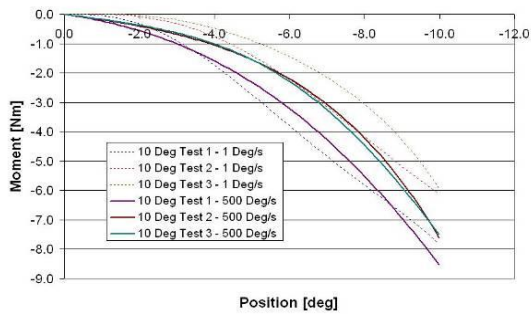
C100800 C4/C5 Extension Tests



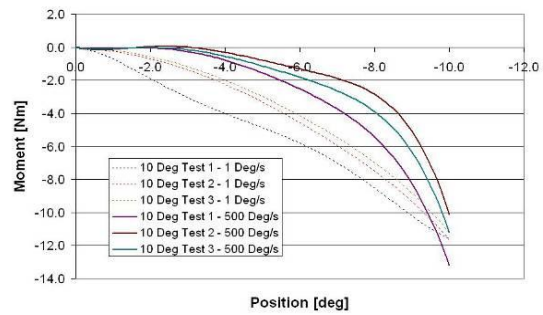
C066985 C4/C5 Extension Tests



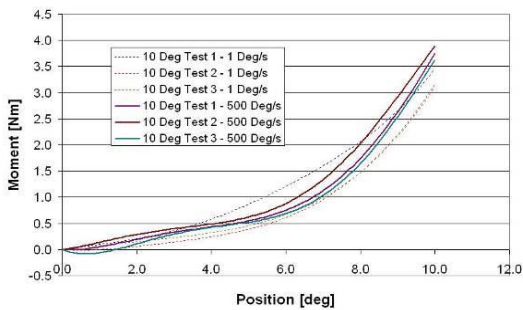
C100386 C4/C5 Extension Tests



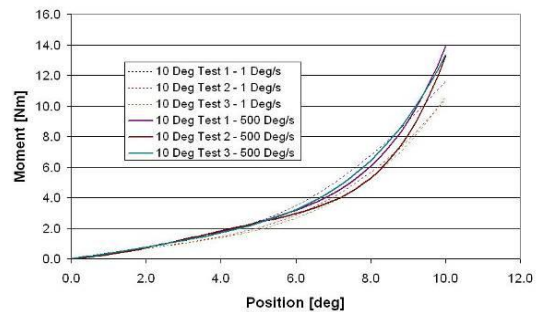
C111187 C4/C5 Extension Tests



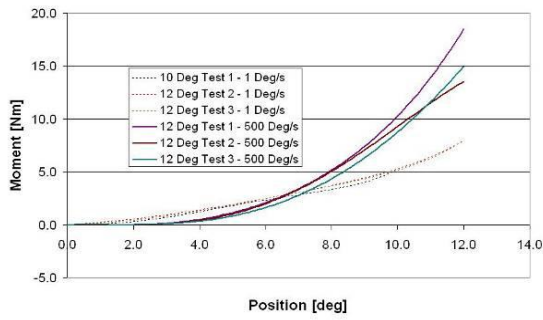
C111141 C5/C6 Flexion Tests



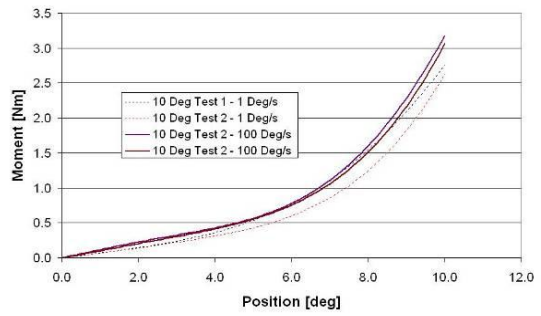
C080914 C5/C6 Flexion Tests



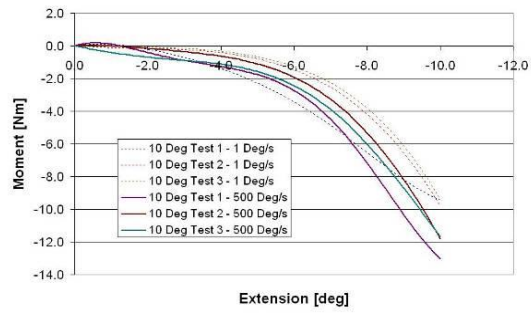
S101442 C5/C6 Flexion Tests



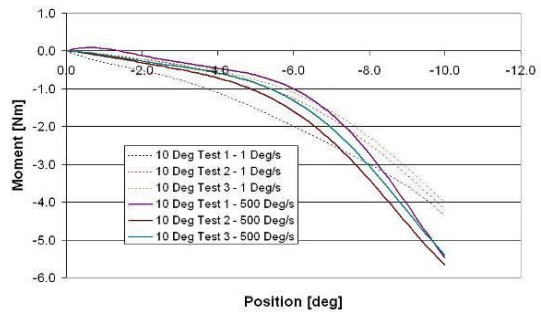
C0065494 C5/C6 Flexion Tests



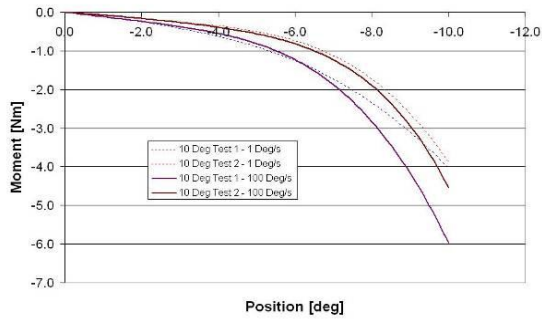
S101442 C5/C6 Extension Tests



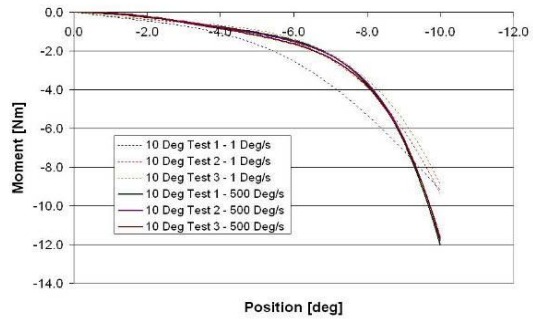
C111141 C5/C6 Extension Tests



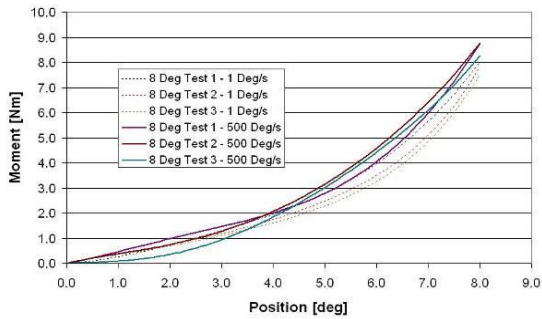
C0065494 C5/C6 Extension Tests



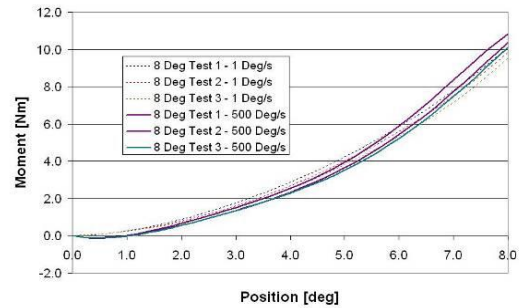
C080914 C5/C6 Extension Tests



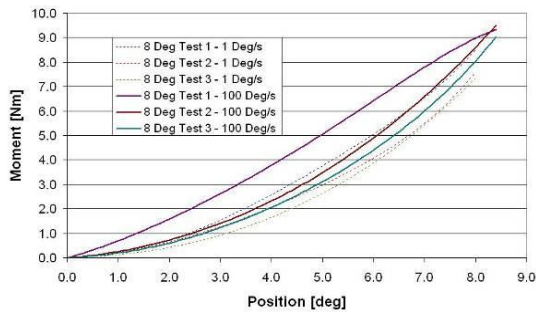
C111187 C6/C7 Flexion Tests



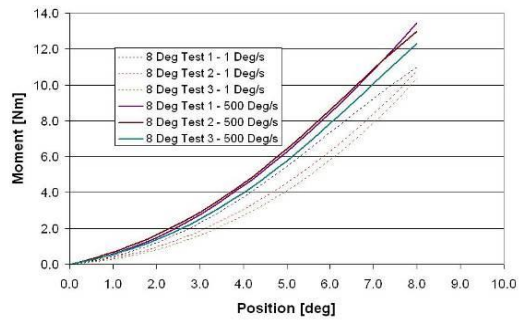
C066985 C6/C7 Flexion Tests



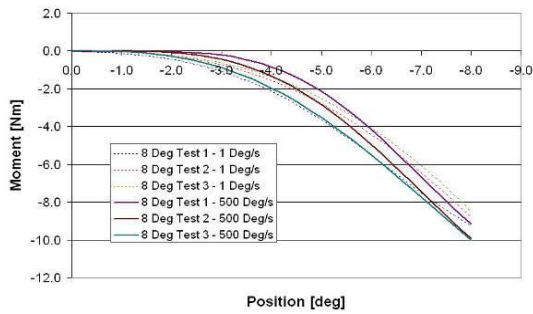
C100386 C6/C7 Flexion Tests



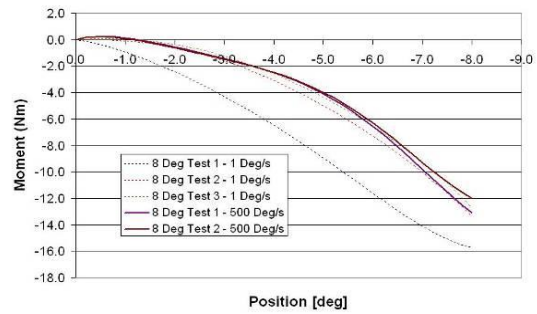
C100800 C6/C7 Flexion Tests



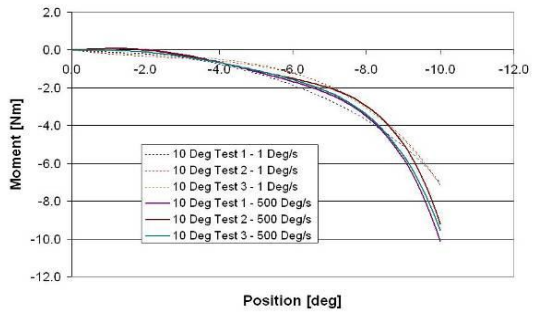
C100800 C6/C7 Extension Tests



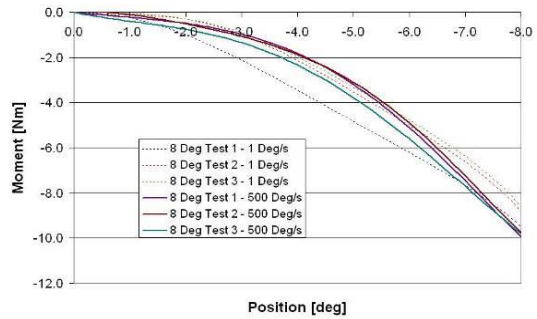
C066985 C6/C7 Extension Tests



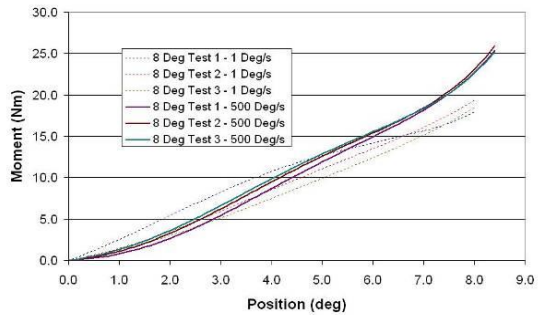
C100386 C6/C7 Extension Tests



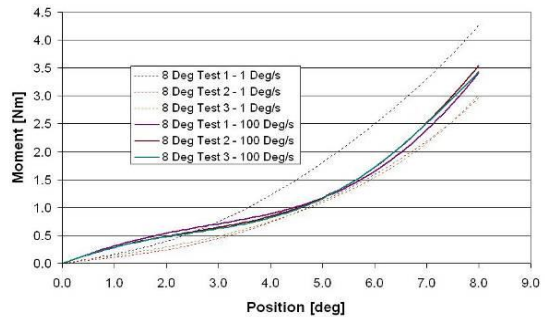
C111187 C6/C7 Extension Tests



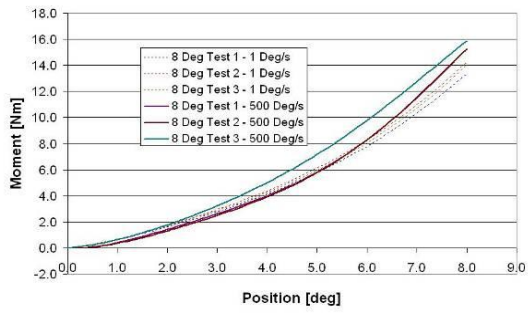
C080914 C7/T1 Flexion Tests



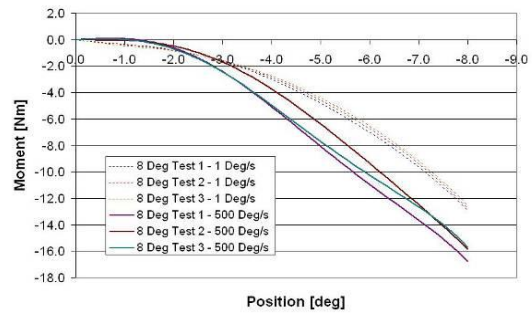
C0065494 C7/T1 Flexion Tests



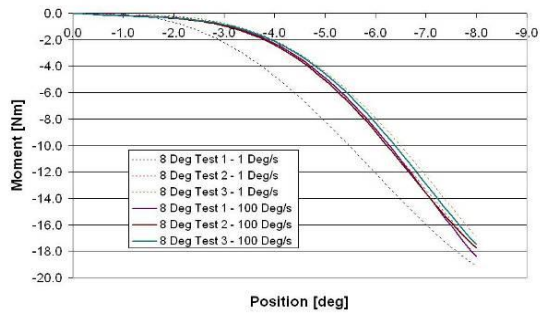
C111141 C7/T1 Flexion Tests



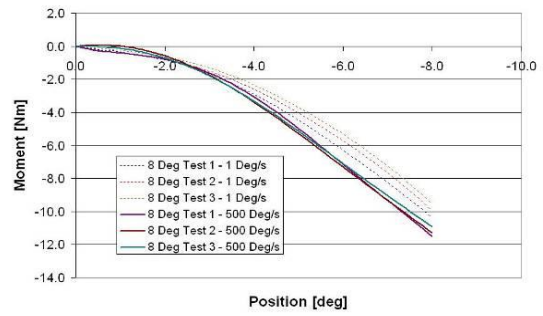
C080914 C7/T1 Extension Tests



C0065494 C7/T1 Extension Tests



C111141 C7/T1 Extension Tests



References

- Abramowitch, S. D., Feola, A., Jallah, Z., & Moalli, P. A. (2009). Tissue Mechanics, Animal Models, and Pelvic Organ Prolapse: A Review. *European Journal of Obstetrics & Gynecology and Reproductive Biology*, 146-158.
- Ashman, R.B., Cowin, S.C., Van Buskirk, W.C., & Rice, J.C. (1984). A Continuous Wave Technique for the Measurement of the Elastic Properties of Cortical Bone. *Journal of Biomechanics*, 17(5), 349-361.
- Bartel, D.L., Davy, D.T., & Keaveny, T.M. (2006) *Orthopaedic Biomechanics: Mechanics and Design in Musculoskeletal Systems*. New Jersey: Pearson Prentice Hall.
- Bass, C. R., Lucas, S. R., & Salzar, R. S. (2007). Failure Properties of Cervical Spinal Ligaments Under Fast Strain Rate Deformations. *Spine*, 32, 7-13.
- Bogduk, N., & Mercer, S. (2000). Biomechanics of the Cervical Spine. I: Normal kinematics. *Clinical Biomechanics*, 15(9), 633-48.
- Camacho, D. L. A., Nightingale, R. W., Robinette, J. J., Vanguri, S. K., Coates, D. J., & Myers, B. S. (1997) Experimental Flexibility Measurements for the Development of a Computational Head-Neck Model Validated for Near-Vertex Head Impact. 41st Stapp Car Crash Conference Proceedings, 41, 473-486.
- Cassidy, J. J., Hiltner, A., & Baer, E. (1989). Hierarchical Structure of the Intervertebral Disc. *Connective Tissue Research*, 23, 75-88.
- Cezayirlioglu, H., Bahniuk, E., Davy, D.T., & Heiple, K.G. (1985). Anisotropic Yield Behavior of Bone under Combined Axial Force and Torque. *Journal of Biomechanics*, 18(1), 61-69.
- Chazal, J., Tanguy, A., & Bourges, M. (1985). Biomechanical Properties of Spinal Ligaments and a Histological study of the Supraspinal Ligament in Traction. *Journal of Biomechanics*, 18(3), 167-176.
- Cheng, S., Clarke, E. C., and Bilston, L. E. (2009). The Effects of Preconditioning Strain on Measured Tissue Properties. *Journal of Biomechanics*, 42(9), 1360-1362.
- Cowen, S.C. (1988) *Bone Mechanics*. Boca Raton Florida: CRC Press Inc.
- Cripton, P. A, Bruehlmann, S. B., Orr, T. E., Oxland, T. R., & Nolte, L. P. (2000). In Vitro Axial Preload Application during Spine Flexibility Testing: Towards Reduced Apparatus-Related Artefacts. *Journal of Biomechanics*, 33(12), 1559-68.
- Dvorak, J., Froehlich, D., Penning, L., Baumgartner, H., & Panjabi, M.M. (1988). Functional radiographic diagnosis of the cervical spine: flexion/extension. *Spine*, 13(7), 748-755.

- Dvorak, J., Panjabi, M.M., Novotny, J.E., & Antinnes, J.A. (1991). In vivo flexion/extension of the normal cervical spine. *Journal of Orthopaedic Research*, 9(6), 828-834.
- Ebara, S., Iatridis, J. C., Setton, L. A., Foster, R. J., Mow, V. C., & Weidenbaum, M. (1996) Tensile Properties of Nondegenerate Human Lumbar Anulus Fibrosus. *Spine*, 21(4), 452-461.
- Elliott, D. M., & Setton, L. A. (2001). Anisotropic and Inhomogeneous Tensile Behavior of the Human Anulus Fibrosus : Experimental Measurement and Material Model. *Journal of Biomechanical Engineering*, 123, 256-263.
- Evans, F.G. (1976). Mechanical Properties and Histology of Cortical Bone from Younger and Older Men. *The Anatomical Record*, 185(1), 1-11.
- Fice, J.B., Cronin, D.S., & Panzer, M.B. (2009) Investigation of Facet Joint Response Under Rear Impact Conditions Using FE Model of the Cervical Spine. *Proceedings of the 21st International Technical Conference on the Enhanced Safety of Vehicles, National Highway Traffic Safety Administration, 2009.*
- Fields, A. J., Lee, G. L., Liu, X. S., Jekir, M. G., Guo, X. E., & Keaveny, T. M. (2011). Influence of Vertical Trabeculae on the Compressive Strength of the Human Vertebra. *Journal of Bone and Mineral Research*, 26(2), 263-269.
- Fujita, Y., Duncan, N. A., & Lotz, J. C. (1997). Radial Tensile Properties of the Lumbar Annulus Fibrosus are Site and Degeneration Dependent. *Journal of Orthopaedic Research*, 15, 814-819.
- Fung, Y.-C. (1993). *Biomechanics: Mechanical Properties of Living Tissues* (2nd Edition ed.). New York: Springer.
- Gallagher, K. M., Howarth, S. J., & Callaghan, J. P. (2010). Effects of Anterior Shear Displacement Rate on the Structural Properties of the Porcine Cervical Spine. *Journal of Biomechanical Engineering*, 132, 3-8.
- Gayzik, F.S., Moreno, D.P., Geer, C.P., Wuertzer, S.D., Martin, R.S., & Stitzel, J.D. (2011). Development of a full body CAD dataset for computational modeling: a multi-modality approach. *Annals of Biomedical Engineering*, 39(10), 2568-2583.
- Goertzen, D. J., Lane, C., & Oxland, T. R. (2004). Neutral Zone and Range of Motion in the Spine are Greater with Stepwise Loading than with a Continuous Loading Protocol . An in Vitro Porcine Investigation. *Journal of Biomechanics*, 37, 257-261.
- Gray, H. (1918). *Anatomy of the Human Body* (20th ed.). Philadelphia: Lea & Febiger.
- Halldin, P. H., Brodin, K., Kleiven, S., Holst, H. V., Jakobsson, L., & Palmertz, C. (2000). Investigation of Conditions that Affect Neck Compression- Flexion Injuries Using Numerical Techniques. 44th Stapp Car Crash Conference Proceedings, 44, 127-138.

- Hedenstierna, S., & Halldin, P. (2008). How Does a Three-Dimensional Continuum Muscle Model Affect the Kinematics and Muscle Strains of a Finite Element Neck Model Compared to a Discrete Muscle Model in Rear-End , Frontal , and Lateral Impacts. *Spine*, 33(8), 236-245.
- Hedenstierna, S., Halldin, P., & Siegmund, G. P. (2009). Neck Muscle Load Distribution in Lateral , Frontal , and Rear-End Impacts A Three-Dimensional Finite Element Analysis. *Spine*, 34(24), 2626-2633.
- Hill, R. (1978). Aspects of Invariance in Solid Mechanics. *Advances in Applied Mechanics* 18, 1 – 75.
- Holzappel, G.A., Schulze-Bauer, C.A.J., Fiegl, G., & Regitnig, P. (2005). Single Lamellar Mechanics of the Human Lumbar Anulus Fibrosus. *Biomechanics and Modeling in Mechanobiology*, 3, 125-140.
- Howarth, S. J., & Callaghan, J. P. (2012). Compressive force magnitude and intervertebral joint flexion / extension angle influence shear failure force magnitude in the porcine cervical spine. *Journal of Biomechanics*, 45(3), 484-490.
- Iida, T., Abumi, K., Kotani, Y., & Kaneda, K. (2002). Effects of Aging and Spinal Degeneration on Mechanical Properties of Lumbar Supraspinous and Interspinous Ligaments. *Spine*, 2, 95-100.
- Iatridis, J.C., Setton, L.A., Weidenbaum, M., & Mow, V.C. (1997). The Viscoelastic Behavior of the Non-Degenerate Human Lumbar Nucleus Pulposus in Shear. *Journal of Biomechanics*, 30(10), 1005-1013.
- Ivancic, P. C., Coe, M. P., Ndu, A. B., & al, E. (2007). Dynamic mechanical properties of intact human cervical spine ligaments. *The Spine Journal*, 7, 659-665.
- Kallemeyn, N., Gandhi, A., Kode, S., & Shivanna, K. (2010). Validation of a C2 – C7 Cervical Spine Finite Element Model using Specimen-Specific Flexibility Data. *Medical Engineering and Physics*, 32(5), 482-489.
- Kemper, A., McNally, C., Manoogian, S., Mcneely, D., Tech, V., Forest, W., & Biomechanics, I. (2006). Stiffness Properties of Human Lumbar Intervertebral Discs in Compression and the Influence of Strain Rate. Center for Injury Biomechanics – Virginia Tech, Wake Forest, Paper Number 07-0471, 1-7.
- Kumaresan, S., Yoganandan, N., & Pintarh, F. A. (1999). Finite Element Analysis of the Cervical Spine: a Material Property Sensitivity Study. *Clinical biomechanics*, 14, 41-53.
- Marchand, F., & Ahmed, A.M. (1990). Investigation of the laminate structure of lumbar disc anulus fibrosus. *Spine*, 15(5), 402-410.
- Markolf, K. L. (1972). Deformation Joints of the Thoracolumbar in Response to External Intervertebral Loads. *Journal of Bone and Joint Surgery*, 54(3), 511-533.
- Mattucci, S.F.E. (2011). Strain Rate Dependent Properties of Younger Human Cervical Spine Ligaments. M.A.Sc Thesis, University of Waterloo.

- Mattucci, S. F. E., Moulton, J. A., Chandrashekar, N., & Cronin, D. S. (2012). Strain rate dependent properties of younger human cervical spine ligaments. *Journal of the Mechanical Behavior of Biomedical Materials*, 10, 216-226.
- McCalden, R. W., McGeough, J. A., Barker, M. B., & Court-Brown, C. M. (1993) Age-related changes in the tensile properties of cortical bone. The relative importance of changes in porosity, mineralization, and microstructure. *Bone and Joint Surg.*, 75-A, 1193-1205.
- McElhaney, H., & Virginia, W. (1966). Dynamic Response of Bone and Muscle Tissue. *Journal of Applied Physiology*, 21(4), 1231-1236.
- Meyer, F., Bourdet, N., Deck, C., & Willinger, R. (2004). Human Neck Finite Element Model Development and Validation against Original Experimental Data. 48th Stapp Car Crash Proceedings, 48, 177-206.
- Moore, K. L., & Dalley, A. F. (1999). *Clinically Oriented Anatomy* (Fourth ed.). Lippincott Williams & Wilkins.
- Morgan, E. F., Bayraktar, H. H., & Keaveny, T. M. (2003). Trabecular Bone Modulus – Density Relationships Depend on Anatomic Site. *Journal of Biomechanics*, 36, 897-904.
- Moroney, S. P., Schultz, A. B., Miller, J. A., & Andersson, G. B. (1988). Load-Displacement Properties of Lower Cervical Spine Motion Segments. *Journal of Biomechanics*, 21(9), 769-79.
- Myklebust, J., Pintar, F., & Yoganandan, N. (1988). Tensile Strength of Spinal Ligaments. *Spine*, 13(5), 526-531.
- Nachemson, A., & Evans, J. (1968). Some Mechanical Properties of the Third Human Lumbar Interlaminar Ligament (Ligamentum Flavum). *Journal of Biomechanics*, 1, 211-220.
- Nightingale, R. W., Carol Chancey, V., Ottaviano, D., Luck, J. F., Tran, L., Prange, M., & Myers, B. S. (2007). Flexion and Extension Structural Properties and Strengths for Male Cervical Spine Segments. *Journal of Biomechanics*, 40(3), 535-42.
- Nightingale, R. W., Winkelstein, B. A, Knaub, K. E., Richardson, W. J., Luck, J. F., & Myers, B. S. (2002). Comparative Strengths and Structural Properties of the Upper and Lower Cervical Spine in Flexion and Extension. *Journal of Biomechanics*, 35(6), 725-32.
- Noyes, F.R., & Grood, E.S. (1972). The Strength of the Anterior Cruciate Ligament in Humans and Rhesus Monkeys. *The Journal of Bone and Joint Surgery*, 58(8), 1074-1082.
- Panjabi, M. M., Crisco, J. J., Vasavada, A, Oda, T., Cholewicki, J., Nibu, K., & Shin, E. (2001). Mechanical Properties of the Human Cervical Spine as Shown by Three-Dimensional Load-Displacement Curves. *Spine*, 26(24), 2692-700.
- Panjabi, M. M., Ito, S., Ivancic, P. C., & Rubin, W. (2005). Evaluation of the Intervertebral Neck Injury Criterion using Simulated Rear Impacts. *Journal of Biomechanics*, 38(8), 1694-701.

- Panzer, M. B., & Cronin, D.S. (2009). C4 – C5 Segment Finite Element Model Development, Validation, and Load-Sharing Investigation. *Journal of Biomechanics*, 42, 480-490.
- Panzer, M. B., Fice, J. B., & Cronin, D. S. (2011). Cervical spine response in frontal crash. *Medical Engineering and Physics*, 33(9), 1147-1159.
- Patwardhan, A. G., Havey, R. M., Carandang, G., Simonds, J., Voronov, L. I., Ghanayem, A. J., Meade, K. P., Gavin, T.M., & Paxinos, O. (2003). Effect of Compressive Follower Preload on the Flexion-Extension Response of the Human Lumbar Spine. *Journal of Orthopaedic Research*, 21, 540-546.
- Pezowicz, C. A., Robertson, P. A., & Broom, N. D. (2005). Intralamellar relationships within the collagenous architecture of the annulus fibrosus imaged in its fully hydrated state. *Journal of Anatomy*, 207(4), 299-312.
- Pugh, J.W., Rose, R.M, & Radin, E.L. (1973). Elastic and Viscoelastic Properties of Trabecular Bone: Dependence on Structure. *Journal of Biomechanics*, 6, 475-485.
- Przybylski, G. J., Carlin, G., Patel, P., & Woo, S. (1996). Human Anterior and Posterior Cervical Longitudinal Ligaments Possess Similar Tensile Properties. *Journal of Orthopaedic Research* , 14, 1005-1008.
- Quinn, K.P., & Winkelstein, B.A. (2011). Preconditioning is Correlated With Altered Collagen Fiber Alignment in Ligament. *Journal of Biomechanics*, 133(6), (064506)1-4.
- Reilly, D. T., & Burstein, A. H. (1975). The Elastic and Ultimate Properties of Compact Bone Tissue. *Journal of Biomechanics*, 8(6), 393-405.
- Shea, M., Edwards, W. T., White, A. A., & Hayes, W. C. (1991). Variations of Stiffness and Strength along the Human Cervical Spine. *Journal of Biomechanics*, 24(2), 95-107.
- Shim, V., Liu, J., & Lee, V. (2005). A Technique for Dynamic Tensile Testing of Human Cervical Spine Ligaments. *Experimental Mechanics*, 46, 77-89.
- Stemper, B.D., Board, D., Yoganandan, N., & Wolfla, C.E. (2010). Biomechanical Properties of Human Thoracic Spine Disc Segments. *Journal of Craniovertebral Junction and Spine*, 1(1), 18-22.
- Stemper, B.D., & Storvik, S.G. (2010): Incorporation of Lower Neck Shear Forces to Predict Facet Joint Injury Risk in Low-Speed Automotive Rear Impacts, *Traffic Injury Prevention*, 11:3, 300-308
- Stokes, I. A., Gardner-Morse, M., Churchill, D., & Laible, J. P. (2002). Measurement of a spinal motion segment stiffness matrix. *Journal of Biomechanics*, 35, 517-521.
- Thompson, R. E., Barker, T. M., & Percy, M. J. (2003). Defining the Neutral Zone of Sheep Intervertebral Joints during Dynamic Motions : an In Vitro Study. *Clinical Biomechanics*, 18, 89-98.

- Townsend, P.R., Rose, R.M., & Radin, E.L. (1975). Buckling Studies of Single Human Trabeculae. *Journal of Biomechanics*, 8, 199-203.
- Wagner, D. R., & Lotz, J. C. (2004). Theoretical Model and Experimental Results for the Nonlinear Elastic Behavior of Human Annulus Fibrosus. *Journal of Biomechanics*, 22, 901-909.
- Wainwright, S.A., Biggs, W.D., Currey, J.D., & Gosline, J.M. (1976) *Mechanical Design in Organisms*. London: Edward Arnold Publishers Limited.
- Wen, N., Lavaste, F., Santin, J.J., & Lassau, J.P. (1993). Three-Dimensional Biomechanical Properties of the Human Cervical Spine in vitro. *Eur Spine Journal*, 2: 2-11.
- Wheeldon, J. A, Pintar, F. A, Knowles, S., & Yoganandan, N. (2006). Experimental Flexion/Extension Data Corridors for Validation of Finite Element Models of the Young, Normal Cervical Spine. *Journal of Biomechanics*, 39(2), 375-80.
- White, A. A., & Panjabi, M. M. (1990). *Clinical Biomechanics of the Spine* (2nd Edition ed.). Philadelphia: Lippincott Company
- Williams, J.L., & Lewis, J.L. (1982). Properties and an Anisotropic Model of Cancellous Bone from the Proximal Tibial Epiphysis. *Journal of Biomechanical Engineering*, 104 (1), 50-56.
- Van der Horst, M.J. (2002). *Human Head Neck Response in Frontal, Lateral and Rear End Impact Loading - Modelling and Validation*. University of Eindhoven. Ph.D Thesis.
- Viejo-Fuertes, D., Liguoro, D., Rivel, J., Midy, D., & Guerin, J. (1998). Morphologic and Histologic Study of the Ligamentum Flavum in the Thoraco-Lumbar Region. *Surgical and Radiologic Anatomy* , 20 (3), 171-176.
- Voo, L. M., Pintar, F. A, Yoganandan, N., & Liu, Y. K. (1998). Static and Dynamic Bending Responses of the Human Cervical Spine. *Journal of Biomechanical Engineering*, 120(6), 693-6.
- Yingling, V. R., Callaghan, J. P., & McGill, S. M. (1997). Dynamic Loading Affects the Mechanical Properties and Failure Site of Porcine Spines. *Clinical Biomechanics*, 12(5), 301-305.
- Yoganandan, N., Kumaresan, S., & Pintar, F. (2000). Geometric and Mechanical Properties of Human Cervical Spine Ligaments. *Journal of Biomechanical Engineering* , 122, 623-629.
- Yoganandan, N., Kumaresan, S., & Pintar, F. (2001). Biomechanics of the cervical spine Part 2. Cervical spine soft tissue responses and biomechanical modeling. *Clinical biomechanics*, 16(1), 1-27.
- Yoganandan, N., Pintar, F., & Butler, J. (1989). Dynamic Response of Human Cervical Spine Ligaments. *Spine*, 14(10), 1102-1110.
- Yoganandan, N., Ray, G., Pintar, F.A., Myklebust, J.B., & Sances, A. (1989b). Stiffness and Strain Energy Criteria to Evaluate the Threshold of Injury to an Intervertebral Joint. *Journal of Biomechanics*, 22(2), 135-142.

Yoon, H.Y., & Katz, J.L. (1984). The Structure and Anisotropic Mechanical Properties of Bone. *IEEE Transactions on Bio-medical Engineering*, 31(12), 878-884.

Zhang, Q. H., Teo, E. C., Ng, H. W., & Lee, V. S. (2006). Finite Element Analysis of Moment-Rotation Relationships for Human Cervical Spine. *Journal of Biomechanics*, 39(1), 189-93.